10
Diffusion in Zeolites

Jörg Kärger and Sergey Vasenkov
Leipzig University, Leipzig, Germany

Scott M. Auerbach
University of Massachusetts Amherst, Amherst, Massachusetts, USA

I. GENERAL INTRODUCTION

The dynamic properties of adsorbed molecules play a central role in reactions and separations that take place within the cavities of zeolites and other shape-selective, microporous catalysts. Selectivity may be strongly influenced, e.g., by the diffusivities of reactant and product molecules. However, with this selectivity comes a price: significant transport resistance. Zeolite scientists are thus interested in better understanding diffusion in zeolites to optimize the balance between high flux and high selectivity. These interests have resulted in a burgeoning field of both experimental and theoretical research, which we review in this chapter.

Although diffusion coefficients for molecular liquids typically fall in the range of 10^{-9}–10^{-8} m^2s^{-1}, diffusivities for molecules in zeolites cover a *much* larger range, from 10^{-19} m^2 s^{-1} for benzene in Ca-Y (1) to 10^{-8} m^2 s^{-1} for methane in silicalite-1 (2). Such a wide range offers the possibility that diffusion in zeolites, probed by both experiment and simulation, can provide an important characterization tool complementary to diffraction, nuclear magnetic resonance (NMR), infrared (IR), etc., because diffusive trajectories of molecules in zeolites sample all relevant regions of the zeolite–guest potential energy surface. We believe that studying diffusion in zeolites can also provide information about structural defects and disorder in zeolite–guest systems, which are very difficult to detect by ''conventional'' characterization methods (see, e.g., Chaps. 3, 6, 7, and 8 in this volume).

In addition to the application-oriented reasons for studying diffusion in zeolites, significant effort has been devoted to revealing the fascinating physical effects that accompany such diffusion systems, including molecular nanoconfinement, connected and disconnected channel systems, ordered and disordered charge distributions, cluster formation, and single-file diffusion. The experimental and theoretical concepts presented and illustrated in this chapter refer mainly to diffusion in zeolites as the most important example of microporous materials. In most cases, however, these concepts can easily be transferred to less ordered or totally amorphous microporous materials as well (3,4).

We hope that this chapter provides a launching point for scientists new to the field of diffusion in zeolites. Toward that end, two excellent monographs (5,6), one collection (7), and several penetrating reviews have been written that address both the experimental (8,9) and theoretical (10–14) issues that arise when studying diffusion in zeolites. To distinguish this

chapter from others on the subject, we critically review the most basic ideas in the field and explore their most recent applications. For example, we present a critical (and hopefully balanced) comparison between the Fickian and Maxwell-Stefan formulations of diffusion. The particular subjects we have chosen to discuss in this chapter necessarily reflect our own interests and experiences in the field; we regret that no review can be complete.

The remainder of this chapter is organized as follows: in Sec. II we discuss the macroscopic phenomenologies used to describe diffusion in zeolites, and in Sec. III we review the microscopic dynamics that underlie these phenomenologies. In Sec. IV we describe the development and application of various experimental methods for probing diffusion in zeolites, and in Sec. V we outline recent efforts to model the dynamics of molecules sorbed in zeolites. Finally, in Sec. VI we summarize the basic insights gained so far and give concluding remarks about important areas of future research.

II. MACROSCOPIC PHENOMENOLOGY OF DIFFUSION IN ZEOLITES

A. Basics of Mass Transfer in Applications of Zeolites

Diffusion is a mass transfer process in multicomponent systems that can be understood from both microscopic and macroscopic viewpoints. From the microscopic view, diffusion results from random thermal motion of molecules, which is also known as Brownian motion or stochastic motion. We treat this microscopic approach in much more detail later in the chapter; we now focus on the macroscopic phenomenology of diffusion. From the macroscopic view, diffusion arises from the tendency for each component in a multicomponent system to disperse homogeneously in space—a direct result of the second law of thermodynamics (15–17). Diffusion is typically monitored by measuring material flux densities (hereafter denoted fluxes), defined as the number of molecules passing through a given surface area per unit time. The fact that such fluxes typically vanish in the absence of concentration gradients motivates Fick's first law, which postulates that material fluxes are proportional to concentration gradients when such gradients are relatively small (17). Below, we elaborate on this and other macroscopic formulations of diffusion; before doing so, we comment on the multicomponent nature of diffusion.

Diffusion is inherently a multicomponent phenomenon (18). To see why, we imagine an extreme case of equilibration of a macroscopic concentration gradient in a single-component system, namely, the expansion of gas into vacuum. At a microscopic level, the particles composing the expanding gas do not move stochastically; rather, they move ballistically, i.e., in straight-line trajectories, until collisions with container walls ensue. At a macroscopic level, expansion into vacuum would better be modeled as flow via the Navier-Stokes equation (18). The presence of other components in a homogeneous system, or an adsorbent in a heterogeneous system, gives rise to collisions that randomize velocities, thus producing stochastic rather than ballistic motion. Even self-diffusion (*vide infra*) in a single-component system is best conceptualized macroscopically as the equimolar mixing of tagged and untagged components, hence a multicomponent system.

Zeolite–guest systems are by construction multicomponent. In most practical applications of zeolite-guest systems, the zeolite crystallites are bound to a fixed macroporous support (19), usually silica or alumina, thus rendering the zeolite as a nondiffusing component. As such, it becomes meaningful to consider single-component diffusion in zeolites when we keep in mind that we are really talking about a multicomponent diffusion system with one fixed component (zeolite) and another diffusing component (guest). Of course, practical applications of zeolites involve multicomponent sorbed guest phases, as arise in both separations (components to be separated, e.g., N_2 and O_2) and reactions (reactants and products, e.g., xylene isomers).

The fact that applications of zeolites do not typically involve large zeolite single crystals, but rather employ supported zeolite crystallites, means that transport through beds of such supported zeolite particles involves many distinct types of diffusion, including diffusion on support surfaces and in support macropores, as well as diffusion on zeolite crystallite surfaces and in zeolite nanopores (see Fig. 1 in Chapter 23 of this volume). When using zeolites for separations and catalysis, one hopes for both high selectivity for and high flux of the most valuable product(s). Unfortunately, high selectivity is usually obtained at the expense of high flux, and vice versa. Because disposal and/or recycle of unwanted byproducts can be rather costly, one often settles for relatively low fluxes if selectivities can be made high enough. Because selectivities are usually conferred by processes taking place in the intracrystalline spaces of zeolites, one expects that the (sometimes relatively low) molecular fluxes emanating from zeolite membranes or beds are also controlled by intracrystalline transport processes. For this reason, we focus in the present chapter on intracrystalline diffusion of neutral molecules in dry zeolites. (In Chapter 21, Sherry discusses diffusion of ions in zeolites as it pertains to ion-exchange applications in hydrated zeolites. And in Chapter 23, Krishna discusses "external" transport resistances that generally arise in applications of zeolites.)

The phenomenon of stochastic molecular motion is not limited to nonequilibrium systems. However, under typical equilibrium conditions, such stochastic motion does not lead to macroscopically observable fluxes. Therefore, diffusion phenomena under equilibrium conditions only become visible if particles of the same type can be distinguished from each other. Conventionally, such experiments are carried out with isotopically labeled particles (15,20,21). As such, this type of particle movement is generally referred to as tracer diffusion or self-diffusion. In the next section, we explore the basic phenomenologies of these diffusion processes in zeolites.

B. Transport and Self-Diffusion via Fick's Laws

As discussed above, Fick's first law postulates that material fluxes are proportional to concentration gradients when such gradients are small, in the spirit of linear response theory (22,23). Such an *ansatz* can be pursued for single-component as well as multicomponent diffusion in zeolites. For the latter case, Fick's first law is given by:

$$\vec{J}_i = -\sum_{j=1}^{N_c} D_{ij} \vec{\nabla} c_j \tag{1}$$

where N_c is the number of components, $\{D_{ij}\}$ are the generalized Fickian diffusion coefficients, and $\vec{J}_i$ and $\vec{\nabla} c_i$ are the flux and local concentration gradient, respectively, of component i perpendicular to a given surface. Implicit in Eq. (1) is the assumption that the microporous host–guest system is quasi-homogeneous because the diffusivities are only labeled by components, and not by particular directions. As a consequence, the volume and plane elements used for the calculations of c_i and $\vec{J}_i$, respectively, must be large in comparison with the pore separation and small in comparison with the zeolite crystallite size. In addition to the linear response *ansatz*, Eq. (1) indicates that the flux of component i is influenced by *all* the concentration gradients in the system, not just by the concentration gradient of component i. Despite the plausibility of Eq. (1), Krishna has argued persuasively that the diffusion coefficients $\{D_{ij}\}$ are not physically illustrative transport coefficients, i.e., that D_{ij} does not represent any particular interaction between particles of components i and j (24). Indeed, we exploit Eq. (1) below only for the purpose of elucidating single-component self- and transport diffusion in zeolites. Diffusion of a multicomponent mixture of guests in zeolites is better characterized by the chemical potential–based approaches discussed in Sec. II.D.

Depending on the experimental situation, the diffusivities in Eq. (1) are given various names. In the simplest case of only one component, Eq. (1) becomes:

$$\vec{J}_1 = -D_{11}\vec{\nabla}c_1 \tag{2}$$

Being associated with matter transport, the coefficient D_{11} is generally referred to as the transport diffusivity. In this chapter, we adopt the notation $D_T \equiv D_{11}$, yielding:

$$\vec{J} = -D_T\vec{\nabla}c \tag{3}$$

which is the more usual expression of Fick's first law. As discussed above in Sec. IIA, the concept of single-component diffusion should be considered with great care. Indeed, if the system were composed of only a single component under the influence of a macroscopic concentration gradient, then there would also exist an overall pressure gradient as well. Mass transport in this situation would be characterized better by the macroscopic phenomenology of flow than it would by diffusion (18). As such, implicit in the single-component expression of Fick's first law is the presence of another, nondiffusing component such as a zeolite or some other heterogeneous material. On the other hand, the Maxwell-Stefan formulation of diffusion in zeolites, which is discussed in Sec. II.D, explicitly includes the zeolite in its expressions.

In practice, extracting transport diffusivities from flux measurements through zeolite membranes is complicated by the fact that experimentalists usually do not measure concentrations gradients, but rather observe macroscopic reservoir properties such as partial pressures. As a result, experimentalists often report zeolite membrane permeances, P, or permeability coefficients, $\mathscr{P}$, given respectively by:

$$\vec{J} = -P\Delta p\hat{z} \tag{4}$$

$$= -\mathscr{P}\frac{\Delta p}{L}\hat{z} \tag{5}$$

where $\hat{z}$ is the transmembrane direction, Δp is the pressure drop across the membrane, and L is the measured membrane thickness. The permeance is useful when absolute fluxes are required for a given membrane and pressure drop, while the permeability coefficient is preferred when comparing properties of different membranes, especially those with different thicknesses. However, the permeability coefficient is useful in this regard only when fluxes scale as L^{-1}, which as we see below in Secs. II. C, III. B, and V.B.2, is by no means guaranteed.

With two components involved, the diffusivities may pertain to rather different physical phenomena depending on the particular experimental setup. For example, in the typical tracer (or self-) diffusion experiment, the properties of components 1 and 2 are essentially identical* (25), with the total concentration $c_1 + c_2$ kept uniform throughout the system. As a result, $\vec{\nabla}(c_1 + c_2) = 0$ and hence $\vec{\nabla}c_1 = -\vec{\nabla}c_2$, yielding:

$$\vec{J}_1 = -D_{11}\vec{\nabla}c_1 - D_{12}\vec{\nabla}c_2$$

$$= -(D_{11} - D_{12})\vec{\nabla}c_1 \equiv D_S\vec{\nabla}c_1 \tag{6}$$

where $D_S = D_{11} - D_{12}$ is defined as the tracer or self-diffusion coefficient. Both the transport and self-diffusion coefficients are functions of temperature and concentration, which in the case of self diffusion is the total concentration of both components.

* Because the mass changes accompanying isotopic substitution change the statistical mechanics of molecular translation and rotation, such labelling does introduce very slight chemical potential gradients. These effects are expected to be rather small and therefore are ignored by most researchers.

The relationship between transport and self-diffusion can be clarified further using Fick's first law by analyzing the diffusion modes for a two-component system of identical but labeled particles (25). In this case, the diffusion matrix ($\{D_{ij}\}_{i,j\,=\,1,2}$) is asymmetrical, and has two eigenvectors that correspond to the two eigenmodes of diffusion for differently labeled, identical particles. The first diffusion eigenmode involves components 1 and 2 diffusing together, with driving forces proportional to their occupancies, so that the labeling of particles does not affect their transport. This is the so-called codiffusion eigenmode and corresponds precisely to transport diffusion. The second eigenmode corresponds to equimolar counterdiffusion, where $\vec{J}_1$ is equal and opposite to $\vec{J}_2$ at constant total loading. The resulting diffusivity for the counterdiffusion eigenmode is exactly the self-diffusion coefficient. As such, the transport and self-diffusion coefficients arise simply from Fick's first law, as two eigenvalues of the diffusion matrix for a two-component system of differently labeled, identical particles.

By combining Eqs. (3) and (6) with the law of matter conservation given by:

$$\frac{dc}{dt} = -\vec{\nabla} \cdot \vec{J} \tag{7}$$

the time dependencies of the intracrystalline concentrations due to transport and self diffusion are given by:

$$\frac{dc}{dt} = \vec{\nabla} \cdot \left(D_{\mathrm{T}} \vec{\nabla} c \right) \tag{8}$$

and

$$\frac{dc^*}{dt} = D_{\mathrm{S}} \nabla^2 c^* \tag{9}$$

respectively, where c^* indicates the concentration of labeled molecules. The general form of Eqs. (8) and (9) is referred to as the diffusion equation, and also as Fick's second law. (In Sec. IV.A.1, we discuss the interpretation of experimental reaction–diffusion data by augmenting the diffusion equation with terms that model reactivity.) The slightly more complex structure of Eq. (8) in comparison with Eq. (9) is caused by the fact that transport diffusion experiments are carried out under nonuniform concentration conditions, so that D_{T}—being generally a function of concentration—must remain within the parentheses in Eq. (8). By contrast, in self-diffusion experiments the total concentration remains constant. Since it is this total concentration (and not the concentration c^* of only the labeled molecules) on which the self diffusivity depends, D_{S} in Eq. (9) may be placed in front of the differential operator $\vec{\nabla}$.

An important example where Eq. (8) reduces to the form of Eq. (9) involves diffusion in Langmuirian host–guest systems. Such systems involve regular lattices of identical sorption sites where particle–particle interactions are ignored, except for exclusion of multiple site occupancy. These model systems exhibit Langmuir adsorption isotherms and give single-component transport diffusivities that are independent of loading (26). As a result, the Langmuirian transport diffusivity can be pulled to the left of the differential operator in Eq. (8), hence reducing to the form of Eq. (9).

Solving Eq. (9) gives the time dependence of the concentration of labeled molecules; the initial condition is dictated either by convenience or by experimental circumstances. Solving for $c^*(\vec{r}, t)$ with the initial condition $c^*(\vec{r}, t = 0) = \delta[\vec{r} - \vec{r}(0)]$ gives a quantity that is proportional to the probability density of the displacements of labeled molecules, i.e., to the conditional probability that a molecule is at $\vec{r}$ at time t given that it was at $\vec{r}(0)$ at time zero. This probability density is given by:

$$P(\vec{r}, t) = \frac{1}{(4\pi D_{\mathrm{S}} t)^{3/2}} e^{-|\vec{r} - \vec{r}(0)|^2 / 4 D_{\mathrm{S}} t} \tag{10}$$

Armed with this probability distribution, also known as the propagator (5), the mean square displacement after time t becomes:

$$\left\langle |\vec{r}(t) - \vec{r}(0)|^2 \right\rangle = 6D_S t \tag{11}$$

Equation (11) is known as the Einstein equation; as with Eq. (9), the Einstein equation can be considered as the defining equation of the self-diffusion coefficient. As with Eq. (1), the Einstein equation above assumes a quasi-homogenous host–guest system. Because many zeolites involve spatially inhomogeneous frameworks, e.g., MFI-type zeolites, it is often more illustrative to resolve displacements along x, y, and z directions according to:

$$\left\langle | r_\alpha(t) - r_\alpha(0) |^2 \right\rangle = 2D_S^\alpha t \tag{12}$$

where $\alpha = x$, y, or z, and $D_S = (D_S{}^x + D_S{}^y + D_S{}^z)/3$. The self-diffusion coefficient for homogeneous systems satisfies $D_S = D_S{}^x = D_S{}^y = D_S{}^z$. It remains interesting to explore the extent to which different zeolite–guest systems produce self-diffusion coefficients that deviate from homogeneity.

Below in Secs. IV and V we describe various experimental and theoretical methods for studying the time dependencies of local concentrations and mean square displacements of molecules in zeolites, for the purpose of describing intracrystalline diffusion coefficients. Despite this focus on diffusion coefficients, application-oriented zeolite scientists are generally more interested in quantifying material fluxes through zeolite beds or membranes. While such fluxes can be influenced by intracrystalline diffusion coefficients, other factors may also play important roles. In particular, when zeolite particles are relatively small, and when zeolite membranes are relatively thin, fluxes can be controlled by rates of desorption from zeolites. In the next section, we analyze the limiting cases of diffusion-limited and desorption-limited transport to reveal which fundamental processes ultimately control permeation through zeolites.

C. Desorption-Limited vs. Diffusion-Limited Fluxes

For the following analysis we assume the simplest possible model (27), namely, a Langmurian host–guest system, which involves a regular lattice of identical sorption sites where particle–particle interactions are ignored, except for exclusion of multiple site occupancy. Although corrections to this model change the precise magnitudes of fluxes, the qualitative conclusions we draw remain unchanged (28). In order to explore how desorption rates influence permeation fluxes, we consider transport through a perfect zeolite membrane that has a thickness of $L + 1$ sites from the top edge to the bottom edge. The model membrane is shown in Fig. 1a–c. Adsorption sites are represented by squares in Fig. 1a–c, while particles are shown as circles. For this diffusion system, it is more convenient to quantify concentrations using the concept of fractional occupancy (also known as loading), defined by $\theta \equiv N/N_{sites} \leq 1$, where N is the number of sorbed molecules and N_{sites} is the total number of sorption sites. A Langmuirian host–guest system at equilibrium with external fluid reservoirs will have an equilibrium sorption isotherm of the form:

$$\theta_{eq} = \frac{1}{1 + k_d/v} \tag{13}$$

where the equilibrium fractional occupancy, θ_{eq}, is uniform throughout the membrane. k_d is the rate coefficient for desorption, via thermally activated hops of a molecule located in an edge site to the fluid phase; v is the rate of insertion attempts of molecules from the fluid phase into each exposed sorption site at the edges of the zeolite; and k_{hop} is the rate coefficient for site-to-site jumps within the membrane. The fundamental diffusion coefficient for this problem (*vide infra*) is given by $D_0 = k_{hop}a^2$, where a is the site-to-site jump distance. D_0 is the single-component

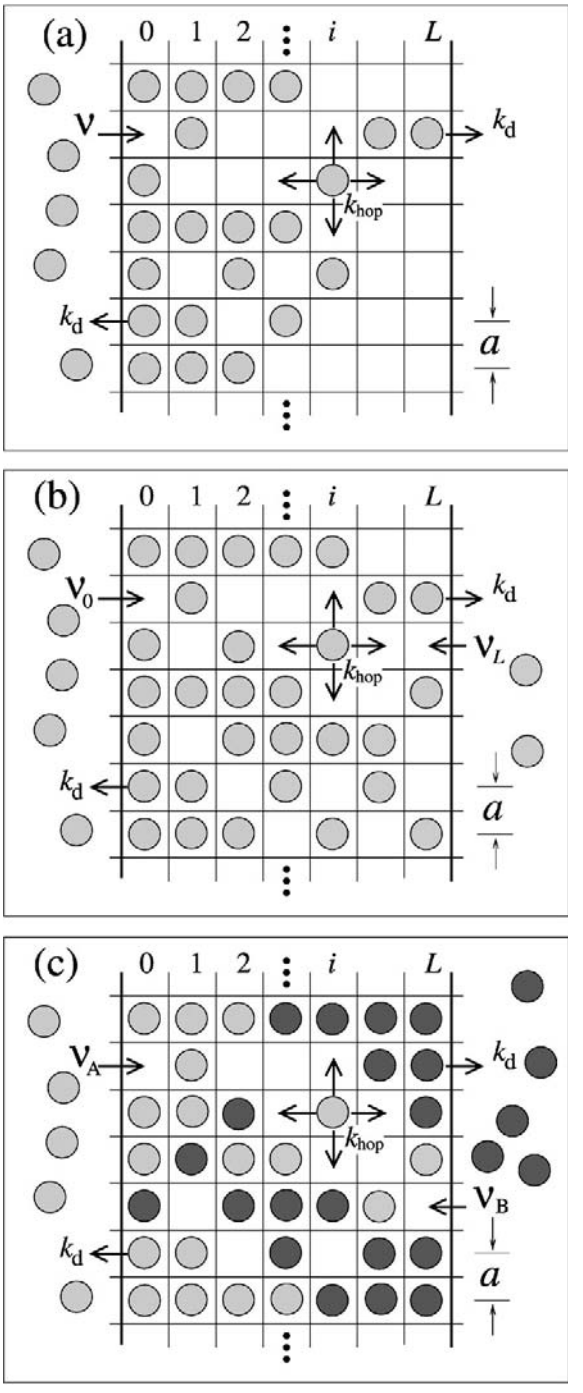

Fig. 1 Two-dimensional Langmuirian zeolite membranes with various boundary conditions: (a) single-component permeation into vacuum, (b) single-component permeation from high to low (but nonzero) pressure, and (c) tracer counterpermeation.

transport diffusivity, as well as the low-loading limit of the self-diffusivity. In what follows we set $a \equiv 1$, which is tantamount to giving membrane thicknesses in units of a.

Case 1. Below we consider three different situations, each depicted in Fig. 1a–c. The first and simplest case, shown in Fig. 1a, involves transport diffusion through the membrane into vacuum, i.e., the rate of insertion attempts on the vacuum side vanishes. Our goal is to determine a formula for the steady-state flux as a function of k_d, ν, D_0, and L. For the following discussion, we express flux as number of particles passing per time per edge site. To obtain this flux, we write down formulas for the fluxes at the high pressure side, J_0, in the interior of the membrane, J_i, and at the low-pressure side, J_L, all as functions of (k_d, ν, D_0, L) as well as the average edge concentrations (θ_0, θ_L). By applying the steady-state constraints, $J_0 = J_i$ and $J_i = J_L$, we solve the resulting 2×2 linear system for (θ_0, θ_L) to cast the steady-state flux in terms of the desired quantities.

Figure 1a suggests that J_0, J_i, and J_L satisfy:

$$\begin{aligned} J_0 &= \nu(1-\theta_0) - k_d\theta_0 \\ J_i &= -D_0\left(\frac{\theta_L - \theta_0}{L}\right) \\ J_L &= k_d\theta_L \end{aligned} \tag{14}$$

Equating the fluxes in Eq. (14) gives the following steady-state flux:

$$J = \frac{\nu k_d D_0}{k_d L(\nu + k_d) + D_0(\nu + 2k_d)} = \frac{k_d\theta_{eq} D_0}{k_d L + D_0(2-\theta_{eq})} \tag{15}$$

where the second equality comes from substituting $\theta_{eq} = \nu/(\nu + k_d)$, which is the loading of the corresponding equilibrium system with both reservoirs presenting insertion attempt frequencies of ν.

We consider the different limiting forms of Eq. (15) by first noting that, because $2 - \theta_{eq}$ is always of order unity, the denominator is controlled by the relative magnitudes of $k_d L$ and D_0. In the limit where $k_d L \gg D_0$, Eq. (15) reduces to:

$$J = \frac{D_0\theta_{eq}}{L} = -D_0\left(\frac{\bar{\theta}_L - \bar{\theta}_0}{L}\right) \tag{16}$$

where $\bar{\theta}_0$ and $\bar{\theta}_L$ are the edge concentrations assuming local thermodynamic equilibrium. In the present case, $\bar{\theta}_0 = \theta_{eq}$ and $\bar{\theta}_L = 0$. In this limit, diffusion through the membrane is much slower than desorption from the edges, so that transport through the membrane is diffusion limited. Since the flux scales with L^{-1}, the permeability coefficient $\mathscr{P}$ in this limit is independent of membrane thickness, as is desired. We also note that in diffusion-limited transport, the flux is directly proportional to the intracrystalline diffusion coefficient, justifying the intense effort to quantify this property.

Inherent in this analysis is the assumption of a fixed, finite jump length between adjacent sites. In the limit where this jump length vanishes while the membrane thickness remains constant, we have that $L \to \infty$ and hence $k_d L \gg D_0$, which again produces the diffusion-limited case (29). This situation is best described by the (differential) diffusion equation, Eq. (8).

In the opposite limit, where $k_d L \ll D_0$, Eq. (15) now reduces to:

$$J = k_d\left(\frac{\theta_{eq}}{2-\theta_{eq}}\right) \tag{17}$$

which is the desorption-limited extreme because the flux is proportional to the desorption rate, k_d, and is totally independent of the intracrystalline diffusion coefficient. Equation (17) reduces simply to k_d when $\theta_{eq} = 1$. In desorption-limited transport, which applies to thin membranes

(and by extension to small zeolite particles as well), the concentration is essentially uniform throughout the membrane, and the flux is independent of membrane thickness. As such, the desorption-limited permeability coefficient is proportional to the membrane thickness, L, rather than being independent of L.

The most important message from this analysis is that zeolite scientists should endeavor to determine whether their systems fall into the diffusion-limited or desorption-limited regime to ensure that the more important property is being studied (i.e. D_0 vs. k_d), and that proper comparisons are being made (i.e., L dependence of $\mathscr{P}$). In practice, real systems often fall between these two extremes, giving transport that depends on both diffusion and desorption.

Case 2. In the second case, depicted in Fig. 1b, we consider transport diffusion from high pressure to low (but nonvanishing) pressure. This problem is very similar to that in Case 1 except that in Case 2 the two reservoirs in contact with the membrane present different insertion attempt frequencies, namely ν_0 and ν_L, with $\nu_0 > \nu_L$. The flux expressions for J_0 and J_i are unchanged except that for J_0, ν is replaced by ν_0. The flux J_L now becomes $k_d\theta_L - \nu_L(1 - \theta_L)$. The resulting steady-state flux, expressed in terms of local thermodynamic equilibrium concentrations $\bar{\theta}_0$ and $\bar{\theta}_L$, is given by:

$$J = \frac{k_d D_0(\bar{\theta}_0 - \bar{\theta}_L)}{k_d L + D_0(2 - \bar{\theta}_0 - \bar{\theta}_L)} \tag{18}$$

This expression reduces to that found in Case 1 by setting $\bar{\theta}_L$ to zero. Although we argued in Case 1 that $(2 - \bar{\theta}_0)$ is always of order unity, and hence need not be considered in comparing $k_d L$ with D_0, now in Case 2 we find that $(2 - \bar{\theta}_0 - \bar{\theta}_L)$ is *not* always of order unity, especially when both insertion attempt frequencies are relatively high. As a result, this concentration-dependent factor must be included when discriminating between different limits.

The diffusion-limited form of Eq. (18), which arises when $k_d L \gg D_0(2 - \bar{\theta}_0 - \bar{\theta}_L)$, is given by:

$$J = -D_0\left(\frac{\bar{\theta}_L - \bar{\theta}_0}{L}\right) \tag{19}$$

which again is Fick's first law under conditions of local thermodynamic equilibrium of the edge concentrations. In the opposite limit of desorption-limited transport, Eq. (18) reduces to:

$$J = k_d\left(\frac{\bar{\theta}_0 - \bar{\theta}_L}{2 - \bar{\theta}_0 - \bar{\theta}_L}\right) \tag{20}$$

Again, the desorption-limited flux scales with k_d, and is independent of D_0 and L. As with Case 1, Eq. (20) reduces to k_d when $\bar{\theta}_0 = 1$. Equation (20) appears to have a pathological limit, however, when both $\bar{\theta}_0$ and $\bar{\theta}_L \to 1$. In this case the driving force for diffusion vanishes; as a result so should the flux. Indeed, Eq. (20) vanishes when $\bar{\theta}_0 = \bar{\theta}_L \to 1$, but that is not the only way to evaluate the limit. Alternatively, we might consider the case where $\bar{\theta}_0 = 1$ while $\bar{\theta}_L \to 1$. In this case the flux does not vanish but instead becomes k_d, a seemingly incongruous result. The conundrum is solved when we recall that in this limit, the system again becomes diffusion limited because $k_d L \gg D_0(2 - \bar{\theta}_0 - \bar{\theta}_L)$, even if the membrane is very thin.

We summarize the main conclusions regarding diffusion vs. desorption control of transport diffusion. Membrane transport is diffusion limited when $k_d L \gg D_0(2 - \bar{\theta}_0 - \bar{\theta}_L)$, which reduces to $k_d L \gg D_0$ under typical circumstances when driving forces are high. Membrane transport becomes desorption limited when $k_d L \ll D_0(2 - \bar{\theta}_0 - \bar{\theta}_L)$, which is especially important for thin membranes and for small zeolite particles. In this case permeability coefficients from membranes with different thicknesses are no longer comparable.

Case 3. In the third case, depicted in Fig. 1c, we consider equimolar counterdiffusion of identical but labeled particles, i.e., tracer counterpermeation (TCP). As discussed above, such counterdiffusion of tagged particles (A particles) and untagged particles (B particles) is isomorphic to self diffusion. Here we derive the steady-state counterflux of one of the two components; the other component produces equal and opposite flux. The fundamental flux expressions for J_0, J_i, and J_L are essentially identical to those in Case 2, except that insertion rates are sensitive to the presence of both components at the edges. As such, $v_0(1 - \theta_0) \rightarrow v_0(1 - \theta_T)$ and $v_L(1 - \theta_L) \rightarrow v_L(1 - \theta_T)$, where θ_T is the total concentration of both components, which is uniform throughout the membrane. By the symmetry of TCP, $\theta_T \equiv \theta_A(z) + \theta_B(z) = \theta_A(z) + \theta_A(L - z) = [1 + k_d/(v_0 + v_L)]^{-1}$, where z labels the location along the transmembrane direction.

The only other change from Case 2 to the present one is that D_0 is replaced by the self-diffusion coefficient, D_s, which depends upon θ_T in a nontrivial way. For the present Langmuirian system, D_s generally decreases with θ_T because blocking sites decreases the likelihood of counterdiffusion. Many other dependencies can arise for more complicated systems. Kärger and Pfeifer have reported the five most common ways that D_s is found experimentally to depend on θ_T for diffusion in zeolites (31), which have also been seen in simulations (*vide infra*) (31,32).

The steady-state TCP flux of labeled particles is given by:

$$J = \frac{D_s(1 - \theta_T)(v_0 - v_L)}{k_d L + 2D_S} \tag{21}$$

In diffusion-limited TCP, where $k_d L \gg D_S$, Eq. (21) reduces to:

$$J = \frac{D_s(1 - \theta_T)(v_0 - v_L)}{k_d L} = -D_S\left(\frac{\bar{\theta}_L - \bar{\theta}_0}{L}\right) \tag{22}$$

where once again $\bar{\theta}_0$ and $\bar{\theta}_L$ are the edge concentrations consistent with local thermodynamic equilibrium. Desorption-limited TCP arises when $k_d L \ll D_S$; in this case Eq. (21) reduces to:

$$J = (1 - \theta_T)(v_0 - v_L)/2 = k_d(\bar{\theta}_0 - \bar{\theta}_L)/2 \tag{23}$$

As in both previous desorption-limited cases, the desorption-limited TCP flux is proportional to k_d, and is independent of both the membrane thickness and the relevant diffusion coefficient (in this case D_S).

The results in this section have been obtained with very few assumptions, most notably Fick's first law, which provides a useful approach for studying single-component transport through Langmuirian adsorbents. Despite the obvious power of Fick's formulation, it can also break down in surprisingly simple circumstances, such as a closed system consisting of a liquid in contact with its equilibrium vapor. In this case, Fick's law predicts a nonzero macroscopic flux because of the concentration gradient at the vapor–liquid interface. The fact that no macroscopic flux is observed suggests that the real driving force for diffusion is not the concentration gradient but rather the chemical potential gradient, which vanishes for this equilibrium two-phase system. Other curiosities can result from the Fickian treatment of multicomponent systems, such as negative Fickian diffusivities (24). Various transport phenomenologies have been developed based on chemical potential gradients; below we review the theories of Maxwell, Stefan, and Onsager.

D. Phenomenologies Based on Chemical Potential Gradients

1. Maxwell-Stefan Formulation

What we presently call the Maxwell-Stefan formulation of diffusion was developed independently by Maxwell in 1866 and by Stefan in 1871 (24,33,34). In Chapter 23, Krishna discusses this phenomenology and its application to diffusion in zeolites. Because understanding this formulation is important for many of the ideas below, we briefly review the Maxwell-Stefan picture of diffusion (see also Ref. 24 for the complete story). For pedagogical reasons, we first develop the Maxwell-Stefan formulation for bulk systems; then we consider its application for surface diffusion as occurs in zeolites. Because the Fickian formulation discussed above in Secs. II.B and II.C tacitly assumes the presence of the zeolite, we compare below Fickian diffusivities with Maxwell-Stefan surface diffusivities.

The Maxwell-Stefan formulation is especially useful when considering transport in multicomponent, multiphase systems, which is to say most industrially important circumstances. Indeed, the simplest system amenable to the Maxwell-Stefan formulation is a two-component bulk fluid, which again points to the fundamentally multicomponent nature of diffusion. In the standard Maxwell-Stefan picture, it is assumed that the n-component fluid under study has no net gradient in the total concentration. The presence of a net macroscopic (molar averaged) velocity is not ruled out; diffusive fluxes are defined relative to this net velocity so that the *total diffusive flux vanishes*. Clearly the Fickian *ansatz* lacks this constraint, which makes the Fickian approach appear to be the more natural treatment of zeolite membrane permeation. In these experiments, the observables of interest are the permselectivities and the (hopefully nonvanishing) total diffusive flux, all measured relative to the zeolite bed or membrane. However, we show below the ingenious way that the Maxwell-Stefan approach manages to treat single-component diffusion in zeolites while still providing the definitive treatment of multicomponent diffusion in zeolites.

We begin by writing down the Maxwell-Stefan *ansatz* for a two-component bulk fluid with a vanishing total diffusive flux. By equating the driving force for diffusion of component 1 (i.e., $-\vec{\nabla}\mu_1$) with the frictional drag exerted by component 2, the macroscopic velocity of component 1 relative to that for component 2 satisfies (24):

$$-\vec{\nabla}\mu_1 = RTx_2\left(\frac{\vec{v}_1 - \vec{v}_2}{D_{12}^{\mathrm{MS}}}\right) \tag{24}$$

where R is the gas constant, T the temperature, x_2 the mole fraction of component 2, $\vec{v}_1$ the macroscropic velocity of component i, and D_{12}^{MS} is defined as the Maxwell-Stefan diffusion coefficient. Equation (24) suggests that the relative velocity of a particular component is linearly proportional to its chemical potential gradient; as such the Maxwell-Stefan *ansatz* involves linear response theory in much the same way as the Fick *ansatz* in Eq. (1). However, whereas the Fick formulation focuses on calculating fluxes, the Maxwell-Stefan picture focuses on balancing forces. In the Maxwell-Stefan approach, the frictional drag exerted by component 2 is assumed to be proportional to the mole fraction of component 2, with a proportionality coefficient given by the friction coefficient RT/D_{12}^{MS}. Although the Maxwell-Stefan approach is still phenomenological, it seems to reveal the essential physics of multicomponent diffusion in ways that the Fickian approach cannot.

To treat surface diffusion, while still constraining the total diffusive flux to vanish, the Maxwell-Stefan equations are augmented by one additional component representing the adsorbent. However, since diffusive fluxes are measured relative to the adsorbent, the latter cannot contribute diffusive flux to balance the permeant fluxes. This problem is solved by

realizing that whenever a molecule jumps, a vacancy makes a counterbalancing jump. Thus, the additional component in the Maxwell-Stefan treatment of surface diffusion is vacant sorption sites. As discussed in Sec. II.C, it is more convenient in surface diffusion problems to express concentrations through fractional occupancies. In terms of these, the Maxwell-Stefan *ansatz* for a two-component sorbed phase takes the form:

$$-\vec{\nabla}\mu_1 = RT\theta_2\left(\frac{\vec{v}_1 - \vec{v}_2}{D_{12}^{\mathrm{MSs}}}\right) + RT\theta_{\mathrm{vac}}\left(\frac{\vec{v}_1 - \vec{v}_{\mathrm{vac}}}{D_{1,\mathrm{vac}}^{\mathrm{MSs}}}\right) \tag{25}$$

where $\theta_{\mathrm{vac}} = 1 - \theta_1 - \theta_2$ is the vacancy loading, and $\vec{v}_{\mathrm{vac}}$ is the macroscopic vacancy velocity. In Eq. (25), D_{12}^{MSs} is the Maxwell-Stefan surface counterdiffusivity (note the augmented superscript) and $D_{1,\mathrm{vac}}^{\mathrm{MSs}}$ is the single-component Maxwell-Stefan surface diffusivity for component 1. This picture is attractive in its ability to disentangle the zeolite–guest$_1$ and guest$_1$–guest$_1$ interactions that determine $D_{1,\mathrm{vac}}^{\mathrm{MSs}}$ from the cross-component, guest$_1$–guest$_2$ forces that determine D_{12}^{MSs}. In the simple case of single-component diffusion in zeolites, Eq. (25) reduces to:

$$-\vec{\nabla}\mu_1 = RT\theta_{\mathrm{vac}}\left(\frac{\vec{v}_1 - \vec{v}_{\mathrm{vac}}}{D_{1,\mathrm{vac}}^{\mathrm{MSs}}}\right) \tag{26}$$

Despite the beauty of the vacancy-based Maxwell-Stefan picture of surface diffusion, zeolite scientists need a formulation that allows the calculation of nonvanishing total diffusive fluxes for comparison with permeation measurements. To arrive at such a Maxwell-Stefan picture, the additional component must be the zeolite itself, whose macroscopic velocity $\vec{v}_{\mathrm{zeo}}$ is taken to be zero. While this seems to make good conceptual sense, it also implies that θ_{vac} in Eqs. (25) and (26) should be replaced by θ_{zeo}, which itself does not make much physical sense. This issue is swept under the rug by defining a new single-component Maxwell-Stefan surface diffusivity according to:

$$D_{1,\mathrm{vac}}^{\mathrm{MSs}} \equiv \frac{D_{1,\mathrm{zeo}}^{\mathrm{MSs}}}{\theta_{\mathrm{zeo}}} \tag{27}$$

Considering that the fractional occupancies $\{\theta_i\}$ were originally derived from mole fractions $\{x_i\}$ in the Maxwell-Stefan formulation for bulk fluids, and that the mole fraction of zeolite is likely to be nearly constant and relatively close to unity, the arbitrariness of the definition in Eq. (27) is not too disturbing.

Now we compare the single-component Fickian transport diffusivity defined in Eq. (3) with the single-component Maxwell-Stefan surface diffusivity defined in Eq. (27). We begin by expressing the chemical potential gradient of component 1 in terms of its loading gradient and fugacity on the left-hand side of Eq. (26). Furthermore, we multiply both sides by θ_1/RT, and after simple algebra we identify the right-hand side as $\vec{J}_1/c_{\mathrm{s}}D_{1,\mathrm{vac}}^{\mathrm{MSs}}$, where $\vec{J}_1$ is the diffusive flux of component 1 and c_{s} is the number of moles of sorption sites per unit volume. Putting these results together yields:

$$\vec{J}_1 = -c_{\mathrm{s}}D_{1,\mathrm{vac}}^{\mathrm{MSs}}\Gamma\vec{\nabla}\theta_1 = -D_{1,\mathrm{vac}}^{\mathrm{MSs}}\Gamma\vec{\nabla}c_1 \tag{28}$$

where $c_1 = c_{\mathrm{s}}\theta_1$ is the local concentration of component 1. In Eq. (28), Γ is a "thermodynamic correction factor" given by $\Gamma = (\partial \ln f_1/\partial \ln \theta_1)_T$, where f_1 is the local fugacity of component 1. Comparing Eq. (28) with Eqs. (2) and (3) shows the relation between the Fickian transport and Maxwell-Stefan surface diffusivities, namely, that:

$$D_{\mathrm{T}} = D_{1,\mathrm{vac}}^{\mathrm{MSs}}\Gamma \tag{29}$$

This result shows that the transport and Maxwell-Stefan surface diffusivities agree for thermodynamically ideal systems, i.e., those for which $f_1 \propto \theta_1$ and hence $\Gamma = 1$.

Equation (29) has been interpreted as suggesting that the Fickian diffusivity actually represents a composite of both legitimate transport effects and thermodynamic effects. This perspective is buoyed by the diffusive properties of bulk fluids, which tend to produce Maxwell-Stefan diffusivities with extremely mild concentration dependencies (24). Because the thermodynamic correction factors can have rather strong concentration dependencies, which are conferred to the Fickian diffusivities, the Maxwell-Stefan bulk diffusivities are rightly trumpeted as the proper bulk transport coefficients because they are not corrupted by thermodynamically induced concentration dependencies. This viewpoint has even been carried over to diffusion in zeolites because for zeolite–guest systems with relatively weak confinement [e.g., methane in silicalite (35)], the single-component Maxwell-Stefan surface diffusivity can also exhibit a rather weak loading dependence. For this reason, the single-component Maxwell-Stefan surface diffusivity is often reported as the "corrected diffusivity" (5,36) because it has been corrected by removing the thermodynamic effects. In this context, Eq. (29) is sometimes called the Darken equation (5).

However, we do not need to remind the reader that most interesting applications of zeolites involve rather strong confinement, where the fundamental mechanism of transport involves infrequent jumps between well-defined sorption sites. As discussed above, the simplest model to describe such strong confinement is the Langmuirian model, for which it is the Fickian transport diffusivity that contains no loading dependence ($D_T = D_0$) (26), while Γ takes the form $1/(1 - \theta_1)$. As such, the Langmuirian Maxwell-Stefan surface diffusivity is given by $D_{1,vac}^{MSs} = D_0(1 - \theta_1)$. In this case, one might regard the Fickian diffusivity as the "corrected diffusivity" because the loading dependence of $D_{1,vac}^{MSs}$ can be removed by multiplying by Γ. Hence, the designation "corrected diffusivity" depends on the physics of the zeolite–guest system.

Below in Sec. III. A, we will argue that the $(1 - \theta_1)$ loading dependence of $D_{1,vac}^{MSs}$ is identical to the loading dependence predicted for the Langmuirian self-diffusion coefficient by mean field theory. This similarity between D_S and $D_{1,vac}^{MSs}$ has prompted some researchers to use an approximate form of the Darken equation, also called the Darken equation for maximum confusion, where the Maxwell-Stefan surface diffusivity is replaced by the self diffusivity. When applied to Langmuirian systems, this approximation actually puts in correlations (see Sec. III.B.) that do not belong. A much better context in which to apply this approximation is for weakly confined diffusion in zeolites, for which $D_{1,vac}^{MSs}$ is nearly independent of loading, so that one can replace $D_{1,vac}^{MSs}$ by the infinite-dilution limit of D_S. This perspective is supported by molecular dynamics simulations performed by Maginn *et al.* (35), and by Skoulidas and Sholl (37).

The Maxwell-Stefan diffusion equations for a general n-component sorbed phase can be recast through matrix algebra into the $(n \times n)$ Fickian form of Eq. (1). Although these manipulations do not shed much more light on the problem, they show in practice that negative Fickian diffusivities can arise from a positive-definite set of Maxwell-Stefan surface diffusivities (24), which casts doubt on the meaningfulness of the multicomponent Fickian formulation. What is perhaps more interesting is the fact that, through the Maxwell-Stefan formulation, measured multicomponent sorption kinetics have been predicted from data on single-component sorption kinetics and multicomponent sorption isotherms (24,38,39). Using this approach, one predicts that the faster diffusing component is generally slowed down to the mobility of the slower diffusing component. Measured deviations from this prediction usually indicate diffusion at grain boundaries, which facilitate unexpectedly rapid motion (40,41) (see also Chapter 17 by Nair and Tsapatsis in this volume).

These predictions of multicomponent sorption kinetics have been facilitated by Krishna's suggestion to estimate cross-component Maxwell-Stefan surface diffusivities according to the following empirical relation (42):

$$D_{ij}^{\mathrm{MSs}} \cong [D_{i,\mathrm{vac}}^{\mathrm{MSs}}(\theta_i = 0)]^{\theta_i/(\theta_i+\theta_j)} [D_{j,\mathrm{vac}}^{\mathrm{MSs}}(\theta_j = 0)]^{\theta_j/(\theta_i+\theta_j)} \tag{30}$$

Equation (30) generalizes the empirical relation, first proposed by Vignes (43) to describe multicomponent diffusion in bulk liquid mixtures, for the case of surface diffusion. Paschek and Krishna tested Eq. (30) by comparing transport coefficients obtained from kinetic Monte Carlo (see Sec. V.B.2) to those obtained from Maxwell-Stefan theory assuming Eq. (30) (44). Although excellent agreement was found, the sensitivity of this agreement to the assumed form of D_{ij}^{MSs} was not tested. As such, it remains to be seen whether this empirical formula embodies the extent to which actual cross-component interactions perturb the dynamics (e.g., barrier crossings) of multicomponent surface diffusion.

In summary, then, the analyses in Secs. II.C and II.D suggest that the Fickian formulation provides a powerful description of single-component diffusion in zeolites, especially for Langmuirian zeolite–guest systems; while the Maxwell-Stefan formulation is preferred for multicomponent diffusion in zeolites, by virtue of the empirical relation Eq. (30). Because both formulations involve linear constitutive relations between driving forces and fluxes, all this analysis begs the question of whether diffusion in zeolites proceeds outside of the linear response regime. The fact that zeolite membranes and crystallites used in experiments and applications tend to be relatively large on a molecular scale may convert relatively large pressure drops into relatively small concentration and chemical potential gradients, thus keeping diffusion in zeolites in the linear response regime. As zeolite scientists explore the use of thinner zeolite membranes and smaller zeolite crystallites for the purpose of reducing or eliminating transport bottlenecks that arise in catalytic applications (45,46), the question of whether diffusion in zeolites still proceeds in the linear response regime will have to be explored with more rigor.

2. Onsager Formulation

Yet another formulation of multicomponent surface diffusion exists, due to Onsager (47), which blends many of the virtues of the Fickian and Maxwell-Stefan approaches (5). In particular, as with the Maxwell-Stefan approach, the Onsager formulation postulates that diffusive fluxes in a multicomponent system are linearly proportional to chemical potential gradients. And, as with the Fickian approach, Onsager's picture focuses on calculating fluxes and not on balancing forces. The Onsager *ansatz* takes the form:

$$\overrightarrow{J_i} = -\sum_{j=1}^{N_c} L_{ij}^{\mathrm{s}} \overrightarrow{\nabla} \mu_j \tag{31}$$

where $\{L_{ij}^{\mathrm{s}}\}$ are the Onsager coefficients for surface diffusion, which are postulated by microscopic reversibility (48) to obey the "reciprocity relations" $L_{ij}^{\mathrm{s}} = L_{ji}^{\mathrm{s}}$. By again expressing the chemical potential gradients in terms of concentration gradients, the Onsager coefficients can be related to both Fickian and Maxwell-Stefan surface diffusivities. For the case of single-component diffusion in zeolites, one finds that $D_{\mathrm{T}} = RTL_{11}^{\mathrm{s}}\Gamma/c_1$, which implies that $D_{1,\mathrm{vac}}^{\mathrm{MSs}} = RTL_{11}^{\mathrm{s}}/c_1$. For the multicomponent case, one finds that the Onsager and Maxwell-Stefan surface diffusivities are related through a simple matrix relation (33). Through this relation one can deduce that the Maxwell-Stefan cross-component surface diffusivities, $\{D_{ij}^{\mathrm{MSs}}\}$, also obey reciprocity: $D_{ij}^{\mathrm{MSs}} = D_{ji}^{\mathrm{MSs}}$. The real virtue of the Onsager coefficients is

that they are related to microscopic dynamic quantities through Green-Kubo correlation function expressions, as discussed below in Sec. III.C.

III. MICROSCOPIC UNDERPINNINGS OF DIFFUSION IN ZEOLITES

The macroscopic treatments of diffusion discussed above serve the following purposes: (a) Given that diffusivities are provided from other sources, macroscopic diffusion theories can predict the transport properties of zeolite–guest systems; (b) given that the transport properties of a particular zeolite–guest system are known, the relevant diffusivities can be extracted by interpreting the transport behavior in light of a macroscopic diffusion theory. Such theories, however, cannot predict diffusivities *a priori*. Zeolite scientists are generally interested in predicting the temperature, loading, and composition dependencies of diffusivities, as well as their overall magnitudes, for various zeolite–guest systems. Microscopic approaches that contain information about stochastic molecular motion in zeolites are required for making such predictions. Below we review the basic microscopic underpinnings—the statistics and dynamics—that control diffusion in zeolites.

A. Stochastic Motion and Jump Diffusion

Diffusive motion in zeolites arises from collisions with the environment (zeolite and other guests) that cause the direction of motion to become randomized. Although such stochastic motion is fundamentally smooth and continuous on the relatively short time scales considered by molecular dynamics (11), on the longer time scales associated with diffusion, stochastic motion can be modeled as jumps chosen randomly in accord with prescribed probabilities. Such approaches are called jump diffusion models (10,12,14), which provide simple pictures of diffusion that turn out to be remarkably relevant to diffusion in zeolites. As will be discussed in detail in Sec. V.B.1, jump diffusion models assume that molecules spend relatively long periods of time vibrating in well-defined sorption sites (e.g., zeolite cages), with jumps between sites themselves taking negligible time. Below we explore simple jump diffusion models to reveal the basic temperature and loading dependencies expected for diffusion in zeolites.

We begin by considering the simplest class of lattices in d-dimensional space, namely, cartesian Langmuirian lattices (see also Sec. II.B), which form linear, square, or cubic sets of identical sorption sites. Such systems ignore particle–particle interactions, except for exclusion of multiple site occupancy. These lattices give Langmuir sorption isotherms and single-component transport diffusivities that are independent of loading (26). The two-dimensional case is pictured in Fig. 1a–c, each with nearest–neighbor sites separated by the length a. The probability to make a particular site-to-site jump is $1/2d$ because the coordination number for each site in d-dimensional space is $2d$, and each of the $2d$ possible jumps occurs with the same fundamental rate coefficient, k_{hop}.

As discussed above in Sec. II.B, the mean square displacement (MSD) provides a measure of the spatial extent of self diffusion as a function of time. After n jumps of a single random walker, the MSD for the d-dimensional lattice can be written as:

$$\langle R^2(n)\rangle \equiv \left\langle \left| \sum_{i=1}^{n} \vec{l}_i \right|^2 \right\rangle = \left\langle \sum_{i=1}^{n} \left| \vec{l}_i \right|^2 \right\rangle + \left\langle \sum_{i\neq j} \vec{l}_i \cdot \vec{l}_j \right\rangle = \left\langle \sum_{i=1}^{n} a^2 \right\rangle = na^2 \qquad (32)$$

Here $\vec{l}_i$ is the displacement vector for the random jump at the ith step, which is averaged in $\langle \cdots \rangle$ according to the Bernoulli distribution (16,49). In Eq. (32) we have used the fact that the term with $i \neq j$ vanishes when jumps are completely uncorrelated from one another.

The result in Eq. (32) is independent of dimensionality and, indeed, holds for any regular lattice in any dimension consisting of only one site type and one jump length scale, e.g., the tetrahedral lattice. However, when expressed as an explicit function of time, the MSD depends on dimensionality as well as lattice topology. To see why, we assume that the average jump time is τ, i.e., that $n = t/\tau$. Equation (32) then becomes $\langle R^2(t)\rangle = a^2 t/\tau$, which shows that in normal diffusion the MSD is proportional to time. This should be contrasted to ballistic motion where the MSD is proportional to t^2. The inverse of the mean site residence time, τ^{-1}, is the total rate of leaving a site, which for cartesian Langmuirian lattices is given by $2dk_{\text{hop}}$ because there are $2d$ identical ways to leave each site. Recalling the Einstein equation, which defines the self-diffusion coefficient in one and three dimensions, namely, Eqs. (11) and (12), we have that $\langle R^2(t)\rangle = 2dD_S t = 2d(k_{\text{hop}}a^2)t$, which shows that $D_S = k_{\text{hop}}a^2$ for cartesian Langmuirian lattices. This is a truly remarkable result, demonstrating how the self-diffusion coefficient can be reduced to fundamental length and time scales. We will show in Sec. III.B that when local correlations arise, the MSD retains its proportionality with time, but when global correlations become important, e.g., in single-file diffusion, the MSD becomes proportional to $t^{1/2}$ (9,50).

We will show below in Sec. III.C that the Maxwell-Stefan and self-diffusion coefficients are identical at infinite dilution for single-component diffusion on surfaces (35). We have already shown in Sec. II.D that the Maxwell-Stefan and Fickian diffusion coefficients agree at infinite dilution. As such, all three diffusion coefficients take the form $k_{\text{hop}}a^2$ at infinite dilution for cartesian Langmuirian lattices. We now explore the temperature dependence of this expression. Because the length scale a has little temperature dependence until the zeolite melts, we focus on k_{hop}. According to transition state theory (10,12,14), we have:

$$k_{\text{hop}}^{\text{TST}} = \left[\frac{\omega(T)}{2\pi}\cdot e^{\Delta S(T)/k_B}\right]\cdot e^{-\beta\Delta E(T)} \tag{33}$$

where T is temperature, k_B is Boltzmann's constant, $\beta = 1/k_B T$, $\omega(T)$ is the temperature-dependent site vibrational frequency, $\Delta S(T)$ is the temperature-dependent activation entropy, and $\Delta E(T)$ is the temperature-dependent activation energy. When considering a broad temperature range including temperatures for which $\beta\Delta E(T) \gg 1$, the Boltzmann factor in Eq. (33) dominates the temperature dependence of k_{hop}, rendering the factor in brackets an apparent pre-exponential constant usually denoted by the apparent frequency, ν. In this case, the three diffusivities exhibit an Arrhenius temperature dependence taking the form $D_0 e^{-\beta E_a}$, where $D_0 = \nu a^2$ and E_a is an apparent activation energy.

On the other hand, when $\beta\Delta E(T) \lesssim 1$, the temperature dependence of the pre-exponential factor can become important. In this case, the resulting temperature dependence of the diffusivities is not obvious and can depend strongly on the details of the zeolite–guest system. Other temperature dependencies can also arise for diffusion in zeolites when the site lattice contains different types of sites, e.g., cation sites and window sites (51). In this case the competition among different mechanisms of cage-to-cage motion can produce non-Arrhenius behavior, even when the fundamental site-to-site rate coefficients obey the Arrhenius temperature dependence (52–54).

The analysis above assumes diffusion at infinite dilution, with only a single molecule in the zeolite. In Sec. II.D, we discussed the loading dependence of the transport and Maxwell-Stefan diffusivities for Langmuirian lattices. Now we estimate the loading dependence of the self-diffusion coefficient. In general this is not easy, even for Langmuirian systems, because of correlations and their dependence on site topology. A simple esimate can be provided by mean field theory (23), which considers the average environment surrounding each random walker. Using mean field theory we obtain $D_S(\theta) \cong D_S(0)(1-\theta) = k_{\text{hop}}a^2(1-\theta)$. The factor $(1-\theta)$ is the fraction of jump attempts that are successful because they are directed to vacancies.

Although this mean field theory estimate can be semiquantitative when each site is connected to several nearest neighbors (e.g., ≥ 6) (55), it can exhibit significant error for lattices with low connectivity, e.g., those used to model diffusion in MFI-type zeolites (56).

In summary, we have used a simple lattice model to reveal the fundamental consequences of stochastic motion in an effort to explore the basic temperature and loading dependencies that can be expected for self diffusion in zeolites. These results hold for diffusion in most microporous materials, as well as diffusion on two-dimensional surfaces such as metals (57). However, the results in this section were obtained by completely ignoring the complications due to correlations. In the next section, we discuss three different kinds of correlations and their impact on diffusion in zeolites.

B. Correlations and Single-File Diffusion

1. Kinetic Correlations

Diffusion in zeolites can be influenced by correlations that arise from kinetic effects, geometrical effects, and vacancy effects (5,54). Kinetic correlations arise from the inertial tendency toward ballistic molecular motion, i.e., Newton's first law applied to zeolite science: a guest molecule moving in a zeolite will tend to move freely until it is forced to do otherwise. Including kinetic correlations generally increases the MSD; indeed, when kinetic correlations dominate motion, the MSD becomes proportional to t^2. In this situation the macroscopic phenomenology changes from diffusion to flow. When diffusion is perturbed only slightly by kinetic correlations, such effects serve to increase the diffusion coefficient. In the context of the cartesian Langmuirian models discussed above in Sec. III.A, kinetic correlations are manifested through "multisite" jumps, i.e., jumps that begin and end at sites other than nearest neighbors. One can show that the self-diffusion coefficient for a cartesian Langmuirian model with multisite jumps becomes (57):

$$D_S = \frac{a^2}{2d} \sum_{\vec{m} \neq \vec{m}_0} k_{hop}(\vec{m}_0 \rightarrow \vec{m}) \mid \vec{m} - \vec{m}_0 \mid^2 \tag{34}$$

where the sum is over all lattice sites indexed by the integers $\vec{m}$, excluding the reference site $\vec{m}_0$, and $\{k_{hop}(\vec{m}_0 \rightarrow \vec{m})\}$ are the multisite jump rate coefficients. Ignoring multisite jumps reduces Eq. (34) back to $D_S = k_{hop}a^2$, where k_{hop} is the nearest-neighbor jump rate coefficient. Including multisite jumps clearly increases the self-diffusion coefficient. The convergence properties of this sum are revealed by defining $m \equiv \mid \vec{m} - \vec{m}_0 \mid$. By the isotropy of space present in cartesian Langmuirian models, the summand in Eq. (34) depends only on m. For large m, the degeneracy in m scales with m^{d-1}, where d is the dimension of space. As such, to retain the phenomenology of diffusion, the multisite rate coefficients must decay faster than $1/m^{d+2}$. In practice, we expect multisite jumps in zeolites to gain importance at high temperatures and low loadings, where molecular energy dissipation is relatively inefficient. Moreover, multisite jumps should be more prevalent in channel-type zeolites (53,54) than in cage-type zeolites (58) because channels are more conducive to ballistic trajectories.

2. Geometrical Correlations

Kinetic and vacancy correlations can influence diffusion in zeolites, as well as diffusion in a wide variety of other homogeneous and heterogeneous systems. Geometrical correlations, on the other hand, pertain especially to zeolites as well as any other anisotropic microporous host. In the language of jump diffusion models, geometrical correlations arise when the sum of jump vectors from a given site does *not* vanish. As such, the lattices we have considered thus far in

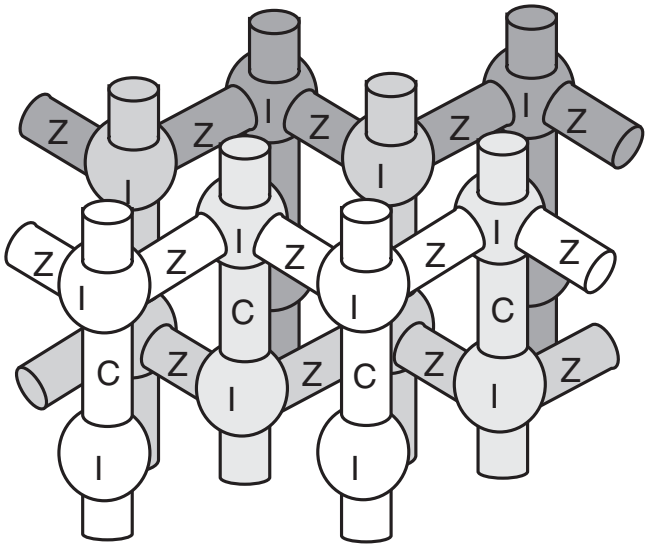

Fig. 2 Channel and site structure of silicalite-1 showing intersection sites (I), straight-channel sites (C), and zig-zag channel sites (Z).

this chapter typically do not exhibit such correlations. Chabazite provides an interesting exception to this rule; diffusion in this zeolite can exhibit geometrical correlations even when jump vectors cancel (59). Geometrical correlations can arise for other reasons as well, as diffusion in MFI-type zeolites provides the prototypical example of geometrical correlations. A schematic of the MFI framework topology is shown in Fig. 2. In this figure, we see that the jumps from each straight channel site (C) cancel, as do the jumps from each zig-zag channel site (Z); thus, these sites present no geometrical correlation. The jumps from each intersection site (I), on the other hand, do not cancel and thus do present geometrical correlations. Because of this diffusion anisotropy, Kärger has suggested the benefit of studying the individual cartesian components of the self-diffusivity—D_S^x, D_S^y, and D_S^z—whose average is the overall self-diffusion coefficient. Indeed, assuming that subsequent jumps from channel intersections are uncorrelated in time, Kärger derived the following geometrical correlation rule:

$$\frac{a^2}{D_S^x} + \frac{b^2}{D_S^y} = \frac{c^2}{D_S^z} \tag{35}$$

where a, b, and c are the lattice constants along the x, y, and z directions, respectively (60,61). While this simple correlation rule was found to be in reasonable agreement with numerous molecular dynamic simulations (62–65), from experimental studies the only conclusion that could be drawn is that the measurements are not inconsistent with the correlation rule (66,67).

Geometrical correlations can also be important for diffusion in zeolites with cubic unit cells, especially in cation-containing zeolites (54). In these cases, molecules can jump away from but not into cations, thus producing geometrical correlations. Jousse *et al.* have shown that ignoring geometrical correlations can result in overestimating self diffusivities by an order of magnitude for benzene in Na-Y and can change the qualitative loading dependence as well (54).

3. Vacancy Correlations

Vacancy correlations are analogous to kinetic correlations, but opposite in sign, since an atom in a metal has a larger probability to move backward to the site it just vacated than it does

to move onward. A completely analogous effect gains importance for diffusion in zeolites at high loadings. Figure 3 schematically depicts a site-to-site jump in a zeolite cage at high loading, which leaves behind a vacancy, i.e., produces particle–vacancy exchange. Subsequent jumps are more likely to fill this vacancy, thus producing correlations that reduce self diffusivities. Since mean field theory ignores correlations, these vacancy effects give self diffusivities lower than mean field theory estimates. The loading dependence of self diffusivities is thus written as:

$$D_S(\theta) = D_S(0)(1-\theta)f(\theta), \tag{36}$$

where $f(\theta) \leq 1$ is the so-called correlation factor. Since Bardeen and Herring's seminal work, a large body of research has been devoted to calculating correlation factors for a variety of lattice geometries using theory and Monte Carlo simulations (68). Although no generally applicable, closed-form expression exists, results have been obtained for a number of different Langmuirian lattices (69,70). Here we give the flavor of how correlation factors can be estimated.

The simplest approach for estimating correlation factors comes from the Maxwell-Stefan formulation of tracer diffusion on surfaces (24,71), involving equimolar counterdiffusion of two identical but labeled species (see also Fig. 1c for an illustration of tracer counterpermeation). The self-diffusion coefficient from the Maxwell-Stefan approach takes the form:

$$D_S(\theta) = \frac{1}{1/D_{1,\text{vac}}^{\text{MSs}} + \theta/D_{12}^{\text{MSs}}}, \tag{37}$$

where $\theta = \theta_1 + \theta_2$ is the total loading, and D_{12}^{MSs} is the Maxwell-Stefan surface diffusivity that controls the facility of exchange between labeled and unlabeled particles. Such exchange is related to vacancy correlations, as we shall illustrate by considering the Langmuirian transport model, where $D_{1,\text{vac}}^{\text{MSs}} = D_0(1-\theta)$. Multiplying the top and bottom of Eq. (37) by $D_{1,\text{vac}}^{\text{MSs}}$ shows that the Maxwell-Stefan correlation factor can be written as:

$$f(\theta) = \frac{1}{1 + (D_{1,\text{vac}}^{\text{MSs}}/D_{12}^{\text{MSs}})\theta}. \tag{38}$$

In the limit where $D_{12}^{\text{MSs}}/D_{1,\text{vac}}^{\text{MSs}} \to \infty$, the correlation factor approaches unity, indicating that facile exchange washes out vacancy correlations. Along these lines, Nelson and Auerbach have

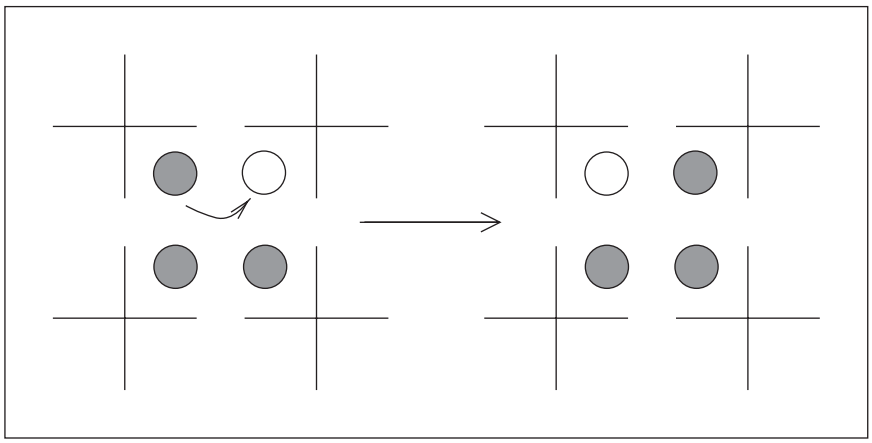

Fig. 3 Schematic depiction of a molecular site-to-site jump; subsequent jumps of molecules (dark) are likely to fill the newly formed vacancy (light).

reported simulations of tracer counterpermeation in anisotropic zeolite membranes, which show that vacancy correlations vanish when transport in the plane of the membrane is fast compared with transmembrane diffusion (27). Such in-plane transport provides a conceptual picture for the mechanism of identical particle exchange.

For finite values of D_{12}^{MSs}, the correlation factor in Eq. (38) is less than 1 as desired. Unfortunately, no theory exists for estimating the loading dependence of D_{12}^{MSs} for tracer diffusion. Indeed, application of Eq. (30) gives $D_{12}^{\mathrm{MSs}} = D_0$ which yields $f(\theta) = 1/[1 + \theta(1 - \theta)]$, predicting erroneously that vacancy correlations vanish as $\theta \to 1$. In the absence of theoretical foundation, Paschek and Krishna suggest a practical approach (71), namely, that $D_{12}^{\mathrm{MSs}} = D_{1,\mathrm{vac}}^{\mathrm{MSs}}$, which in essence equates the rate of particle–vacancy exchange with that of particle–particle exchange. Although the physical validity of this assumption is questionable, the resulting correlation factor, $f(\theta) = 1/(1+ \theta)$, gives remarkably good agreement with the results of kinetic Monte Carlo simulations (71).

One can also estimate the role of vacancy correlations using statistical mechanics. We begin by recalling the general formula for the MSD given in Eq. (32); the second term, with $i \neq j$, contains the correlations we seek to understand. To obtain the self diffusivity in the form of Eq. (36), we factor out the first term in Eq. (32), which gives uncorrelated MSDs proportional to $D_S(0)(1 - \theta)$. As such, the correlation factor becomes:

$$f(\theta) = 1 + 2\sum_{i=1}^{n}\sum_{j>1}\left\langle \vec{l}_i \cdot \vec{l}_j \right\rangle \Big/ \sum_{i=1}^{n}\left\langle \vec{l}_i \cdot \vec{l}_i \right\rangle \tag{39}$$

$$= 1 + 2\sum_{k=2}^{n}(n-k+1)\left\langle \vec{l}_1 \cdot \vec{l}_k \right\rangle \Big/ n\left\langle \vec{l}_1 \cdot \vec{l}_1 \right\rangle \tag{40}$$

$$= 1 + 2\sum_{k=2}^{n}\left\langle \vec{l}_1 \cdot \vec{l}_k \right\rangle \Big/ \left\langle \vec{l}_1 \cdot \vec{l}_1 \right\rangle + \frac{2}{n}\sum_{k=2}^{n}(1-k)\left\langle \vec{l}_1 \cdot \vec{l}_k \right\rangle \Big/ \left\langle \vec{l}_1 \cdot \vec{l}_1 \right\rangle, \tag{41}$$

where in Eq. (39) we have exploited the fact that the off-diagonal sum contains two identical copies of every $i \neq j$ combination. Equation (40) arises by viewing the quantity $\langle \vec{l}_i \cdot \vec{l}_j \rangle$ as an equilibrium correlation function (5,23,56), which depends only on $i-j$. As such, the off-diagonal sum in the numerator gives $(n-k+1)$ terms equal to $\langle \vec{l}_1 \cdot \vec{l}_k \rangle$ for each value of k, while the denominator gives n identical terms equal to $\langle \vec{l}_1 \cdot \vec{l}_1 \rangle$. In the long-time limit required by diffusion, where $n \to \infty$, the third term in Eq. (41) is of order $1/n$ compared with the second term, and as such is ignored. The second term in Eq. (41) (without the factor of 2) was identified by Coppens *et al.* as a correlation function–type expression, denoted C_n, which describes the persistence of correlations as a function of time (56). The sequence C_n converges to a finite value for large n, denoted C_∞, which is negative when vacancy correlations dominate. The correlation factor is thus given as $f(\theta) = 1+ 2C_\infty$.

Coppens *et al.* studied the convergence of C_n to C_∞ for various lattice topologies and loadings by performing kinetic Monte Carlo simulations (*vide infra*) (56), observing three interesting results. First, correlation factors are smaller for lattices with lower connectivities, especially for the MFI lattice which has an average connectivity of $Z = 8/3$ despite its three-dimensional structure ($Z = 6$ for simple cubic). Second, the more poorly connected lattices exhibit slower convergence of C_n to C_∞, suggesting longer correlation lengths and times for such systems. Third, for a given lattice topology, the normalized correlation function, C_n/C_∞, could be fitted to the stretched-exponential $1-e^{-[(n-1)/n_c]\gamma}$, where n_c and γ depend on the lattice topology but were found to be *independent of loading*, thus providing a universal characteristic of each lattice type.

Although evaluating Eq. (41) analytically remains challenging in general, progress can be made by assuming the Langmuirian model described above. In this case, C_n reduces to:

$$C_n = \sum_{k=2}^{n} \left\langle \vec{l}_1 \cdot \vec{l}_k \right\rangle \Big/ \left\langle \vec{l}_1 \cdot \vec{l}_1 \right\rangle = \sum_{k=1}^{n-1} \left\langle \vec{l}_1 \cdot \vec{l}_{k+1} \right\rangle \Big/ \left\langle \vec{l}_1 \cdot \vec{l}_1 \right\rangle$$
$$\equiv \sum_{k=1}^{n-1} \langle \cos\theta_k \rangle = \sum_{k=1}^{n-1} \langle \cos\theta_1 \rangle^k = \frac{\langle \cos\theta_1 \rangle - \langle \cos\theta_1 \rangle^n}{1 - \langle \cos\theta_1 \rangle} \tag{42}$$

where θ_k is defined as the angle between the jump vector $\vec{l}_i$ and $\vec{l}_{i+k}$, which implies that θ_1 is the angle between successive jump vectors for a given molecule. For lattices with sufficient symmetry, one can show that $\langle \cos\theta_k \rangle = \langle \cos\theta_1 \rangle^k$ (5), as has been assumed in Eq. (42). To obtain the correlation factor, $f(\theta) = 1 + 2C_\infty$, we note that because $|\langle \cos\theta_1 \rangle| < 1$, $\langle \cos\theta_1 \rangle^n$ vanishes in the limit $n \to \infty$. Thus we obtain the classical expression for the correlation factor:

$$f(\theta) = \frac{1 + \langle \cos\theta_1 \rangle}{1 - \langle \cos\theta_1 \rangle}. \tag{43}$$

Equation (43) deserves several remarks: First, this result shows that vacancy correlations in simple lattices result from correlations between successive hops only. Second, the loading dependence of the correlation factor arises from the loading dependence contained in $\langle \cos\theta_1 \rangle$. Third, if kinetic correlations dominate (at low loadings), then $\langle \cos\theta_1 \rangle$ is positive, which increases the self diffusivity from the mean field estimate. Next, when $\langle \cos\theta_1 \rangle$ is negative, which is expected at higher loadings when vacancy correlations are important, the correlation factor is indeed less than 1. In practice, the quantity $\langle \cos\theta_1 \rangle$ can be evaluated from Monte Carlo simulations or with simple probabilistic arguments (72).

4. Single-File Diffusion

The correlation function approach of Coppens *et al.* shows that vacancy effects can be associated with finite correlation lengths, which grow when considering lattices with smaller connectivities. Vacancy correlations take on a whole new demeanor in single-file self-diffusion, where molecules can only diffuse in one dimension and cannot move past one another (9). In this case the correlation length becomes macroscopic, which changes the phenomenology of diffusion. In particular, one can show that the MSD becomes proportional to $t^{1/2}$ for single-file diffusion in infinitely long files (51,73–75). It is interesting to note that the propagator characterizing molecular displacements during single-file diffusion remains Gaussian (76), even though the time dependence of the second moment of this propagator (i.e., the MSD) deviates from that found in normal diffusion.

The prediction of single-file diffusion has spurred great interest in observing experimentally the signature and consequences of single-file diffusion in zeolites, culminating in two reports of ethane single-file diffusion in $AlPO_4$-5 by pulsed-field gradient (PFG) NMR (77,78). Despite these reports, some controversy remains because of quasi-elastic neutron scattering data consistent with normal diffusion for this same system (79). (These experimental methods are discussed in Sec. IV.) The neutron scattering data for cyclopropane in $AlPO_4$-5 did show the single-file diffusion signature, but only for sufficiently high cyclopropane loadings so that guest–guest collisions were likely on the experimental time scale.

Complicating the unambiguous identification of single-file diffusion are (at least) two phenomena occurring on widely different time scales. First, although particle exchange may be unlikely, experimental observation on the time scales of such exchange may obfuscate or even eliminate the $t^{1/2}$ signature of single-file diffusion (80,81). Second, real zeolite single files are finite in length, which introduces the possibility of a new, "compound" diffusion mode that

becomes important on the time scale for vacancies to permeate through the single file (80,82,83). For times shorter than the vacancy diffusion time, i.e., $t < t_c = L^2/\pi D_0$ where L is the file length, particle transport proceeds via the non-Fickian, single-file diffusion mode, with MSDs increasing with the square root of time. For times longer than t_c, however, Nelson and Auerbach have shown that self diffusion in single-file systems is completely described by Fick's laws, except that the "Fickian" self-diffusion coefficient depends on file length according to (83):

$$D_{SF} = \frac{D_0 \theta_T k_d^2 L}{(1-\theta_T) vL(vL + 2D_0) - 2D_0 \theta_T k_d}, \tag{44}$$

where the parameters (k_d, v, θ_T) pertain to TCP as shown in Fig. 1c. Equation (44) was obtained by analyzing steady-state TCP fluxes under single-file conditions and was verified by open-system kinetic Monte Carlo simulations (see Sec. V.B.2). When single-file transport is diffusion limited, i.e., for large L, Eq. (44) reduces to (80,83):

$$\lim_{L\to\infty} D_{SF} = \frac{D_0(1-\theta_T)}{L\theta_T}, \tag{45}$$

which was originally derived by Hahn and Kärger (80). Equation (45) shows that the correlation factor for finite single files is given by $f(\theta) = 1/L\theta$, thus unifying vacancy correlations with single-file diffusion. The L dependence of this correlation factor also shows the seeds of the $t^{1/2}$ signature of single-file diffusion, namely, that dividing the diffusivity by L in a diffusion problem is essentially the same as dividing the linear time dependence of the MSD by $t^{1/2}$.

Nelson and Auerbach found that the fraction of time in the single-file diffusion mode scales inversely with file length for long files, suggesting that Fickian self-diffusion *dominates transport* in longer single-file zeolites. They predicted that the crossover time between (medium-time) single-file diffusion and (long-time) Fickian diffusion is just above the experimental window for PFG NMR experiments, suggesting that longer-time PFG NMR would observe this transition.

We close this section by discussing another type of correlation that has been predicted to arise in single-file systems, involving correlated cluster dynamics where instead of imagining molecules jumping one at a time, they are predicted to jump together (84). Several characteristics of the zeolite–guest system must conspire for this mechanism to gain importance. In particular, the guests must feel sufficient guest–guest attractions, the lattice of sites for an individual guest must be such that many guests cannot simultaneously fill different sites without crowding, and, finally, the guests must be constrained to diffuse in one dimension. Assuming these all hold, Sholl and Fichthorn found that activation energies for these cluster jumps are strongly size dependent and are lower than the barriers for monomer diffusion.

Having now discussed the various types of correlations that can arise for diffusion in zeolites, we now discuss the most powerful way to quantify such effects, and indeed the diffusion coefficients themselves, through the use of statistical mechanical correlation functions.

C. Correlation Functions

The relationships between transport coefficients and correlation functions are made explicit by using linear response theory and the fluctuation–dissipation theorem (23), which in turn are motivated by Onsager's regression hypothesis (47). This hypothesis, first articulated in 1931, asserts that correlations between spontaneous equilibrium fluctuations decay according to the same phenomenology (e.g., the diffusion equation or facsimile) as do externally induced nonequilibrium disturbances. This relationship between equilibrium fluctuations and nonequilibrium relaxation only holds strictly when the nonequilibrium disturbances are relatively small, since spontaneous equilibrium fluctuations are themselves very small in macroscopic systems. The interested reader is

referred to the authoritative sources on correlation functions (85,86), and also to the lucid review on correlation functions as they pertain to diffusion in zeolites by Theodorou *et al.* (10). To feign completeness, we review below the ideas most relevant for understanding how correlation functions can shed light on diffusion in zeolites.

1. Self Diffusion

We begin by rewriting the Einstein equation, which serves to define the self-diffusion coefficient, in an effort to express D_S in terms of a correlation function. Following Chandler's approach (23), we write the classical MSD as:

$$\langle R^2(t)\rangle = \langle |\ \vec{r}(t) - \vec{r}(0)\ |^2\rangle = \left\langle \int_0^t dt'\,\vec{v}(t') \cdot \int_0^t dt''\,\vec{v}(t'')\right\rangle, \tag{46}$$

where in the last equality we have exploited the fact that $[\vec{r}(t) - \vec{r}(0)] = \int_0^t dt'\,\vec{v}(t')$, where $\vec{v}(t)$ is the velocity of the tagged particle at time t. Next we differentiate the Einstein equation with respect to time and divide by 6 to obtain:

$$D_S = \frac{1}{6}\lim_{t\to\infty}\frac{d}{dt}\left\langle \int_0^t dt'\,\vec{v}(t') \cdot \int_0^t dt''\,\vec{v}(t'')\right\rangle = \frac{2}{6}\lim_{t\to\infty}\langle\,\vec{v}(t)\cdot[\,\vec{r}(t) - \vec{r}(0)]\rangle \tag{47}$$

$$= \frac{1}{3}\lim_{t\to\infty}\langle\,\vec{v}(0)\cdot[\,\vec{r}(0) - \vec{r}(-t)]\rangle = \frac{1}{3}\int_{-\infty}^{0} dt\langle\,\vec{v}(0)\cdot\vec{v}(t)\rangle$$

$$= \frac{1}{3}\int_0^{\infty} dt\langle\,\vec{v}(0)\cdot\vec{v}(t)\rangle. \tag{48}$$

The last equality in Eq. (47) comes from differentiating the square using the fundamental theorem of calculus; the first equality in Eq. (48) arises from the stationarity property of equilibrium correlation functions (23); the final equality in Eq. (48) is valid because by stationarity, equilibrium autocorrelation functions are even functions of time. We have thus arrived at a so-called Green-Kubo formula, which relates a transport coefficient to an integrated (velocity) autocorrelation function (VACF).

In practice, using the final result in Eq. (48) is only really useful when studying stochastic molecular motion in the absence of large energy barriers, e.g., in bulk fluids or very weakly confining zeolite–guest systems. For strongly confined zeolite–guest systems, with large energy barriers separating sorption sites, Eq. (48) is much less useful because velocity correlations typically decay well before rare jump events occur. When relatively large barriers are present, the VACF reveals vibrational information, which can be understood by comparing the Green-Kubo relation in Eq. (48) to the so-called vibrational power spectrum, $G(\omega)$, given as:

$$G(\omega) = \frac{1}{\pi c}\int_0^{\infty} dt\,\frac{\langle\,\vec{v}(0)\cdot\vec{v}(t)\rangle}{\langle\,\vec{v}(0)\cdot\vec{v}(0)\rangle}e^{i\omega t} \tag{49}$$

where ω is the vibrational frequency. Comparison of Eqs. (48) and (49) shows that using the integrated VACF to calculate the self diffusivity for a trapped particle will reveal instead the low-frequency vibrations of the trapped guest molecule.

We gain some insight into the physical origins of the Maxwell-Stefan formulation by supposing that the VACF decays exponentially according to the functional form (see Fig. 4):

$$\left\langle \vec{v}(0)\cdot\vec{v}(t)\right\rangle = \frac{3k_BT}{m}e^{-\eta t/m}, \tag{50}$$

where m is the particle mass and η is a friction coefficient describing the drag felt by the particle from its environment. Indeed, the exponential relaxation posited in Eq. (50)

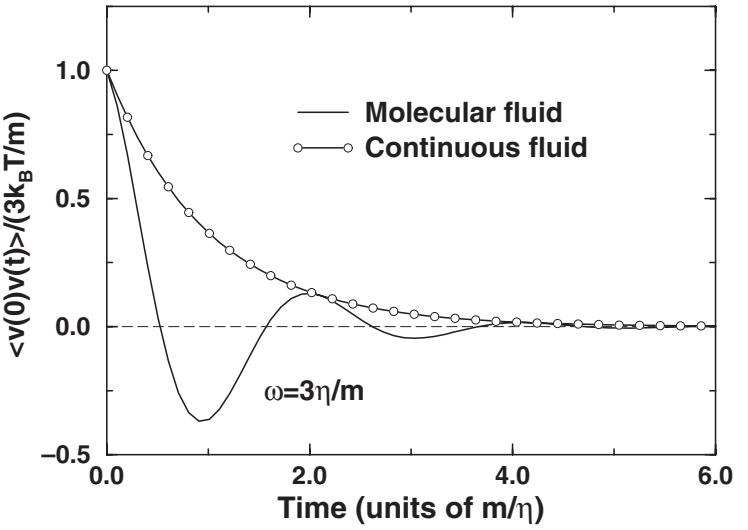

Fig. 4 Normalized velocity autocorrelation functions: (circles) continuous fluid giving exponential decay; (line) molecular fluid showing back-scattering oscillations.

arises from the phenomenology of friction. The pre-exponential factor results from the second moment of the Maxwell-Boltzmann distribution. Plugging this VACF into the Green-Kubo formula gives $D_S = k_BT/\eta$ or, alternatively for the friction coefficient, $\eta = k_BT/D_S$, which is the basic physical assumption in the Maxwell-Stefan picture of diffusion. This may explain why the Maxwell-Stefan formulation is so natural for describing diffusion in bulk fluids and in weakly confined zeolite–guest systems, where the phenomenology of friction works best.

The assumption of simple exponential relaxation considered above breaks down at both short and long times. At long times, the VACF is found to decay as $t^{-d/2}$ in d-dimensional space, which implies by further analysis that diffusion as a phenomenology is invalid in two dimensions (86). At short times, simple exponential decay ignores the molecularity of dense fluids, where back-scattering on picosecond time scales produces negative lobes and subsequent oscillations in the VACF, as shown in Fig. 4. A simple VACF expression to account for this short-time effect is given by:

$$\left\langle \vec{v}(0) \cdot \vec{v}(t) \right\rangle = \frac{3k_BT}{m} e^{-\eta t/m} \cos(\omega t), \tag{51}$$

where m and η are the same as before, and ω is an effective vibrational frequency in the fluid. The resulting self-diffusion coefficient takes the form:

$$D_S = \left(\frac{k_BT}{m}\right) \frac{\eta/m}{(\eta/m)^2 + \omega^2}. \tag{52}$$

In the limit where several vibrations are required to produce velocity relaxation, i.e., $\omega \gg \eta/m$, the self-diffusion coefficient reduces to $D_S = k_BT\eta/(m\omega)^2$, which is now quite different from the Maxwell-Stefan type of expression. As is typical with constitutive relations, the phenomenology associated with the Maxwell-Stefan formulation [*cf.* Eq. (24)] is consistent with long-time dynamics but breaks down for shorter-time phenomena.

When considering self diffusion at finite loadings, one might tag a particular guest molecule and evaluate Eq. (48) from its center-of-mass VACF. Instead, one might utilize all of the statistics available from this many-body system according to:

$$D_S = \frac{1}{3N}\sum_{i=1}^{N}\int_0^\infty dt\langle \vec{v}_i(0)\cdot\vec{v}_i(t)\rangle \tag{53}$$

where N is the number of molecules and $\vec{v}_i(t)$ is the velocity of the ith molecule at time t. This form will be useful for comparison with other diffusivities below.

2. Transport Diffusion

The above analysis demonstrates the power of correlation functions to elucidate the dynamics underlying self diffusion. What is really impressive is the ability of correlation functions to shed light on transport diffusion of both single-component (35,37,87–90) and multicomponent systems in zeolites (91,92). In particular, one can use linear response theory (93) to show that the single-component Onsager coefficient takes the form (85):

$$L_{11}^{s} = \frac{1}{3VRT}\int_0^\infty dt\left\langle \vec{J}(0)\cdot\vec{J}(t)\right\rangle, \tag{54}$$

where V is the system volume and $\vec{J}(t)$ is the spatially averaged, collective flux of the sorbed phase at time t, given by:

$$\vec{J}(t) = \sum_{i=1}^{N}\vec{v}_i(t). \tag{55}$$

Substituting Eq. (55) into Eq. (54) gives:

$$L_{11}^{s} = \frac{1}{3VRT}\sum_{i=1}^{N}\sum_{j=1}^{N}\int_0^\infty dt\langle \vec{v}_i(0)\cdot\vec{v}_j(t)\rangle \tag{56}$$

which shows that transport diffusion arises from velocity correlations between *different* molecules. Recalling the relation between L_{11}^{s} and the single-component Maxwell-Stefan surface diffusivity, $D_{1,\,vac}^{MSs} = RTL_{11}^{s}/c_1$, we obtain for $D_{1,\,vac}^{MSs}$

$$D_{1,vac}^{MSs} = \frac{1}{3N}\sum_{i=1}^{N}\sum_{j=1}^{N}\int_0^\infty dt\langle \vec{v}_i(0)\cdot\vec{v}_j(t)\rangle \tag{57}$$

$$= \frac{1}{3N}\sum_{i=1}^{N}\int_0^\infty dt\langle \vec{v}_i(0)\cdot\vec{v}_i(t)\rangle + \frac{1}{3N}\sum_{i\neq j}\int_0^\infty dt\langle \vec{v}_i(0)\cdot\vec{v}_j(t)\rangle \tag{58}$$

$$= D_s + \frac{1}{3N}\sum_{i\neq j}\int_0^\infty dt\langle \vec{v}_i(0)\cdot\vec{v}_j(t)\rangle \tag{59}$$

This last result deserves several remarks. First, as with self diffusion, using the velocity correlation function in Eq. (57) to evaluate diffusivities is practical only for systems confined by relatively small barriers. Second, in the limit of low loading where correlations between different particles are unlikely, the second term in Eqs. (58) and (59) can be ignored, confirming our assertion made in Sec. III.A that the self diffusivity and Maxwell-Stefan surface diffusivity agree at infinite dilution (35). Third, the fact that $D_{1,vac}^{MSs}$ can be expressed through such a correlation function, arising purely from dynamics, gives further credence to the idea that $D_{1,vac}^{MSs}$ is a "proper" transport coefficient, while the Fickian diffusivity involves a composite of transport and thermodynamics.

The same steps that relate D_S to the VACF can be reversed for $D_{1,vac}^{MSs}$ to give the following mean collective displacement:

$$D_{1,vac}^{MSs} = \frac{1}{6N} \lim_{t\to\infty} \frac{d}{dt} \sum_{i=1}^{N} \sum_{j=1}^{N} \langle [\vec{r}_i(t) - \vec{r}_i(0)][\vec{r}_j(t) - \vec{r}_j(0)] \rangle \tag{60}$$

This expression is useful in numerical simulations for both fluid motion and jump diffusion, which can be modeled with molecular dynamics and kinetic Monte Carlo, respectively (we discuss these simulation methods in Sec. V). However, despite the versatility of Eq. (60), its evaluatation is complicated relative to that for self-diffusion for two reasons. First, as opposed to the MSD, which averages a quantity that is either positive or zero, the collective displacements that are averaged in Eq. (60) can be negative, which can complicate statistical convergence. Second, further complicating the statistics is the fact that, whereas for self diffusion all molecules contribute separate statistics, here for collective motion the entire system contributes one batch of statistics. In general, these challenges arise from the common origin that Eq. (60) attempts to describe nonequilibrium relaxation by averaging spontaneous equilibrium fluctuations, which is a formidable statistical task. Despite these challenges, Sanborn and Snurr successfully used Eq. (60) to simulate transport diffusion in siliceous FAU under a variety of conditions (91,92), by performing many independent simulations and averaging the results.

For multi-component systems, Onsager's approach leads to the following correlation function for the coefficient $L_{\alpha\beta}^{s}$, which couples components α and β (86):

$$L_{\alpha\beta}^{s} = \frac{1}{3VRT} \int_0^\infty dt \left\langle \vec{J}_\alpha(0) \cdot \vec{J}_\beta(t) \right\rangle, \tag{61}$$

where $\vec{J}_\alpha(t)$ is the collective flux for component α at time t. Assuming there are N_α and N_β molecules in components α and β, respectively, $L_{\alpha\beta}^{s}$ becomes

$$L_{\alpha,\beta}^{s} = \frac{1}{3VRT} \sum_{i=1}^{N_\alpha} \sum_{j=1}^{N_\beta} \int_0^\infty dt \langle \vec{v}_{i\alpha}(0) \cdot \vec{v}_{j\beta}(t) \rangle, \tag{62}$$

which shows that multicomponent transport diffusion is controlled by velocity correlations between different molecules in different components. In practice, Sanborn and Snurr found it most convenient to calculate the $\{L_{\alpha\beta}^{s}\}$ coefficients using Eq. (62) averaged by molecular simulations, and then to transform these to Fickian transport diffusivities, $\{D_{\alpha\beta}\}$, for phenomenlogical interpretation (91,92).

Having now explored the macroscopic phenomenologies and microscopic underpinnings of diffusion in zeolites, we now focus on perhaps the most important task at hand: measuring diffusion in zeolites.

IV. METHODS OF MEASURING DIFFUSION IN ZEOLITES

Conceptually understanding zeolitic diffusion is not only complicated by the various physical situations under which diffusion phenomena may occur. It is also complicated by the fact that the ranges over which diffusion phenomena may be perceived can be dramatically different for different experimental techniques. It has become common to distinguish between macroscopic, mesoscopic, and microscopic techniques (4,6,94). In macroscopic techniques, intracrystalline transport phenomena are recorded by analyzing the response of an assembly of crystals to well-defined changes in the surrounding atmosphere. Mesoscopic techniques focus on an individual crystal without being able to resolve intracrystalline molecular transport. Only in the microscopic techniques, the primary experimental data directly result from transport phenomena with

molecular displacements smaller than the zeolite crystallites. It should be noted that this latter definition of a microscopic technique must not be confused with a convention generally used in statistical thermodynamics where concentrations and fluxes—being mean values over many particles—are considered to be macroscopic quantities, while microscopic quantities are characteristics of the individual particles. However, in zeolite science and technology it has also become common for concentration- or flux-based techniques to be called microscopic, as soon as a resolution within the crystallites, i.e., over microscopic dimensions, becomes possible. This section presents a short description of the fundamentals of the various experimental techniques of diffusion measurement, together with typical examples of the results obtained.

A. Macroscopic Methods

1. Steady-State Methods

a. Membrane Permeation

With zeolite material being synthetically available nowadays as membranes (see Chapter 17 by Nair and Tsapatsis in this volume), diffusion measurements may immediately be based on Fick's first law, by determining the flux through the membrane for a given difference in the sorbate concentrations in the membrane faces. Diffusion measurements of this type assume that transport through the membrane is diffusion limited (see Sec. II.C), which implies that observed fluxes are proportional to diffusivities, and that intracrystalline concentrations in the membrane faces can be calculated from sorption isotherms given the gas phase pressures (or concentrations) of the diffusants. By rearranging Fick's first law, the diffusivity results simply from

$$D_{\mathrm{T}} = \frac{|\vec{J}|\, L}{\Delta c} \tag{63}$$

where L is the membrane thickness and Δc is the concentration drop across the membrane, estimated from the pressure drop and the sorption isotherm. Permeation studies can be carried out to determine both transport and self diffusivities. In the latter case, the flux and concentration difference refer to the labeled component in, e.g., tracer counterpermeation experiments. When studying transport diffusion, one has to take into account that Eq. (63) only applies strictly for a sufficiently small concentration difference over the membrane, so that for concentration-dependent transport diffusivities, the diffusivity within the membrane can be taken as a constant equal to its effective mean value.

Permeation studies with zeolites have been carried out with both compact polycrystalline membranes (95–97) and single crystals suitably involved in impermeable foils (98–100). The data on intracrystalline diffusion provided from permeation studies with polycrystalline membranes are still heavily corrupted by membrane defects (28,97). However, as a consequence of their substantial potential for advanced technologies in separation and catalysis (101), there is no doubt that the quality of zeolite membranes will improve rapidly in the next few years. At least from the view of fundamental research, permeation studies with embedded single crystals appear to provide more reliable data on intracrystalline zeolitic diffusion. Measurements of this type, which may be referred to as mesoscopic, shall be presented in Sec. IV.B.

b. Reaction under Diffusion Control

Another class of steady-state experiments for diffusion measurement is based on the involvement of chemical reactions (102,103). In the simplest case of a unimolecular, irreversible

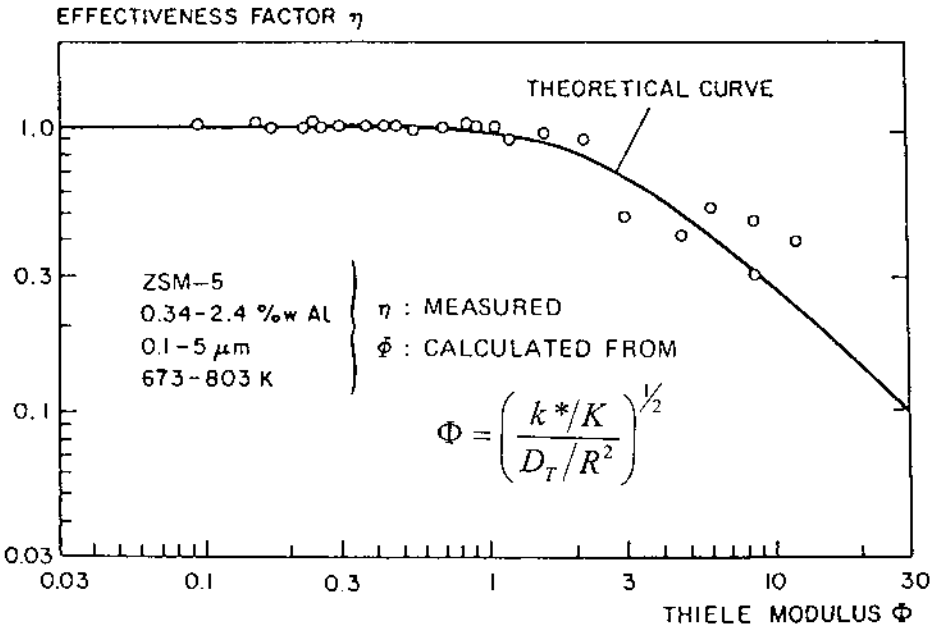

Fig. 5 Measured effectiveness factors (η) for the conversion of 2,2-dimethylbutane over H-ZSM-5 catalysts, as a function of the Thiele modulus (Φ). Data are calculated from diffusivities, obtained by conventional sorption studies, and compared with the theoretical curve that relates the two. (From Ref. 103.)

reaction A→B of first order (5,6,104), the evolution of concentration of species A obeys the relation:

$$\frac{dc_A}{dt} = \vec{\nabla} \cdot \left(D_T \vec{\nabla} c_A \right) - k_{rxn} c_A \tag{64}$$

which results from Eq. (8) by adding the first-order reaction term. Under steady-state conditions, i.e., for $dc_A/dt = 0$, the distribution c_A (and hence the total number) of the reactant molecules over the individual crystallites becomes a function of the intrinsic diffusivity. Thus, from the effective reactivity (the "effectiveness factor") being proportional to the total number of A-type molecules, one is able to determine their intracrystalline diffusivity. More correctly, one determines the mutual diffusivity of the A and B molecules, which—by assuming their microdynamic equivalency—has to coincide with their self diffusivities. As an example, Fig. 5 demonstrates the excellent agreement between the experimentally determined effectiveness factor for the conversion of 2,2-dimethylbutane over ZSM-5 with the theoretical dependence determined on the basis of gravimetric diffusion measurements (103). Conversely, the effectiveness factor of catalytic conversion may thus be used to determine intracrystalline diffusivities.

2. Transient Methods

a. Uptake Methods

The conventionally most common technique of diffusion measurement is following the response of the zeolitic host–guest system to a change in the pressure and/or composition in the surrounding atmosphere. For recording the response, a large variety of techniques are in use. The most direct one is following the molecular uptake by, for example, a gravimetric

device. For a spherical particle of radius R, subject to a step change in sorbate concentration at the external surface, molecular uptake $M(t)$ under isothermal conditions and diffusion control is given by (105):

$$\frac{M(t)}{M(\infty)} = 1 - \frac{6}{\pi^2}\sum_{n=1}^{\infty}\frac{1}{n^2}e^{-n^2\pi^2 D_T t/R^2}, \tag{65}$$

which exhibits the short-time limit of:

$$\lim_{t\to 0}\frac{M(t)}{M(\infty)} = \frac{6}{R}\sqrt{\frac{D_T t}{\pi}}, \tag{66}$$

and the long-time limit of:

$$\lim_{t\to \infty}\frac{M(t)}{M(\infty)} = 1 - \frac{6}{\pi^2}e^{-\pi^2 D_T t/R^2}. \tag{67}$$

The corresponding expressions for other particle shapes may be found, e.g., in (5,105,106). There is in fact little numerical difference between the response from a spherical particle and that from a different geometry, but with the same (external) surface-to-volume ratio. As discussed in Sec. II.C, transient uptake adsorption/desorption measurements yield the most reliable diffusivity data for large crystals and small diffusivities, where transport is diffusion limited. Regardless of whether transport is limited by diffusion or desorption, such measurements provide important time scales for zeolite scientists to gauge rates of molecular sorption. Detailed information on the influence of other processes on molecular uptake can be found in the literature (5,36,106,107); in what follows, we give a short introduction to these processes.

Any adsorption process gives rise to a temperature enhancement of the sample as a consequence of the release of the heat of adsorption. In parallel to the particle flux into each individual crystallite, establishment of equilibrium therefore as well requires heat dissipation toward the surroundings. For sufficiently fast intracrystalline diffusion, this latter process may become rate limiting for the overall phenomenon. Its analysis on the basis of Eqs. (65–67) would lead to completely erroneous diffusivities. During desorption experiments, temperature reduction as a consequence of the consumed heat of desorption leads to completely analogous effects. Note that this effect cannot be remedied by reducing the pressure step, since the reduced temperature changes would be paralleled by corresponding reductions in the internal concentration gradients (108–110). Heat effects do not occur in tracer exchange experiments, since here adsorption (or desorption) of the labeled component is exactly counterbalanced by desorption (or adsorption) of the unlabeled one (*cf.* Sec. IV.A.3).

The real structures of zeolites are likely to differ substantially from the ideal textbook structures. This is particularly true for the external surfaces of the zeolite crystallites. As a zone of pronounced structural heterogeneity, the external crystal surface is predestined to collapse, e.g., under hydrothermal treatment (111,112). Simultaneously, the external crystal surface is a favorite location of coke deposition (113,114). In both cases, the uptake rates can be limited by the permeation through the outer surface rather than by intracrystalline diffusion. Molecular uptake then should follow the simple exponential expression (5):

$$\frac{M(t)}{M(\infty)} = 1 - e^{-3k_d t/R}, \tag{68}$$

where k_d is the surface permeativity as shown in Fig. 1a–c.

When deducing intracrystalline diffusivities from macroscopic uptake measurements, it is generally assumed that immediately after the change in the surrounding atmosphere, the concentration in the surface layers of an individual crystallite attains its new equilibrium value. Such an assumption is clearly only valid for sufficiently fast mass transfer through the bed of

crystallites (115). To quantify this effect one has to relate the dimension of individual crystallites (radius R) and that of the bed ("radius" R_b) with the respective diffusivities. The effective bed diffusivity is given by (4,94):

$$D_b = \frac{D_p \epsilon_p}{\epsilon_p + (1 - \epsilon_p)K} \tag{69}$$

where ϵ_p and D_p are the volume fraction of and diffusivity in the macropores, respectively. The equilibrium constant K is the ratio of the concentrations in the sorbed and gaseous phases. Uptake is limited by intracrystalline diffusion under the condition $R_b^2/D_b \ll R^2/D_T$. In the opposite limit, uptake is limited by bed diffusion. Equations (65–67) still apply to bed-limited diffusion, except with D_T and R replaced by D_b and R_b, respectively. In this case, interpreting the uptake results in terms of intracrystalline diffusion would lead to completely erroneous results.

As a final pitfall, uptake measurements under "piezometric" conditions, i.e., constant volume–variable pressure conditions, can be corrupted significantly by the finite rate at which the atmosphere around the sample follows the pressure step in the gas reservoir. Consideration of this "valve" effect in the calculation of the intracrystalline diffusivity from the observed pressure data (116–118) can impede the rigor of the experimental procedures (119).

According to Eq. (65), the time constant of molecular adsorption/desorption (when limited by intracrystalline diffusion) should be proportional to R^2/D_T. This time constant can be expressed as:

$$\tau_{intra} = \int_0^\infty dt[1 - M(t)/M(\infty)] \tag{70}$$

which is denoted as the first moment of the uptake curve (106,120,121), and also as the mean intracrystalline molecular residence time. Evaluating Eq. (70) using Eq. (65) gives:

$$\tau_{intra} = \frac{R^2}{15 D_T} \tag{71}$$

Assuming that uptake is limited by intracrystalline diffusion and that the distribution of zeolite particle sizes is reasonably monodisperse, Eq. (71) predicts that the uptake time constant should vary with the square of the crystal radius. As an example, Fig. 6 shows this proportionality as found in uptake measurements with 2,2-dimethylbenzene in ZSM-5. The constancy of D_T with varying crystal size can thus be used as a criterion for the validity of the determined diffusivities.

b. Zero Length Column

A number of disadvantages of the conventional uptake method are overcome by the zero length column (ZLC) technique. In this technique, one follows the desorption of sorbate from a previously equilibrated sample of adsorbent into an inert carrier stream (122,123). The concentration of sorbate in the gas stream is usually recorded by chromatographic detection. The time dependence of this concentration is a direct image of the residence time distribution of the molecules within the sorbate particles, which directly provides the intracrystalline diffusivity. The sensitivity of ZLC is high enough that the amount of adsorbent can be reduced to a few milligrams. Mass transfer resistances by bed effects can thus be excluded. Moreover, the carrier gas excludes any heat effects. As a consequence of the very principle of ZLC, during measurements the intracrystalline sorbate concentration drops to zero from the initial value as determined by the partial pressure of the sorbate in the carrier gas. In order to circumvent ambiguities due to concentration-dependent diffusivities, the measurements are therefore generally performed at concentrations close to zero. Variants of the ZLC technique have been applied to the measurement of zeolitic diffusion under liquid phase conditions (124). In some

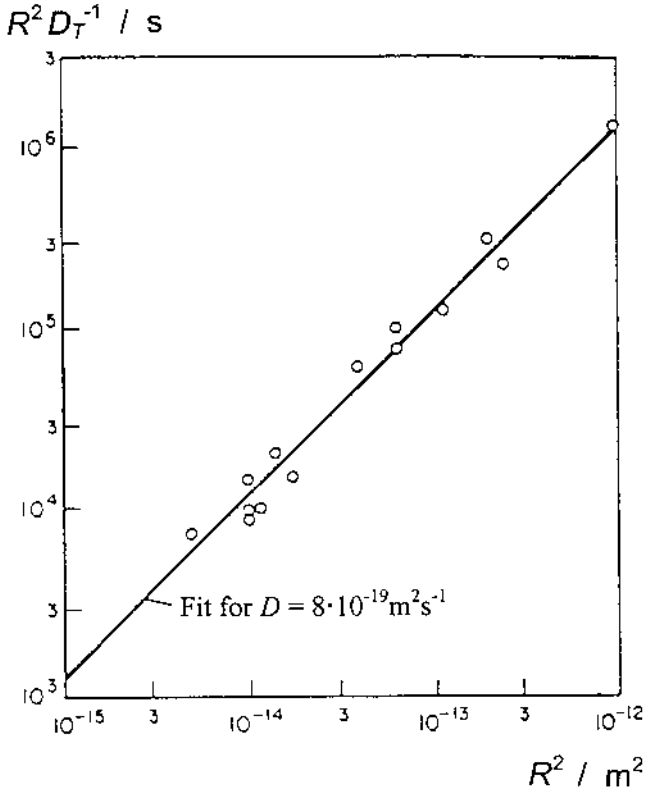

Fig. 6 Variation of the (gravimetric) diffusional time constant, R^2/D_T, with the square of the crystal radius, showing conformity with the diffusion model. (From Ref. 103.)

cases, e.g., branched alkanes in silicalite-1, these diffusivities were found to be dramatically larger than in gas phase measurements (125). This behavior seems to indicate that under fully saturated conditions, the silicalite-1 framework swells slightly so that these species are no longer as severely hindered by interactions with the pore wall. Another variant, tracer ZLC, shall be presented in Sec. IV.A.3.

c. Frequency Response

Both features of a steady-state and a transient method may be recognized in the frequency response (FR) technique (126–128). In this technique one follows the response of the sample to a regular periodic perturbation, such as a sinusoidal variation of the system volume with frequency ω. As a consequence, both the induced pressure variation and the amount adsorbed are also sinusoidally varying functions. They are interrelated by a complex factor of proportionality, which is a function of the frequency of the volume variation. Its real and imaginary parts are commonly referred to as the in-phase and out-of-phase characteristic functions, respectively. They may be calculated from experimentally directly accessible quantities, i.e., the amplitude of pressure variation and the phase shift between volume and pressure variation. The diffusivities are determined by matching the experimental curves to the theoretical expressions for a given model. As a rule of thumb, the out-of-phase characteristic function passes through a maximum at $\omega = D_T/L^2$, where L is the characteristic length of the particles under study. The out-of-phase characteristic function is also expected to approach zero

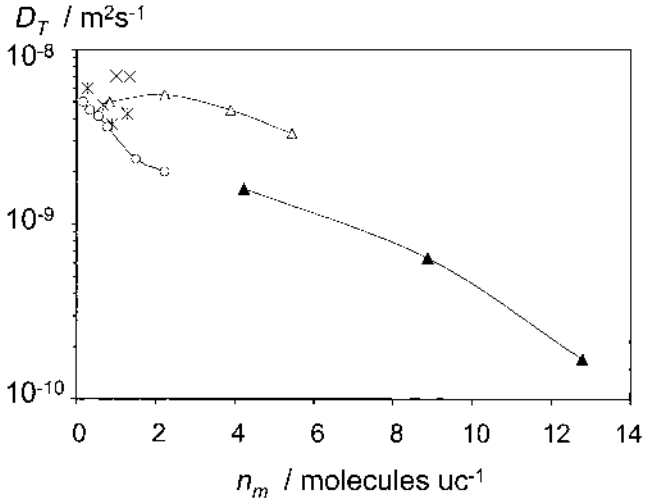

Fig. 7 Corrected diffusivities [*cf.* Eq. (2.29)] of propane in silicalite-1 obtained by the frequency response technique (○: 323 K, ×: 363 K, *: 348 K) by uptake measurement (i.e., "single-step frequency response") (△: 333 K) and by PFG NMR (▲: 333 K). (From Ref. 128.)

for frequencies both much larger and much smaller than this "resonance frequency" (4). There is essentially no instrumental limitation to apply the frequency response technique at very large frequencies, corresponding to time constants in the millisecond regime. As a nonequilibrium technique, however, the frequency response method is subject to thermal effects, which may become rate determining (128,129).

d. Infrared Detection Methods

By combining the frequency response (FR) method with temperature measurement by an infrared (IR) sensor, heat effects can actually be used for an even more complete recording of the parameters varying during the adsorption/desorption measurement cycles (129–131). Using this thermal FR (TFR) method, experimental observables should more reliably be attributed to the corresponding models of mass transfer. Figures 7 and 8 present typical results of the application of the frequency response and the TFR methods to diffusion studies with zeolites. The extrapolation of the pulsed-field gradient (PFG) NMR results in Fig. 7 to smaller concentrations yields satisfactory agreement with the results obtained by the FR techniques. In all these studies, the diffusivity is found to decrease with increasing concentration. This type of concentration dependence (consistent with patterns 1 and 2 of the concentration dependencies presented in Figure 7.2 of Ref. 5) is common for zeolite–guest systems with no specific adsorption sites. The decrease of the diffusivity with increasing concentration can be explained qualitatively by the $(1 - \theta)$ volume exclusion factor discussed in Sec. III.A. The same general tendency of decreasing diffusivity with increasing loading is reflected by the data in Fig. 8. In addition, the presence of water molecules is found to lead to a much more pronounced decay in the propane diffusivities. This behavior can be explained by the formation of ion–water complexes in the windows between adjacent supercages, which can significantly reduce propane propagation rates. We note that the PFG NMR and TFR data are in reasonable agreement in both their qualitative trends and their absolute values. When carrying out diffusion measurements by PFG NMR and the TFR method in the same concentration range, satisfactory agreement between the data obtained by these two techniques can also be seen in Fig. 8.

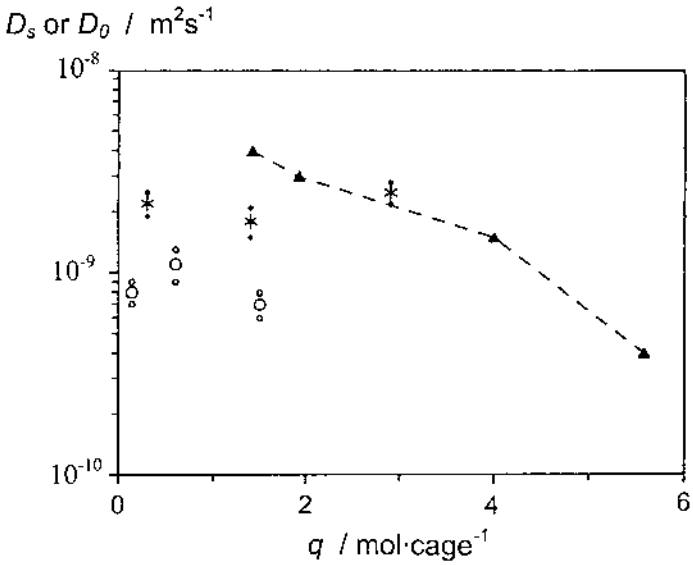

Fig. 8 Corrected diffusivities [*cf.* Eq. (2.29)] of propane in NaX at 303 K in an anhydrous (*) and a hydrated (○) sample, compared with PFG NMR diffusivities (▲). (From Ref. 131.)

Following molecular uptake by recording the time-dependent mass of the zeolite–guest system (gravimetric methods), or the pressure and/or temperature responses (piezometric and frequency response measurements, respectively) only provides information about overall adsorption/desorption kinetics. In many cases of practical application, however, one is interested in the mobility of individual components. Therefore, the application of IR spectroscopy to the study of sorption phenomena has afforded a significant breakthrough for diffusion studies in multicomponent zeolite–guest systems (132–134). Figure 9 shows the evolution of the primary data (IR bands) in a counterdiffusion experiment with H-ZSM5 where, under the influence of a concentration step of ethylbenzene in the surrounding atmosphere (bands at 1496 cm^{-1} and 1453 cm^{-1} for the adsorbed ethylbenzene), a substantial fraction of the previously adsorbed benzene molecules (band at 1478 cm^{-1}) is forced out of the crystallites.

Figure 10 shows the kinetics of the replacement of benzene by ethylbenzene in H-ZSM-5, together with the diffusivities calculated by matching the kinetic curves to the appropriate solutions of Fick's second law. Diffusivities deduced under such conditions are referred to as coefficients of counterdiffusion. The quantity β is a fitting parameter, which accounts for the fact that the sorbate partial pressures are not instantaneously established at the location of the sample. The diffusivities shown in Fig. 10 indicate that adding the ethyl substituent onto benzene does not greatly alter its transport properties, presumably because the "kinetic diameter" of the molecule is not greatly altered. A bigger change is expected when comparing benzene to *ortho*- or *meta*-xylene, which do have significantly greater effective diameters.

In addition to the conventional chromatographic methods (135), other more sophisticated experimental techniques have recently been applied to the study of molecular diffusion in assemblages of zeolite crystallites, including positron emission profiling (PEP) (136,137), temporal analysis of products (TAP) (138,139), and (nuclear) magnetic resonance tomography (MRT) (140,141). Since reliable information about intracrystalline diffusion can be obtained only if the observed processes are strongly influenced by intracrystalline mass transfer, these

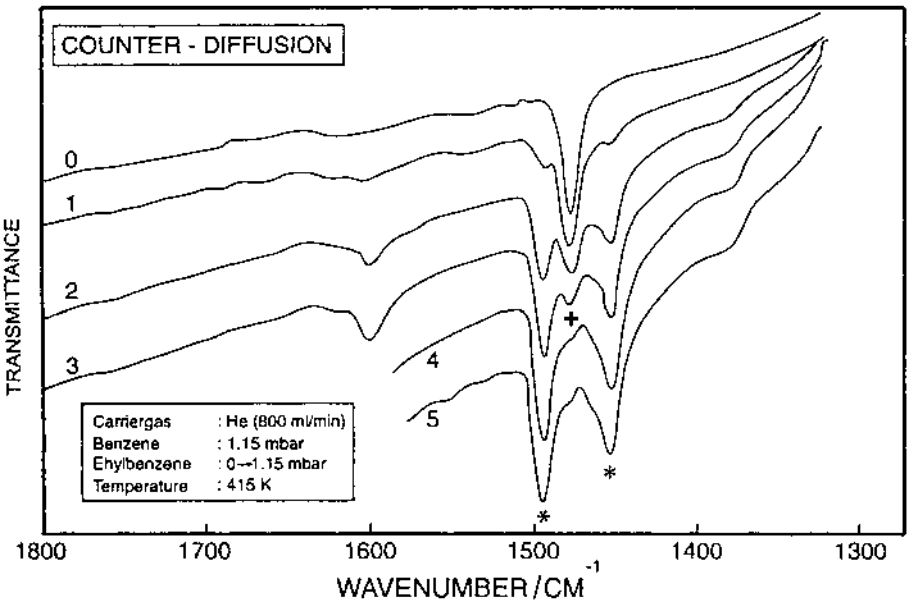

Fig. 9 Set of IR spectra for successive replacement of preadsorbed benzene by ethylbenzene. (+) Strongest benzene band; (*) bands of ethylbenzene. (From Ref. 134.)

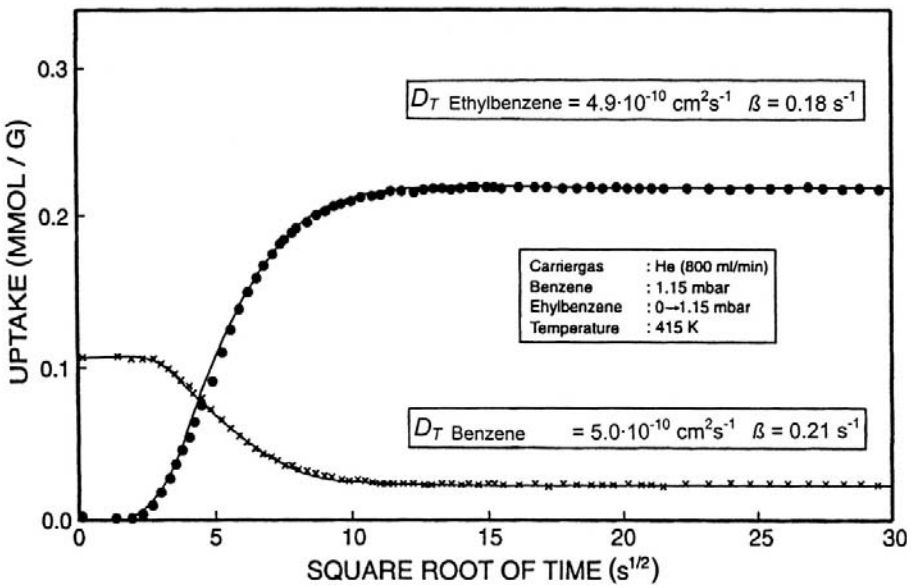

Fig. 10 Uptake curves of counterdiffusion as derived from the evolution of IR spectra (*cf* Fig. 9) for ethylbenzene vs. benzene in H-ZSM-5. (From Ref. 134.)

techniques measure intracrystalline diffusion in zeolites only under rather special conditions (138,142,143).

3. Tracer Methods

By involving isotopically labeled and unlabeled molecules, most of the procedures described in Secs. IV.A.1 and IV.A.2 can be adapted to diffusion measurements under equilibrium, i.e., to the measurement of tracer of self-diffusion. Tracer permeation measurements necessitate different partial pressures of the labeled component on the two sides of the membrane (preferably zero on one side), while the total pressure of the sorbate, i.e., the sum of the partial pressures of the labeled and unlabeled components, must be the same on both sides of the membrane. In Sec. II.C, we refer to this experimental setup as tracer counterpermeation (TCP), as shown in Fig. 1c. In tracer uptake measurements, the process of measurement is initiated by replacing a certain fraction of the sorbate molecules in the surrounding atmosphere by labeled ones (144). Flux or uptake analyses are generally performed by mass spectrometry, which readily allows discrimination between labeled and unlabeled molecules.

a. Tracer Zero Length Column

By performing ZLC with labeled and unlabeled particles, i.e., tracer ZLC or TZLC, the range of applicability of the ZLC technique can be greatly enhanced. In TZLC, the sorbate in the carrier gas is switched from a labeled (e.g., deuterated) to an unlabeled species (145,146). Under these conditions, the purging rate of the labeled component directly yields the intracrystalline self-diffusivity. In contrast to ZLC, which is essentially confined to very low sorbate concentrations, TZLC can probe the whole concentration range from zero to saturation. As an example, Fig. 11 shows the results of self-diffusion measurements of methanol in Na-X by TZLC in comparison

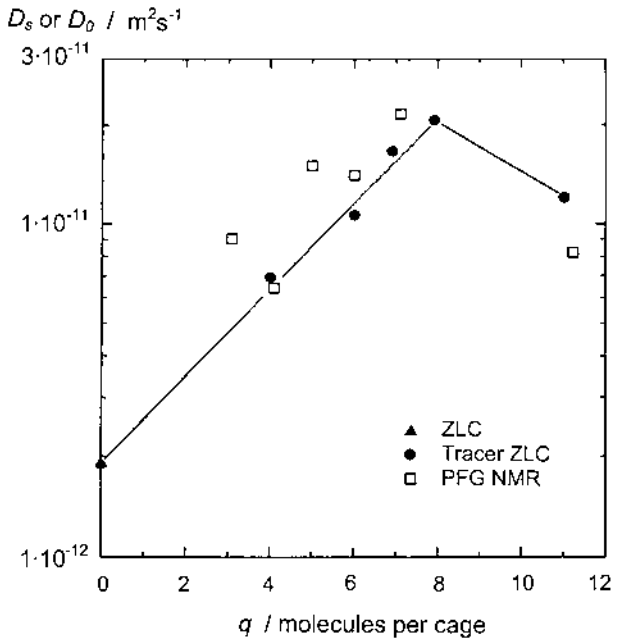

Fig. 11 Self diffusivities of methanol in NaX at 373 K measured by TZLC and PFG NMR, compared to the transport diffusivity at infinite dilution determined by (normal) ZLC. (From Ref. 146.)

with ZLC and PFG NMR data. The self-diffusivities in Fig. 11 have magnitudes of order 10^{-11} m^2 s^{-1}. These data represent an example where satisfactory agreement between various techniques, in particular between macroscopic and microscopic measurements, has been observed. We have presented herein additional examples of satisfactory agreement between the results of different techniques, e.g., in Figs. 7 and 8. The loading dependence of the diffusivities in Fig. 11 exhibits an initial increase at low to medium loadings, followed by a subsequent decrease at high loadings. This behavior indicates the presence of special adsorption sites for methanol in Na-X, presumably over supercage Na cations, because filling these sites increases the rate of self diffusion. However, when the system approaches saturation, the blocking of sites takes over and the self diffusivity begins to decrease with loading.

However, there are also systems that reveal systematic discrepancies between the results obtained by different techniques. As an example, Fig. 12 shows the results of diffusion studies with benzene in zeolite Na-X by TZLC, FR, and PFG NMR (147). The decreasing loading dependence observed by both FR and PFG NMR is consistent with the absence of particularly stable adsorption sites, whereas the increasing loading dependence observed by TZLC signals the presence of such stable sites (31,32). Until now, no fully satisfactory explanation of this discrepancy has been reported. As discussed below in Secs. IV.D and V.C, this discrepancy is most likely caused by structural heterogeneities in the Na-X zeolites considered. Defects in the framework topology and/or disorder in the Al/Na distributions can produce different self diffusivities, depending on the length scales probed by different experimental methods (148,149).

Other variants of nonequilibrium measurements, which have been applied to self-diffusion studies by the use of labeled molecules, include the measurement of molecular uptake from a surrounding liquid (150) and in closed-loop recycling (151,152). Being sensitive to the concentrations of, e.g., deuterated and nondeuterated substances, spectroscopic methods such as IR (132–134) and NMR (153) allow the direct monitoring of labeled and unlabeled molecules in the sorbed phase.

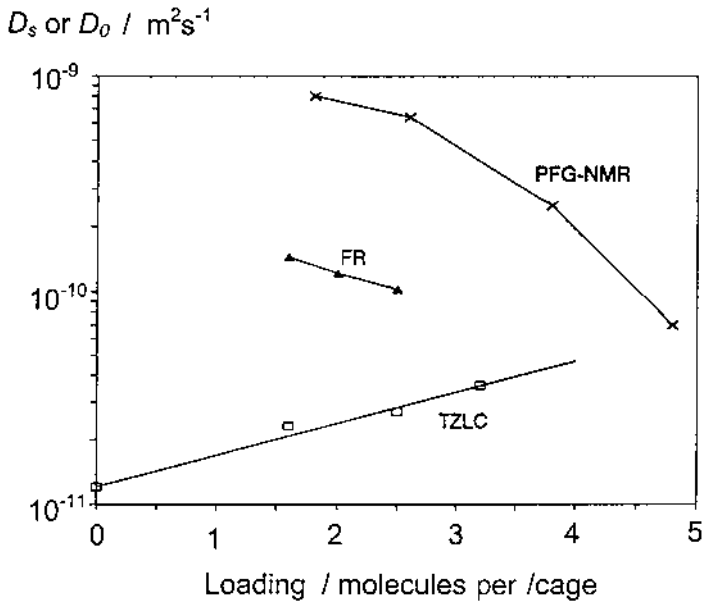

Fig. 12 Comparison of benzene diffusivities in NaX obtained by TZLC, frequency response (FR) and PFG NMR. (From Ref. 147.)

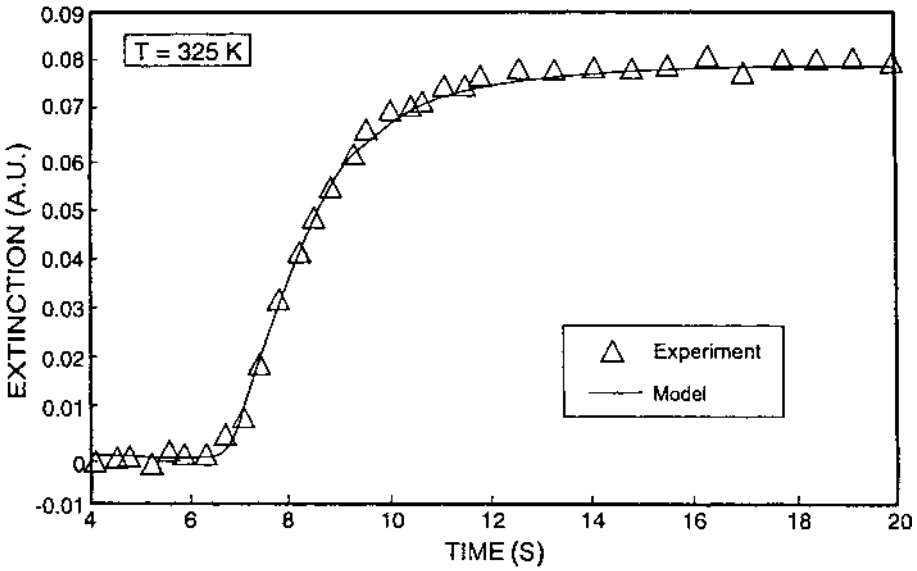

Fig. 13 Uptake kinetics of *n*-heptane on a single crystal of H-ZSM-5 as measured by micro-FTIR spectroscopy. (From Ref. 134.)

B. Mesoscopic Methods

The first mesoscopic measurements of diffusion in zeolites were carried out by Wernick and Osterhuber (154) and by Hayhurst and Paravar (155), who measured molecular fluxes through crystallites embedded in impenetrable polymer matrices. In addition to permeation measurements through ordered arrangements of MFI-type zeolites in metallic membranes (156), Caro and coworkers considered the rate of molecular uptake by restricting access to only one side of the membrane, while the crystallite faces on the other side remained covered by a metal foil. In these measurements the diffusivities were found to depend strongly on the crystallographic direction (99). Recently, molecular uptake by individual crystals has been monitored by micro-Fourier transform (FT) IR (134). The uptake curve of *n*-heptane by an individual H-ZSM-5 crystal in Fig. 13 presents an example of such measurements, showing that uptake in such systems requires on the order of 10 s to reach saturation.

C. Microscopic Methods

1. Transport Diffusion

a. Interference Microscopy

Using interference microscopy, the microscopic measurement of transport diffusion in zeolites has been achieved for the first time (157,158). In this technique, one determines the change in sorbate concentration integrated along the observation direction through the crystallite, by following the change of the optical density of the zeolite crystallites during transient molecular adsorption or desorption. This information can be resolved down to pixels of about $1 \times 1\ \mu m^2$ over the cross-section of the crystal under study. For crystals of cubic symmetry, these integrated data can be translated into concentration maps by deconvolution (158). As an example, Fig. 14 shows the evolution of methanol concentration in zeolite NaCa-A during adsorption, plotted as

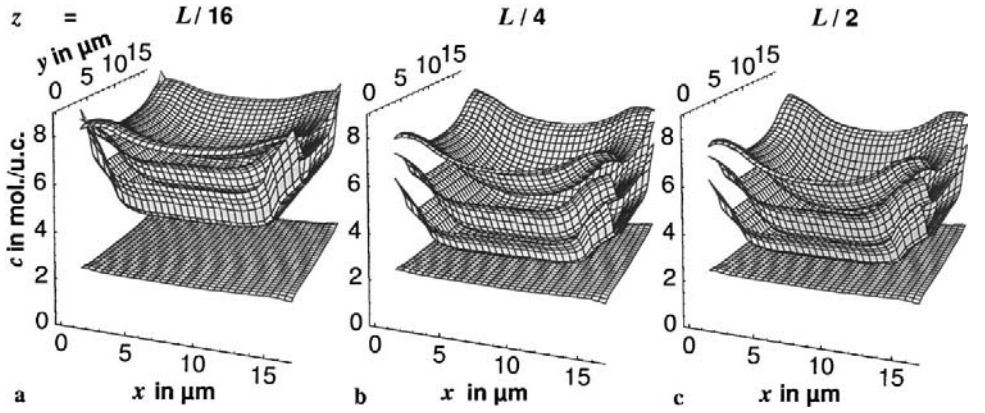

Fig. 14 Concentration profiles $c(x, y, z; t)$ of methanol in an NaCaA-type single crystal of edge length L at 293 K at different times $t = 0$, 40, 80, and 160 s (from bottom to top) after the sorption has started. Data are represented for different planes parallel to one outer face at z values indicated on top of the figures. (From Ref. 157.)

concentration maps over three different cross-sections through the crystallites, parallel to and at different distances from one of the external faces. These data permit the direct determination of intracrystalline transport diffusivities by interpreting the spatial-temporal dependence of measured concentrations using Fick's second law, Eq. (8). The data in Fig. 14 probe adsorption on time scales of 40-s multiples and give a transport diffusivity for methanol in NaCa-A of $(8 \pm 2) \times 10^{-14}$ m^2 s^{-1}, which is in reasonable agreement with PFG NMR data. This diffusivity is less than that for methanol in Na-X by more than three orders of magnitude, presumably because of the much smaller windows in A zeolite, but also because of the stronger charge-dipole attraction between methanol and Ca ions in NaCa-A.

Moreover, interference microscopy provides a sensitive tool for probing structural properties of zeolite crystallites, which are important in determining their transport behavior and which are difficult to detect by other techniques. MFI-type zeolite crystals are well known to have an internal hour-glass-like structure, indicating that they are of twinned rather than of monocrystalline structure (159,160). In order to evaluate the importance for molecular transport of the internal intersections separating different intergrowth components of the crystals, the results obtained by interference microscopy have been compared with corresponding integral concentrations resulting from Monte Carlo simulations (161). In the case of isobutane, such comparisons provide clear evidence that molecular uptake proceeds mostly via the external crystal surface. In this case, the internal interfaces serve as mild transport resistances for diffusion of isobutane from one intergrowth component to another rather than as additional diffusion paths enhancing the penetration rate into the zeolite particles. Such a situation is different from that found in solid-state diffusion with grain boundary effects (162). The findings reported in Ref. 161 are in contrast to observations with iodine, where the iodine molecules have been found to permeate slowly from the gas phase along the internal interfaces of the crystals filled with large aromatic molecules (163).

2. Self-Diffusion

As a consequence of the microscopic size of typical zeolite crystallites, the conventional techniques of isotopic labeling have thus far failed to be applied to the direct observation of intracrystalline self diffusion. The only techniques that have been applied to this purpose are

spectroscopic methods, which provide information about the propagation probabilities of guest molecules within the zeolite sample.

a. Quasi-Elastic Neutron Scattering

Diffusion measurement by quasi-elastic neutron scattering (QENS) is based on analysis of the (quasi-elastic) broadening in the energy distribution of an outgoing neutron beam. The broadening is a consequence of the Doppler shift caused by the interaction of the neutrons with the diffusants. In this way, the different rates of motion of the diffusants are recorded in the spectra of neutron energy transfer. The relevant experimental observable is the so-called double-differential cross-section ($\partial^2\sigma/\partial\Omega\partial E$), which represents the fraction of neutrons scattered into a solid angle in the interval $[\Omega, \Omega + d\Omega]$, and with energies in the interval $[E, E + dE]$. This cross-section can be split into incoherent and coherent contributions according to (164,165):

$$\frac{\partial^2\sigma}{\partial\Omega\partial E} = \sigma_{\text{inc}} S_{\text{inc}}(k,\omega) + \sigma_{\text{coh}} S_{\text{coh}}(k,\omega), \tag{72}$$

where σ_{inc} (σ_{coh}) denotes the incoherent (coherent) cross-section, which is a characteristic quantity for each type of nucleus. The functions $S_{\text{inc}}(k, \omega)$ and $S_{\text{coh}}(k, \omega)$ denote the incoherent and coherent scattering functions, respectively, given by (166):

$$S_{\text{inc}}(k,\omega) = \frac{1}{2\pi}\int d\vec{r}\int dt\; e^{i(\vec{k}\cdot\vec{r}-\omega t)} G_{\text{s}}(\vec{r},t) \tag{73}$$

$$S_{\text{coh}}(k,\omega) = \frac{1}{2\pi}\int d\vec{r}\int dt\; e^{i(\vec{k}\cdot\vec{r}-\omega t)} G(\vec{r},t) \tag{74}$$

These are the double Fourier transforms of the correlation functions of particle propagation, with the momentum transfer $\hbar\vec{k}$ and energy transfer $\hbar\omega$ as the Fourier variables conjugate to $\vec{r}$ and t, respectively. In Eq. (73), $G_{\text{s}}(\vec{r},t)$ denotes the self-portion of the density–density autocorrelation function in space and time, i.e., $G_{\text{s}}(\vec{r},t) \propto \langle \delta\rho_i(\vec{0},0)\delta\rho_i(\vec{r},t)\rangle$. For $r = |\vec{r}|$ large compared to zeolite unit cells, $G_{\text{s}}(\vec{r},t)$ corresponds to the propagator in Eq. (10), which solves the diffusion equation with a δ-function initial condition. Inserting Eq. (10) into Eq. (73) leads to a neutron energy distribution whose width is given by (164,165):

$$\Delta E \equiv \hbar\Delta\omega(\vec{k}) = \hbar k^2 D_{\text{S}} \tag{75}$$

Equation (75) shows that plotting the energy distribution ΔE of the scattered neutrons as a function of $k^2 = |\vec{k}|^2$ yields a straightforward means for determining the self diffusivity D_{s}. For jump diffusion one obtains (167):

$$\Delta E = \frac{\hbar}{\tau}\left[1 - e^{-k^2\langle l^2\rangle/6}\right], \tag{76}$$

where τ is an apparent mean residence time, and $\langle l^2\rangle$ is an apparent mean square jump length. These quantities may correspond to fundamental jump lengths and times, but they may also represent composites of fundamental jump processes, depending on the underlying dynamics. Interpreting QENS data via Eq. (76) allows the determination of both the mean residence time (for large values of k) and the self diffusivity (for small values of k), where Eqs. (75) and (76) coincide. Combining both types of information thus allows the determination of the mean square jump length.

The function $G(\vec{r},t)$ is proportional to the full density autocorrelation function, i.e., $G(\vec{r},t) \propto \langle \delta\rho(\vec{0},0)\delta\rho(\vec{r},t)\rangle$, which is related to the probability density that after time t, a particle is found at a displacement $\vec{r}$ from the position where this or any other particle was located at time $t = 0$. In this way, the coherent scattering function probes collective motions, giving rise to the measurement of transport diffusivities.

Table 1 Diffusivities and Root Mean Square Displacements Accessible by QENS and PFG NMR

Observable	PFG NMR	QENS
D_S (m^2 s^{-1})	$>10^{-15}$	$>10^{-14}$
$\sqrt{\langle R^2(t)\rangle}$(m)	$>10^{-7}$	$<10^{-8}$

According to Eq. (72), the relative values of coherent and incoherent cross-sections indicate which scattering process prevails for a given nucleus. Neutron scattering with hydrogen-containing molecules is essentially incoherent because of the relatively large incoherent cross-section ($\sigma_{inc}(^1H) = 79.9 \times 10^{-28}$ m^2, $\sigma_{coh}(^1H) = 1.76 \times 10^{-28}$ m^2). In comparison with all other nuclei, neutron-hydrogen scattering provides the best prospects for self-diffusion measurements. Interestingly enough, proton-containing molecules are also the best suited for diffusion measurements by PFG NMR, but for a completely different reason, namely, the large gyromagnetic ratio of protons. Table 1 provides an order-of-magnitude comparison between the key quantities characterizing the range of diffusion measurements by QENS and PFG NMR.

With deuterium ($\sigma_{inc}(^2H) = 2.04 \times 10^{-28}$ m^2, $\sigma_{coh}(^2H) = 5.97 \times 10^{-28}$ m^2), the coherent contribution to neutron scattering prevails. The first measurement of transport diffusion in zeolites via coherent QENS was carried out for molecular deuterium (D_2) in Na-X zeolite (168). As such, QENS turns out to be the only technique so far that allows the simultaneous measurement of transport and self diffusion with one and the same system. In this study, it was found that the self and transport diffusivities do indeed have similar values at low D_2 concentrations. For higher loadings, the transport diffusivity increases rapidly and exceeds the self-diffusivity, in complete agreement with the predictions of Eq. (29) for fluid-like motion.

A survey of the range of self diffusivities accessible by incoherent QENS is provided in Fig. 15, showing diffusivities of *n* alkanes in ZSM-5 as a function of the chain length. The

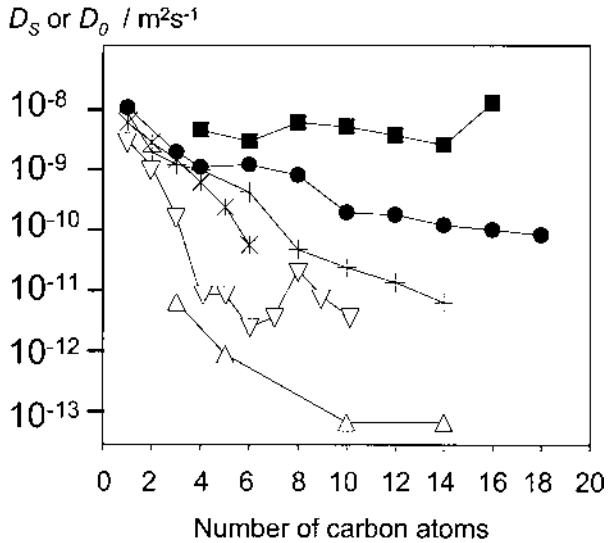

Fig. 15 Intracrystalline self diffusivities of *n*-alkanes at low loadings in MFI zeolites at 300 K, as a function of alkane chain length, obtained by MD simulations (■); Brownian dynamics (●); QENS (+); single-crystal membrane permeation (▽); ZLC (△); and PFG NMR (*) (Data from Refs. 164 and 178.)

results of other experimental techniques and of molecular simulations are also included in Fig. 15 (164,169). These data provide another example of the large differences among diffusivities obtained with different experimental techniques—discrepancies that arise for some but not all systems. It is remarkable that even the results of the two microscopic techniques, namely QENS and PFG NMR, do not agree quantitatively for pentane and hexane diffusion in ZSM-5. Figure 15 exhibits three different types of trends regarding how the diffusivity varies with alkane chain length: (a) roughly independent of chain length [molecular dynamics simulation (170)]; (b) monotonically decreasing with chain length [Brownian dynamics simulation (171), QENS (164), PFG NMR (169), and ZLC (172)]; and (c) nonmonotonically decreasing with chain length [single-crystal membrane permeation (100)]. The question is: which trend is correct?

The membrane permeation data in Fig. 15, if they are correct, indicate that octane (C_8) diffuses much faster than does heptane (C_7) and nonane (C_9). As such, these data suggest the possibility of "resonant diffusion," where the diffusivity is maximal when the hydrocarbon chain length is an integer multiple of the lattice repeat unit (and minimal for half integer multiples) (173). Although only one experiment in Fig. 15 observed resonant diffusion, this phenomenon has received considerable attention from theorists (170,173–175). Indeed, the simulation results reported by Runnebaum and Maginn suggest that while alkane diffusivities in silicalite decrease monotonically with chain length when considering motion in the x and z-directions, they exhibit resonant diffusion along the y direction with octane exhibiting the maximum diffusivity (170). In order to determine whether resonant diffusion actually takes place in zeolites, the many discrepancies among experimental data shown in Fig. 15 will have to be resolved.

b. Pulsed-Field Gradient NMR

Molecular self-diffusion measurements by the pulsed-field gradient (PFG) NMR technique can be understood on the basis of the classical model of NMR, in which the spins—i.e., the magnetic moments of individual nuclei, each with their associated angular momentum—are assumed to rotate about the direction of a magnetic field $\vec{B}$ with the Larmor frequency given by:

$$\omega = \gamma B, \tag{77}$$

where $B = |\vec{B}|$ is the magnetic field strength. The direction of $\vec{B}$ is usually defined by convention as the laboratory-fixed z axis. The gyromagnetic ratio, γ, is a characteristic quantity of the nucleus under study, attaining the highest value for hydrogen ($\gamma_H = 2.675 \times 10^8\ T^{-1}\ s^{-1}$). In field gradient NMR, the magnetic field $\vec{B}$ is the sum of a spatially constant field with strength B_0, and a strongly inhomogeneous field with magnitude $B_{add} = gz$. As such, according to Eq. (77), the Larmor frequency becomes a function of location along the z axis, i.e., $\omega = \omega(z)$.

In PFG NMR, the additional inhomogeneous field B_{add} is applied over two short time intervals δ as the so-called field gradient pulses. By applying a suitable sequence of radio frequency (rf) pulses (see also Refs. 5,16,176, and 177) one generates a transient NMR signal, the "spin echo." One can show that, for each individual molecule, when the difference in Larmor frequencies between two field gradient pulses increases, the spin-echo intensity decreases. The quantitative relation is given by Refs. 5,16,176–178:

$$\psi(g\delta, t) = \int d\vec{r}\, P(\vec{r}, t)\, \cos(\gamma \delta g z), \tag{78}$$

where $P(\vec{r}, t)$ is the Fickian propagator given in Eq. (10). The observation time t is given by the separation between the two gradient pulses. After substituting Eq. (10) into Eq. (78), the PFG NMR spin-echo attenuation due to diffusion in homogeneous media is given by:

$$\psi(g\delta, t) = e^{-\gamma^2 \delta^2 g^2 D_s t}, \tag{79}$$

hence providing a direct measurement of the self diffusivity. In heterogeneous systems, in particular under the influence of restricting barriers, it is convenient to introduce an effective diffusivity given by $D_{\text{eff}} = \langle R^2(t)\rangle/6t$. Deviations from homogeneity can often be accounted for by simply replacing D_S in Eq. (79) by D_{eff}. For diffusion in homogeneous systems, D_{eff} clearly coincides with the genuine self diffusivity. However, for inhomogeneous systems, D_{eff} can exhibit time dependence (148), reflecting the various transport resistances probed during the PFG NMR measurement.

While the range of diffusivities accessible by PFG NMR and QENS are similar, with about 10^{-14} m^2s^{-1} as a typical lower limit, the observed displacements (and hence the corresponding observation times) are distinctly different, as shown in Table 1. Typical displacements covered in PFG NMR are between a few hundred nanometers up to hundreds of micrometers, with observation times of milliseconds to seconds. By contrast, the displacements observable by QENS are limited to a few nanometers. This has been exploited by Jobic *et al.* who used QENS to measure benzene self diffusivities in Na-Y (179), where crystallites are typically too small (about 1 μm) for reliable PFG NMR measurements of intracrystalline self-diffusion. The benzene self-diffusivities measured by Jobic *et al.* decrease with benzene loading, in contrast to the increasing loading dependence predicted by Saravanan and Auerbach on the basis of kinetic Monte Carlo simulations (31). If the loading dependence observed by QENS is correct, then the Monte Carlo simulations overestimate the extent to which Na–benzene interactions provide specific adsorption sites in Na-Y.

Owing to the quite general relation between the observed spin-echo attenuation and the patterns of propagation in Eq. (78), PFG NMR is particularly suitable for diffusion studies with heterogeneous systems such as beds of zeolites. Varying the observation time and hence the covered displacements, PFG NMR is able to probe both intracrystalline diffusion (for $\sqrt{\langle R^2(t)\rangle} \ll R$) as well as long-range diffusion (for $\sqrt{\langle R^2(t)\rangle} \gg R$), where R is the mean crystallite radius. The long-range diffusivity is the counterpart in self-diffusion of the effective bed diffusivity discussed in Eq. (69). Further transport-related phenomena observable in such studies include diffusion anisotropy (59,66), the formation of transport resistances (111–114), deviations from ordinary diffusion such as single-file diffusion (77,78,180) and diffusion on fractals (181), multicomponent diffusion (182–185), and diffusion accompanied by catalytic reactions (186–188).

Before we close this section on PFG NMR, we note that several other NMR methods have been developed for and applied to measuring *orientational* dynamics of molecules in zeolites. In general, NMR measurements probe an orientational correlation function of some molecular axis (189). NMR relaxation and linewidth measurements (190–196) typically assume that this correlation function decays exponentially. With this assumption, the exponential decay time constant, i.e., the correlation time τ_c, can be deduced from spin-spin and spin-lattice relaxation times. Alternatively, the exchange-induced sidebands NMR method can measure the correlation function itself (197). Favre *et al.* applied this approach to benzene dynamics in Ca-Y zeolite (1), finding a biexponential correlation function whose short- and long-time dynamics were interpreted in terms of intracage and intercage motion, respectively (198). Having measured the cage-to-cage rate constant, Favre *et al.* reported the self-diffusivity of benzene in Ca-Y as $D_S = 10^{-19}$–10^{-18} m^2 s^{-1} in the temperature range 338–368 K, perhaps the smallest self diffusivities ever measured for a zeolite–guest system. An even more sophisticated approach is the two-dimensional exchange NMR method (199–201), which measures the orientational correlation function, and also the most important jump angles in the dynamics, which facilitates the interpretation of the measured time scales. In general, diffusion coefficients can be extracted from these orientational data only if the orientational correlation function decay is controlled by cage-to-cage or otherwise long-length scale dynamics. Because such

length scales are typically not measured in these NMR approaches, one should regard a diffusional interpretation of such data with great care.

D. Correlating Results from Different Measurements

Applying PFG NMR to the investigation of diffusion in zeolites (5,114,190,202) has revealed intracrystalline diffusivities that are up to five orders of magnitude larger than those previously assumed on the basis of macroscopic measurements. Subsequent critical reconsiderations of classical uptake measurements (36,107–121) and their interpretations led in many cases to much better agreement among the results of different measuring techniques. These comparisons are complicated by the fact that different techniques often probe fundamentally different physical situations (e.g., equilibrium vs. nonequilibrium conditions) as well as completely different ranges of observation (e.g., nanoscopic vs. macroscopic dimensions). Comparing results obtained under such different conditions necessitates a theoretical framework for correlating equilibrium and nonequilibrium processes, as well as providing independent evidence about the structural homogeneity of crystallites. Both problems are topics of intense current work (8,10,12–14,203,204). The data in Fig. 15 emphasize that even in the most recent studies, where the pitfalls of the various techniques and of their interpretations should have been ameliorated by now, there remain substantial discrepancies. Indeed, a particularly alarming result is shown in Fig. 16, where the self diffusivities of alkanes in MFI-type zeolites are shown to depend significantly on the mean diffusion path probed by PFG NMR (149). While the measurements at higher temperatures and over larger distances yield constant diffusivities as observed in numerous previous PFG NMR studies (205,206), recent progress in PFG NMR

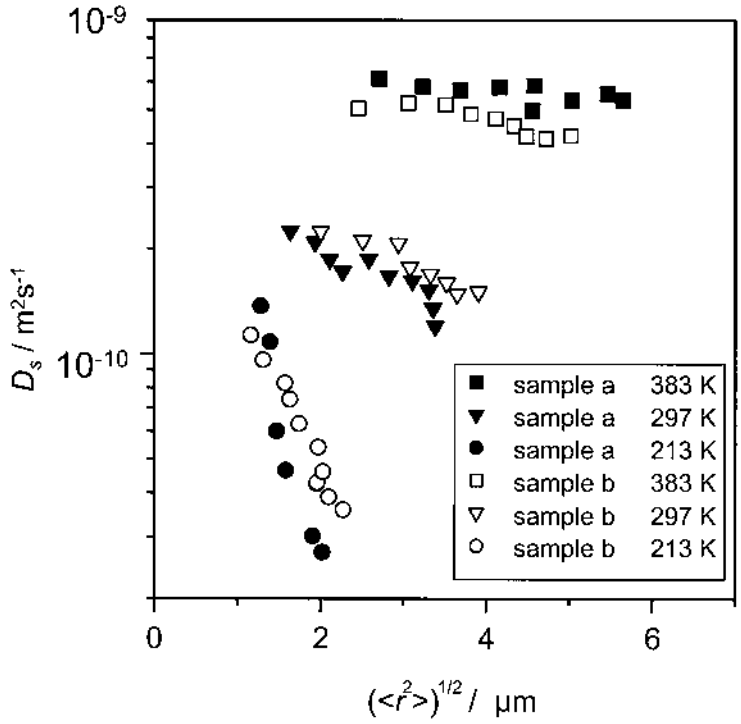

Fig. 16 Dependencies of self-diffusion coefficients on the measured root mean square displacements for *n*-butane in two different samples of silicalite-1 (a and b). (From Ref. 149.)

instrumentation (207) allows diffusion measurements over much smaller distances, where the diffusivities are found to decrease with increasing displacements. This experimental finding appears to support one of the old explanations of the discrepancies between different techniques, namely, that there exists a hierarchy of diffusion barriers (36). Clarifying the origin of these discrepant diffusion measurements is undoubtedly one of the great challenges of future zeolite research. The eventual solution is intimately associated with progress in our understanding of real crystal structures and with our ability to synthesize sufficiently ideal zeolite crystallites.

V. METHODS OF SIMULATING DIFFUSION IN ZEOLITES

The wide range of diffusional length and time scales encountered by molecules in zeolites presents unique challenges to the modeler, requiring that various simulation tools, each with its own range of applicability, be brought to bear on modeling dynamics in zeolites. In particular, when transport is relatively rapid, the molecular dynamics technique can be used to simulate both the temperature and loading dependencies of self diffusion (7,11). On the other hand, when molecular motion is relatively slow because free-energy barriers separating sorption sites are large compared with thermal energies, transition-state theory and related methods must be used to simulate the temperature dependence of site-to-site jump rate constants. In this regime, kinetic Monte Carlo and mean field theory can then be used to model the loading dependence of activated diffusion in zeolites (12,14,208). When diffusional length scales become large because of disorder in zeolite structure, field theories such as the renormalization group approach can be applied. In this section, we describe the techniques and applications of these methods, focusing on how the interplay between guest–zeolite adhesion and guest–guest cohesion controls diffusion in zeolites.

A. Atomistic Methods

The goals of simulating molecular dynamics in zeolites with atomistic detail are twofold: to predict the transport coefficients of adsorbed molecules and to elucidate the mechanisms of intracrystalline diffusion. Below we discuss the basic assumptions and force fields underlying such simulations, as well as the dynamics methods used to model both rapid and activated motion through zeolites.

1. Basic Assumptions and Force Fields

a. Ordered Zeolite Models

Modeling the dynamics of sorbates in zeolites requires an adequate representation of the zeolite sorbent. Zeolites are crystalline materials, which simplifies tremendously the modeler's task as compared with the task of modeling amorphous or disordered microporous materials such as silica gels or activated carbons. Zeolite framework structures are well known from many crystallographic studies and easily accessible from reference material such as Meier and Olson's *Atlas of Zeolite Structure Types* (209), commercial (210) or internet databases (211). Moreover, the typical size of a zeolite crystallite is 1–100 μm, i.e., much larger than the length scale probed by atomistic molecular dynamics (MD) simulations. Size effects therefore can often be neglected except for single-file systems (83), and an adequate modeling of the sorbent is obtained with only a few unit cells included in the simulation cell, with periodic boundary conditions to represent the crystallite's extent.

However, a zeolite structure presents some heterogeneities at the atomistic scale: the arrangement of Si and Al atoms in the structure (or Al and P for $AlPO_4$'s) usually does not present any long-range ordering; and in the general case, extraframework cations also occupy

crystallographic positions without full occupancy or long-range ordering. The simplest way to tackle this problem is to ignore it completely; indeed, a good 80% of all MD studies of guest dynamics in zeolites published since 1997 concern aluminum-free, cation-free, defect-free, all-silica zeolite analogs rather than zeolites. These structures sometimes exist, such as silicalite-1, silicalite-2, and ZDDAY, the respective analogs of ZSM-5 (structure MFI), ZSM-11 (structure MEL), and Na-Y (structure FAU). However, the siliceous analogs sometimes do not exist but in the modeler's view, such as LTL, the analog of the cation-containing zeolite L. Nevertheless, these models can be very useful for studying the influence of zeolite structure or topology on an adsorbate's dynamics, irrespective of the cations (212), or to determine exactly, by comparison, the cations' influence (196,213). Furthermore, some zeolites of industrial interest such as ZSM-5 present high Si:Al ratios, so that their protonated forms have very few protons per unit cell. Heink *et al.* have shown, for example, that the Si:Al ratio of ZSM-5 has very little influence on hydrocarbon diffusivity (169). In these cases, it is safe to assume that studying diffusion in a completely siliceous zeolite analog will display most characteristics of diffusion in the protonated form. This assumption simplifies several factors of the simulation and of the subsequent analysis: fewer parameters for the guest–zeolite interaction potential are needed, the system does not present any heterogeneity, and electrostatic interactions can be neglected when using adequate van der Waals interaction parameters, thus decreasing the computational cost of a force evaluation.

b. Charge Distributions

There are many cases in which such a simplified representation is inadequate: in particular, exchangeable cations create an intense local electric field (amounting to 3 V/Å next to a Ca^{2+} cation in Na-A, according to induced IR measurements) (214) so that, unless the cation is inaccessible to the sorbate, one cannot neglect its Coulombic interaction with an adsorbed molecule. The number of cations in the frame depends on the Si:Al ratio: each Al atom brings one negative charge to be compensated by the adequate number of mono- or multivalent cations. Thus, the Si:Al ratio strongly influences the adsorptive properties of zeolites, so much that a change in the amount of Al brings a change in nomenclature: for example, FAU-type zeolites are denoted zeolite X for Si:Al < 1.5 and zeolite Y for Si:Al > 1.5. Many groups have investigated the distribution of Al and Si atoms in zeolites to determine whether there is any local arrangement of these atoms (215–220). Since X-ray crystallography does not distinguish Si from Al, this is necessarily determined from indirect techniques such as Si or Al NMR. Löwenstein's rule forbids any Al-O-Al bonds, which brings perfect ordering for Si:Al = 1, such as in Na-A. In most other cases, no local ordering has been found in the studies mentioned above. An exception is zeolite EMT, where rich Si and Al phases have been found from crystallographic measurements, when synthesized using crown ethers as templates (221). In zeolite L, aluminum atoms preferentially occupy T_1 rather than T_2 sites, as demonstrated by neutron crystallography (222).

In the absence of local ordering, a common modeling procedure involves neglecting the local inhomogeneity of the Si:Al distribution, and replacing all Al or Si by an average tetrahedral atom T, which is exactly what is observed crystallographically. The Si:Al ratio then is reflected by the average charge of this T atom, the charges on framework oxygen atoms, and the number of charge compensating cations. This T-site model has been used in many recent modeling studies and performs very well for reproducing adsorptive properties of zeolites (223,224). Indeed, few studies of guest adsorption in zeolites consider explicit Al and Si atoms (225–227).

The most important inhomogeneity inside cation-containing zeolites comes from the cation distribution. Indeed, except for very special values of the Si:Al ratio, the possible cation sites are not completely or symmetrically filled, and crystallographic measurements only give

average occupancies. A common procedure is to use a simplified model, with just the right Si:Al ratio that allows complete occupancy of the most probable cation sites and no cations in other sites. This has been used, e.g., by Santikary and Yashonath in their modeling of diffusion in zeolite Na-A: instead of Si:Al = 1, they used a model Na-A with Si:Al = 2, thus allowing complete occupancy of cation site I, which gives cubic symmetry of the framework (228). Similarly, Auerbach and coworkers used a model zeolite Na-Y with Si:Al = 2 in a series of studies on benzene diffusion, so that the model would contain just the right number of Na cations to fill sites I′ and II, thereby giving tetrahedral symmetry (58,196,229). In studying Na-X, which typically involves Si:Al = 1.2, they used Si:Al = 1 so that Na(III) would also be filled (196). This type of procedure is generally used to level off inhomogeneities that complicate the analysis.

It is instructive to observe the effect of the Si:Al ratio of FAU-type zeolites on the behavior of benzene diffusion, as determined from modeling (196,229,230). For very high Si:Al ratios no cations are accessible to sorbed benzene, which only experiences a weak interaction with the framework, and hence diffuses over shallow energetic barriers. These reach only 10 kJ mol^{-1} between the supercage sites and window sites, where benzene adsorbs in the plane of the 12 T-atom ring (12R) window separating two adjacent supercages (230). As the Si:Al ratio decreases toward Na-Y, cation sites II begin to fill in as indicated in Fig. 17. These Na(II) cations at tetrahedral supercage positions create strong local adsorption sites for benzene (the S_{II} site), while the window site remains unchanged. As a consequence, the energetic barrier to diffusion increases to about 40 kJ mol^{-1} (229). The spread in measured activation energies for benzene in Na-Y shown in Fig. 17 reflects both intracage and cage-to-cage dynamics (198) because both NMR relaxation data (intracage) and diffusion data (cage-to-cage) are shown. When the Si:Al ratio further decreases toward Na-X, the windows are occupied by strongly adsorbing site III cations. As a consequence, the window site is replaced by a strong S_{III} site where benzene is facially coordinated to the site III cation, so that transport is controlled by smaller energy barriers reaching only about 15 kJ mol^{-1} (196). Figure 17 (top and middle) schematically presents this behavior, while on the bottom part we compare the expected behavior of the activation energy (full line) as a function of the Si:Al ratio to the available experimental observations (points). The correlation between simulation and experiments is qualitatively reasonable considering the spread of experimental data. Figure 17 shows the success of using a particular Si:Al ratio to simplify the computation, and furthermore shows that adding cations to the structure does not necessarily result in increased diffusion activation energy.

Despite the success of treating disordered charge distributions as being ordered, Chen *et al.* have suggested that electrostatic traps created by disordered Al and cation distributions can significantly diminish self diffusivities from their values for corresponding ordered systems (148). In addition, when modeling the dynamics of exchangeable cations (231) or molecules in acidic zeolites (227), it may be important to develop more sophisticated zeolite models that completely sample Al and Si heterogeneity, as well as the possible cation distributions. For example, Newsam and coworkers proposed an iterative strategy allowing the placement of exchangeable cations inside a negatively charged framework (232), implemented within MSI's Cerius2 modeling environment. In addition, Jousse *et al.* constructed a model zeolite H-Y (Si:Al = 2.43) by randomly placing aluminum atoms in the frame, and distributing protons using the following three rules: (a) protons are linked to an oxygen close to an Al atom; (b) no two hydroxyl groups can be linked to the same silicon atom; (c) no proton can be closer than 4.0 Å from another (227). Although these rules do not completely determine the proton positions, they found that several different proton distributions were broadly equivalent as far as sorption of benzene is concerned. It is clear from the above examples that the real issue in modeling the dynamics of sorbed molecules in zeolites comes from the interaction potentials, also known as force fields when computed from empirical functional forms. Before discussing these force

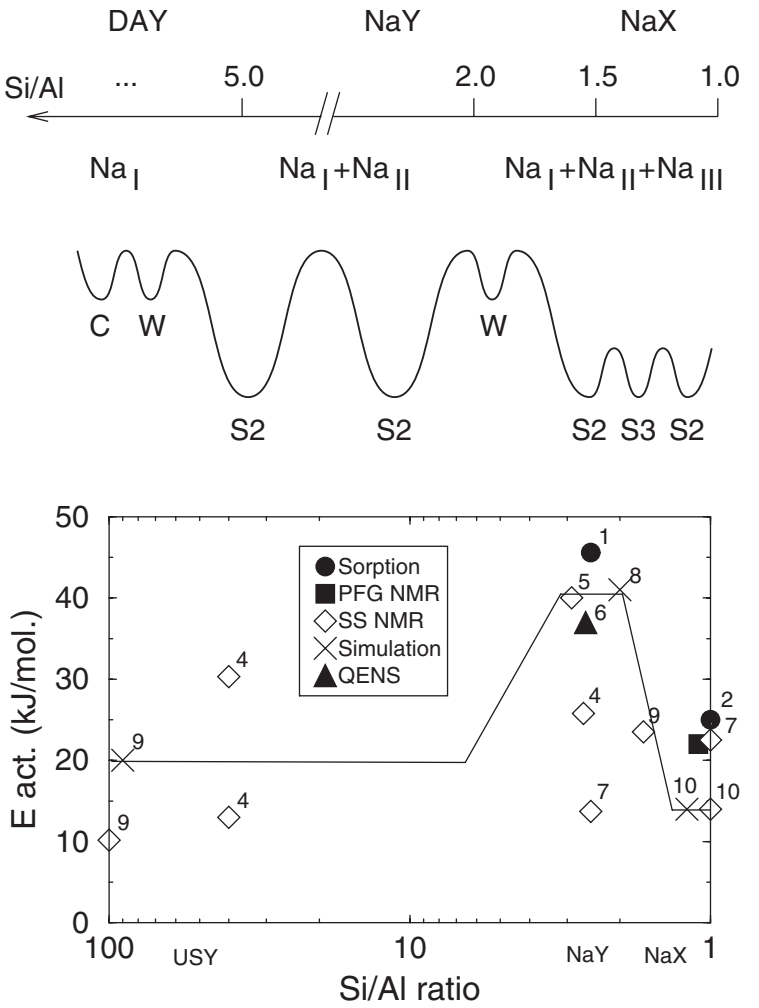

Fig. 17 Activation energies of benzene diffusion in FAU-type zeolites. The top part shows Si:Al ratios of FAU-type zeolites, with the corresponding occupied cation sites. The middle part represents schematic benzene adsorption sites and the energy barriers between them arising from different cation distributions. C is a benzene supercage site far from a cation, W is a benzene window site far from a cation, S2 is a cage site close to an S_{II} cation, S3 is a window site close to an S_{III} cation. The bottom part gives diffusion activation energies for various Si:Al ratios. The solid line shows the overall trend from simulations; symbols are particular experiment or simulation results: 1. Forni *et al.* (Ref. 400), 2. Bülow *et al.* (Ref. 378), 3. Lorenz *et al.* (Ref. 401), 4. Sousa-Gonçalves *et al.* (Ref. 195), 5. Isfort *et al.* (Ref. 201), 6. Jobic *et al.* (Ref. 179), 7. Burmeister *et al.* (Ref. 402), 8. Auerbach *et al.* (Ref. 229), 9. Bull *et al.* (Ref. 194) and 10. Auerbach *et al.* (Ref. 196).

fields in the context of dynamics, however, we examine a hot topic among scientists in the field: whether framework vibrations influence the dynamics of guest molecules in zeolites.

c. Framework Flexibility

This question has long remained an open one, but many recent studies have made systematic comparisons between fixed and flexible lattice simulations, based on several examples: methane and light hydrocarbons in silicate-1 (64,233–236), methane in cation-free LTA

(237), Lennard-Jones adsorbates in Na-A (228) and in Na-Y (238), benzene and propylene in MCM-22 (239), benzene in Na-Y (240–242), and methane in $AlPO_4-5$ (243). In cation-free zeolites, these recent studies have found that diffusivities are virtually unchanged when including lattice vibrations. Fritzsche *et al.* (237) explained earlier discrepancies on methane in cation-free LTA zeolite by pointing out that inappropriate comparisons were made between rigid and flexible framework studies. In particular, the rigid studies used crystallographic coordinates for the framework atoms, while the force field used to represent the framework vibrations gave a larger mean window size than that in the rigid case, thereby resulting in larger diffusivities in the flexible framework. By comparing with a model rigid LTA minimized using the same force field, they found almost no influence on the diffusion coefficient. Similarly, Demontis *et al.* have studied the diffusion of methane in silicalite-1, with rigid and flexible frameworks (234). They conclude that the framework vibrations do not influence the diffusion coefficient, although they affect local dynamic properties such as the damping of the velocity autocorrelation function. Following these findings, numerous recent diffusion studies of guest hydrocarbons or Lennard-Jones adsorbates in cation-free zeolites keep the framework rigid (81,166,175,185,212,244–248).

However, there are some counterexamples in cation-free zeolites. In a recent MD study of benzene and propylene in MCM-22 zeolite, Sastre *et al.* found differences between the diffusion coefficients calculated in the rigid and flexible framework cases (239). Bouyermaouen and Bellemans also observe notable differences for *i*-butane diffusion in silicalite-1 (236). Snurr *et al.* used transition state theory (TST) to calculate benzene jump rates in a rigid model of silicalite-1 (249), finding diffusivities that are one to two orders of magnitude smaller than experimental values. Forester and Smith subsequently applied TST to benzene in flexible silicalite-1 (250), finding essentially quantitative agreement with experiment, thus demonstrating the importance of including framework flexibility when modeling tight-fitting guest–zeolite systems.

Strong framework flexibility effects might also be expected for molecules in cation-containing zeolites, where cation vibrations strongly couple to the adsorbate's motions, and where diffusion is mostly an activated process. However, where a comparison between flexible- and fixed-framework calculations has been performed, surprisingly little influence has been found. This has been shown by Santikary and Yashonath for the diffusion of Lennard-Jones adsorbates of varying size in Na-A. They found a notable difference on the adsorbate density distribution and external frequencies, but not on diffusion coefficients (228). Mosell *et al.* found that the potential of mean force for the diffusion of benzene in Na-Y remains essentially unchanged when framework vibrations are included (240). Jousse *et al.* also found that the site-to-site jump probabilities for benzene in Na-Y do not change when including framework flexibility, in spite of very strong coupling between benzene's external vibrations and the Na(II) cation (242). The reasons behind this behavior remain unclear, and it is also doubtful whether these findings can be extended to other systems. Nevertheless, direct examination of the influence of zeolite vibrations on guest dynamics suggests the following: a strong influence on local static and dynamic properties of the guest, such as low-frequency spectra, correlation functions, and density distributions; a strong influence on the activated diffusion of tight-fitting guest–zeolite systems; but a small influence on diffusion of smaller molecules such as unbranched alkanes.

The preceding discussion on framework flexibility, and its impact on molecular dynamics, has the merit of pointing out the two important aspects for modeling zeolites: structural and dynamical. On the structural side, the zeolite cation distribution, channel diameters, and window sizes must be well represented. On the dynamic side, for tight-fitting host–guest systems, the framework vibrations must allow for an accurate treatment of the activation energy for molecular jumps through flexing channels and/or windows. Existing zeolite framework force fields are numerous and take many different forms, but they are

generally designed for only one of these purposes. It is beyond the scope of this chapter to review all zeolite framework force fields (11); we simply wish to emphasize that one should be very cautious in choosing the appropriate force field designed for the properties to be studied.

d. Guest–Zeolite Force Fields

The guest–framework force field is the most important ingredient for atomistic dynamic models of sorbed molecules in zeolites. Force fields for guest–zeolite interactions are at least as diverse as those for the zeolite framework—even more so, in fact, as most studies of guest molecules involve a reparameterization of potential energy functions to reproduce some typical thermodynamic property of the system, such as adsorption energies or adsorption isotherms. Since force fields are but an analytical approximation of the real potential energy surface, it is essential that the underlying physics is correctly captured by the analytical form. Every researcher working in the field has a different opinion on what the correct form should be; therefore the following discussion must necessarily remain subjective, and we refer the reader to the original articles to sample different opinions.

Physical contributions to the interaction energy between host and guest are numerous. Most important are the short-range dispersive and repulsive interactions, and the electrostatic multipolar and inductive interactions. Nicholson and coworkers developed precise potentials for the adsorption of rare gases in silicalite-1, including high-order dispersive terms (251), and have shown that all terms contribute significantly to the potential energy surface (252), with the largest contributions coming from the two- and three-body dispersion terms. Cohen de Lara and coworkers developed and applied a potential function including inductive terms for the adsorption of diatomic homonuclear molecules in A-type zeolites (253,254). Here also the induction term makes a large contribution to the total interaction energy. A general force field would have to account for all of these different contributions, but most force fields completely neglect these terms for the sake of simplicity. Simplified expressions include only a dispersive-repulsive short-ranged potential, often represented by a Lennard Jones 6–12 or a Buckingham 6-exponential potential, possibly combined with electrostatic interactions between partial charges on the zeolite and guest atoms, according to:

$$U_{ZG} = \sum_I \sum_j \left\{ \frac{q_I q_j}{r_{Ij}} - \frac{A_{Ij}}{r_{Ij}^6} + \frac{B_{Ij}}{r_{Ij}^{12}} \right\}. \tag{80}$$

In general, parameters A and B are determined by some type of combination rule from "atomic" parameters and adjusted to reproduce equilibrium properties such as adsorption energies or adsorption isotherms. It is unlikely, however, that such a potential is transferable between different guest molecules or zeolite structures. As such, the first step of any study utilizing such a simple force field on a new type of host or guest should be the computation of some reference experimental data, such as the heat of adsorption, and eventually the reparametrization of force field terms. Indeed, general-purpose force fields such as CVFF do not give generally adequate results for adsorption in zeolites (255,256).

The simplification of the force field terms can proceed further: in all-silica zeolite analogs with small channels, the electric field does not vary much across the channel and as a consequence the Coulombic term in Eq. (80) can often be neglected. This is of course not true for cation-containing zeolites, where the cations create an intense and local electric field that generally gives rise to strong adsorption sites. Since evaluating electrostatic energies is so computationally demanding, neglecting such terms allows for much longer dynamics simulations. Another common simplification is to represent CH_2 and CH_3 groups in saturated hydrocarbons as united atoms with their own effective potentials. These are very frequently used to model hydrocarbons in all-silica zeolites (175,237,244,245,257). There is, however,

active debate in the literature about whether such a simplified model can account for enough properties of adsorbed hydrocarbons (258–260).

The standard method for evaluating Coulombic energies in guest–zeolite systems is the Ewald method (261,262), which scales as $n\ln n$ with increasing number of atoms n. In 1987 Greengard and Rokhlin (263) presented the alternative "fast multipole method" (FMM) which only scales as n, and therefore offers the possibility of simulating larger systems. In general, FMM only competes with the Ewald method for systems with many thousand atoms (264) and therefore is of little use in zeolitic systems where the simulation cell can usually be reduced to a few hundreds or a few thousand atoms. However, in the special case where the zeolite lattice is kept rigid, most of the terms in FMM can be precomputed and stored; in this case, Jousse and Auerbach have shown that FMM becomes faster than Ewald summation for benzene in Na-Y (58).

This section would not be complete without mentioning the possibility of performing atomistic simulations in zeolites without force fields (265), using *ab initio* molecular dynamics (AIMD) (266,267). Following the original work of Car and Parrinello, most such studies use density functional theory and plane wave basis sets (268). This technique has been applied recently to adsorbate dynamics in zeolites (269–277). Beside the obvious interest of being free of systematic errors due to the force field, this technique also allows the direct study of zeolite catalytic activity (269–271). However, AIMD remains so time consuming that a dynamic simulation of a zeolite unit cell with an adsorbed guest only reaches a few picoseconds at most. This time scale is too short to follow diffusion in zeolites, so that current simulations are mostly limited to studying vibrational behavior (269–274). Similarly, catalytic activity is limited to reactions with activation energies on the order of thermal energies (269,271,275). However, the potential of AIMD to simulate transport coefficients has been demonstrated for simpler systems (278,279) and will likely extend to guest–zeolite systems in the near future as computers and algorithms improve.

2. Equilibrium and Nonequilibrium Molecular Dynamics

Since the first application of equilibrium MD to guest molecules adsorbed in zeolites in 1986 (280), the subject has attracted growing interest (10–14,281,282). Indeed, MD simulations provide an invaluable tool for studying the dynamic behavior of adsorbed molecules over times ranging from picoseconds to nanoseconds, thus correlating atomistic interactions to experiments that probe molecular dynamics, including solid-state NMR, PFG, NMR, inelastic neutron spectroscopy (INS), quasi-elastic neutron scattering (QENS), IR and Raman spectroscopy.

The molecular dynamics of guest molecules in zeolites is conceptually no different from MD simulations of any other nano-sized system. Classical MD involves numerically integrating classical equations of motion for a many-body system. For example, when using cartesian coordinates, one can integrate Newton's second law: $\mathbf{F}_i = m_i\mathbf{a}_i$ where m_i is the mass of the ith particle, $\mathbf{a}_i = d^2\mathbf{r}_i/dt^2$ is its acceleration, and $\mathbf{F}_i = -\Delta_{\mathbf{r}_i}V$ is the force on particle i. The crucial inputs to MD are the initial positions and velocities of all particles as well as the system potential energy function $V(\mathbf{r}_1, \mathbf{r}_2, \ldots, \mathbf{r}_n)$. The output of MD is the dynamic trajectory $[\mathbf{r}_i(t), \mathbf{v}_i(t)]$ for each particle. All modern techniques arising in the field can be applied to the simulation of zeolites, including multiple time scale techniques, thermostats, and constraints. The interested reader is referred to textbooks on the method (262,283,284), and to modern reviews (285,286). In this section we shall describe only those aspects of MD that are especially pertinent to molecules in zeolites. A comprehensive review on MD of guest molecules in zeolites was published in 1997 by Demontis and Suffritti (11). Because the review by Demontis and Suffritti discusses virtually all applications of the method up to 1996, we will limit our examples to the most recent MD studies.

a. Parameters

We estimate that the current limiting diffusivity below which adsorbate motion is too slow for equilibrium MD, is around $D_{\min} \approx 5 \times 10^{-10}$ m^2 s^{-1}, obtained by supposing that a molecule travels over 10 unit cells of 10 Å during a 20-ns MD run. This value of $D_{\min}$ is higher than most measured diffusivities in cation-containing zeolites (5), explaining why so many MD studies focus on hydrocarbons in all-silica zeolite analogs. Even then, the simplifications discussed above are required to perform MD runs of several nanoseconds in a manageable time: simple Lennard-Jones force fields on united atom interaction centers without Coulombic interactions, bond constraints on C-C bonds allowing for longer time steps, and the use of fixed frameworks.

b. Ensembles

A flexible zeolite framework typically provides an excellent thermostat for the sorbate molecules. The framework temperature exhibits minimal variations around its average value, whereas the sorbate energy fluctuates in a way consistent with the canonical ensemble. This is valid either for a microcanonical (*NVE*) ensemble run, or a canonical (*NVT*) ensemble run involving mild coupling to an external thermostat. We caution that coupling the system too strongly to an external bath will almost surely contaminate the actual sorbate dynamics.

The problem is clearly more complex when the zeolite framework is kept rigid. Ideally, one should run the dynamics in the canonical ensemble, with just the right coupling constant to reproduce the fluctuations arising from a flexible framework. However, when these fluctuations are unknown, it is not obvious whether a canonical or microcanonical run is better. In the *NVE* ensemble, the sorbate does not exchange energy with a bath, which may lead to incorrect energy statistics. This is particularly true at low loading but may remain true for higher loadings as well. Indeed, in a direct study of the kinetic energy relaxation of Lennard-Jones particles in Na-Y, Schrimpf *et al.* found that thermalization due to interactions with the framework is considerably faster than thermalization due to mutual interactions between the adsorbates (238). Therefore, it is probably better to run the dynamics in the *NVT* ensemble, with sufficiently weak coupling to an external thermostat to leave the dynamics uncontaminated. On the other hand, Jousse *et al.* have shown that for nonrigid benzene in Na-Y, there is very rapid energy redistribution from translational kinetic energy into benzene's internal vibrational degrees of freedom (242), which proceeds on a time scale comparable to the thermalization due to interactions with the flexible frame. This suggests that for sufficiently large, flexible guest molecules, the transport behavior can be adequately modeled in the *NVE* ensemble even at infinite dilution.

Although most simulations of diffusion in zeolites have focused on self diffusion for computational simplicity, we note growing interest in performing nonequilibrium MD (NEMD) simulations on guest–zeolite systems to model transport diffusion. As an aside, we note that MD experts would classify thermostatted MD, and any non-Newtonian MD for that matter, as NEMD (287,288). We shall be much more restrictive and limit the nonequilibrium behavior to studies involving an explicit gradient along the system, resulting in a net flow of particles. This is especially interesting in zeolite science because most applications of zeolites are run under nonequilibrium conditions, and also because of recent progress in the synthesis of continuous zeolite membranes (289,290) (see also Chapter 17 by Nair and Tsapatsis in this volume). In this case we seek the Fickian or transport diffusivity, discussed thoroughly in Sec. II.B; here we only wish to discuss ensembles relevant to this NEMD.

A seminal study was reported in 1993 by Maginn *et al.*, reporting NEMD calculations of methane transport diffusion through silicalite-1 (35). They applied gradient relaxation MD as well as external field MD (EFMD), simulating the equilibration of a macroscopic concentration gradient and the steady-state flow driven by an external field, respectively. They found that EFMD provides a more reliable method for simulating the linear response regime. Fritzsche *et al.*

applied NEMD methods to calculate the transport diffusivity of methane in cation-free LTA (zeolite A) (291), obtaining results in excellent agreement with the Darken equation [Eq. (29)].

Since then, NEMD methods in the grand canonical ensemble have been reported. Of particular interest is the dual-control volume–grand canonical molecular dynamics (DCV-GCMD) method, presented by Heffelfinger and van Swol (292). In this approach the system is divided into three parts: a central and two boundary regions. In the central region, regular molecular dynamics is performed, whereas in the boundary regions creation and annihilation of molecules are allowed to equilibrate the system with a given chemical potential, following the grand canonical Monte Carlo procedure. This or similar methods have been applied to the simulation of fluid-like behavior in slit pores of very small dimensions (down to a few molecular diameters) (293–298). Martin *et al.* applied DCV-GCMD to the simulation of methane permeation through thin silicalite membranes (299). They found that for very thin membranes the external surface resistance is significant, requiring large spatial separations between external surfaces and grand canonical control volumes to avoid interferences with the grand canonical statistics.

Arya *et al.* (90) compared the computational efficiencies and accuracies of DCV-GCMD and EFMD, both applied to transport diffusion in $AlPO_4$-5. The accuracies of both methods were benchmarked against equilibrium MD (EMD) calculations of the Onsager coefficient according to Eq. (56). Arya *et al.* found that EMD and EFMD yield identical transport coefficients for all systems studied. However, the transport coefficients calculated using DCV-GCMD were lower than those obtained from EMD and EFMD unless (a) a large ratio of stochastic to dynamic moves is used for each control volume, and (b) a streaming velocity is added to all inserted molecules. In general, these authors found that DCV-GCMD is much less efficient than either the EMD or EFMD techniques (90).

c. Data Analyses

Although MD becomes inefficient for modeling activated diffusion, MD can provide useful information about such transport when barriers are comparable to k_BT. In this case, MD can be used to define a coarse-grained model of diffusion (300,301). This coarse graining requires two inputs: the lattice of sites on which diffusion takes place, and the kinetic law governing the motions between those sites. The analysis of MD trajectories as a jump diffusion process allows one to determine the adsorption sites by monitoring the positions of maximal probability of the adsorbate during the dynamics (301), as well as the details of the kinetic law. It has generally been found that residence time distributions follow a simple exponential dependence, characteristic of random site-to-site jumps. In Fig. 18, we present such a residence time distribution for the example of benzene diffusing in zeolite LTL that clearly shows this signature. These observations support the usual assumption of Poisson dynamics, central to many lattice models of guest diffusion in zeolites (see Sec. V.B.1). However, one often finds correlations between jumps that complicate the coarse-grained representation of diffusion (53,54,301).

d. Dynamics of Hydrocarbons in Silicalite-1 and 10R Zeolites

Zeolite ZSM-5 is used in petroleum cracking, which explains the early interest in modeling the diffusion of alkanes in silicalite-1, the all-silica analog of ZSM-5 (62,64,65,233,234,300,302). This early work has been reviewed by Demontis and Suffritti in 1997 (11); therefore, we only wish to outline recent studies.

As pointed out earlier, the relatively rapid diffusivity of alkanes in the channels of all-silica zeolites, at room temperature or above, makes these systems perfect candidates for MD simulations. In general, very good agreement is found between MD self diffusivities and those of microscopic types of experiments, such as PFG NMR or QENS. Figure 19 gives an example of this agreement for methane and butane in silicalite-1 at 300 K (MD data slightly spread for

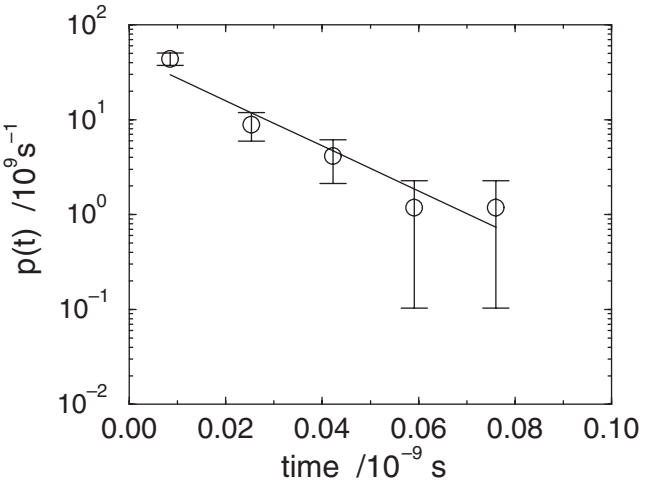

Fig. 18 Cage residence time distribution of benzene in zeolite LTL showing agreement with Poisson statistics, computed from a 1-ns molecular dynamics simulation at 800 K with a single benzene molecule in the simulation cell.

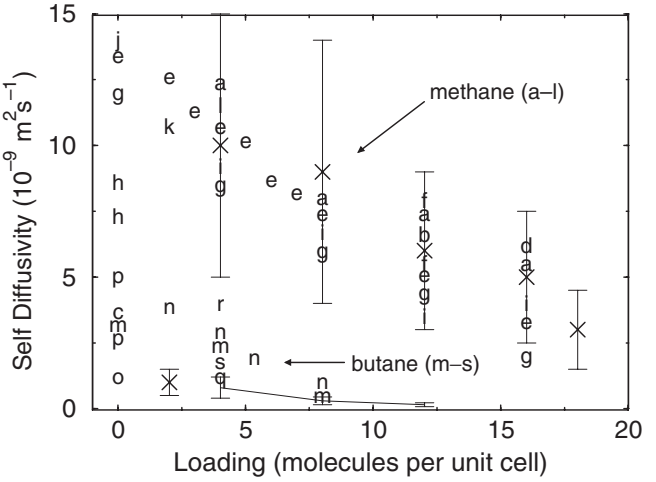

Fig. 19 Self-diffusion concentration dependence of methane and butane in silicalite-1 at 300K, from PFG NMR, QENS, and MD simulations, showing good agreement with the $(1-\theta)$ loading dependence predicted by mean field theory. Crosses are NMR data from Caro *et al.* (Ref. 2) for methane and Heink *et al.* (Ref. 169) for butane, while the star shows QENS butane data from Jobic *et al.* (Ref. 404). In all cases, error bars represent an estimated 50% uncertainty. Letters are MD results (slightly spread for clarity): a-1 for methane and m-s for butane, from the following references: (a) June *et al.* (Ref. 62), (b) Demontis *et al.* (Ref. 64), (c) Catlow *et al.* (Ref. 233), (e) Goodbody *et al.* (Ref. 65), (f) Demontis *et al.* (Ref. 234), (g) Nicholas *et al.* (Ref. 405), (h) Smirnov (Ref. 235), (i) Jost *et al.* (Ref. 185), (j) Ermoshin and Engel (Ref. 406), (k) Schuring *et al.* (Ref. 175), (l) Gergidis and Theodorou (Ref. 248), (m) June *et al.* (Ref. 300), (n) Hernández and Catlow (Ref. 407), (o) Maginn *et al.* (Ref. 171), (p) Bouyermaouen and Bellemans (Ref. 236), (q) Goodbody *et al.* (Ref. 65), (r) Gergidis and Theodorou (Ref. 248), and (s) Schuring *et al.* (Ref. 175).

clarity). This good agreement, in spite of the crudeness of the potentials used, shows that the diffusivity of light alkanes in silicalite-1 depends on the force field properly representing the host–guest steric interactions, i.e., on the size and topology of the pores. Recognizing this, many recent studies focus on comparing diffusion coefficients for different alkanes in many different zeolite topologies, in an effort to rationalize different observed catalytic behaviors. Jousse *et al.* studied the diffusion of butene isomers at infinite dilution in 10R zeolites with various topologies: TON, MTT, MEL, MFI, FER, and HEU. They observed in all cases, except for the structure TON, that *trans*-2-butene diffuses more rapidly than all other isomers (303). Webb and Grest studied the diffusion of linear decanes and *n*-methylnonanes in seven 10R zeolites: AEL, EUO, FER, MEL, MFI, MTT, and TON (212). For MEL, MTT, and MFI, they observe that the self-diffusion coefficient decreases monotonically as the branch position is moved toward the center (and the isomer becomes bulkier), whereas for the four other structures, D_s presents a minimum for another branch position, suggesting that product shape selectivity might play some role in determining the zeolite selectivity. More recently, Webb *et al.* studied linear and branched alkanes in the range $n = 7$–30 in TON, EUO, and MFI (247). Again they observe lattice effects for branched molecules, where D_s presents a minimum as a function of branch position dependent on the structure. They note also some ''resonant diffusion effect'' as a function of carbon number, noted earlier by Runnebaum and Maginn (170): the diffusivity becomes a periodic function of carbon number, due to the preferential localization of molecules along one channel and their increased diffusion in this channel. Schuring *et al.* studied the diffusion of C_1 to C_{12} in MFI, MOR, FER, and TON for different loadings (175). They also find some indication of a resonant diffusion mechanism as a function of chain length. Their study also indicates that the diffusion of branched alkanes is significantly slower than that of their linear counterparts, but only for structures with small pores where there is a tight fit between the adsorbates and the pores.

Another current direction of research concerns the diffusion of mixtures of adsorbates. Although the currently preferred atomistic simulation method applied to the adsorption of mixtures is grand canonical Monte Carlo (304–308), MD simulations are also used to determine how the dynamics of one component affects the diffusion of the other (185,248,257,309). Sholl and Fichthorn investigated how a binary mixture of adsorbates diffuses in unidirectional pores (309), finding a dual mode of diffusion for certain mixtures, wherein one component undergoes normal unidirectional diffusion while the other performs single-file diffusion. Jost *et al.* studied the diffusion of mixtures of methane and xenon in silicalite-1 (185). They find that the diffusivity of methane decreases strongly as the loading of Xe increases whereas the diffusivity of Xe is nearly independent of the loading of methane, which they attribute to the larger mass and heat of adsorption of Xe. On the other hand, Gergidis and Theodorou in their study of mixtures of methane and *n*-butane in silicalite-1 (248) found that the diffusivity of both molecules decreases monotonically with increasing loading of the other. Both groups report good agreement with PFG NMR (185) and QENS experiments (257).

e. Single-File Diffusion

Single-file diffusion designates the particular collective motion of particles diffusing along a one-dimensional channel and unable to pass each other. As already mentioned, in that case the long-time motions of the particles are completely correlated, so that the limit of the MSD depends on the boundaries of the system. Exact treatments using lattice models show that the MSD has three limiting dependencies with time (310,311): plateau for fixed boundaries, linear with t for periodic boundaries or open boundaries (83), and $\sqrt{t}$ for infinite pore length. Experimental evidence for the existence of single-file behavior in unidimensional zeolites (76,78,180,312) has prompted renewed interest in the subject during the last few years

(83,84,245,246,313–316). In particular, several MD simulations of more or less realistic single-file systems have been performed in order to determine whether the single-file $\sqrt{t}$ regime is not an artifact of the simple lattice model on which it is based (81,245,246,315,316). Since the long-time motions of the particles in the MD simulations are necessarily correlated, great care must be taken to adequately consider the system boundaries. In particular, when using periodic boundary conditions, the system size along the channel axis must be sufficiently large to avoid the linear behavior due to the diffusion of the complete set of molecules.

Hahn and Kärger studied the diffusion of Lennard-Jones particles along a straight tube in three cases: (a) without external forces acting on the particles from the tube, (b) with random forces, and (c) with a periodic potential from the tube (316). They find for the no-force case that the MSD is proportional to t, whereas for random forces and a periodic potential it is proportional to $\sqrt{t}$, in agreement with the random walk model. Keffer *et al.* performed MD simulations of Lennard-Jones methane and ethane in an atomistic model of $AlPO_4-5$ (315). The methane molecules, which are able to pass each other, display undirectional but otherwise normal diffusion with the MSD linear with t whereas ethane molecules, which have a smaller probability to pass each other, display single-file behavior with an MSD proportional to $\sqrt{t}$. For longer times, however, the nonzero probability to pass each other destroys the single-file behavior for ethane. Similar behavior was found by Tepper *et al.* (81). Sholl and coworkers investigated the diffusion of Lennard-Jones particles in a model $AlPO_4-5$ (84,245,246) and found that diffusion along the pores can occur *via* concerted diffusion of weakly bound molecular clusters, composed of several adsorbates. These clusters can jump with much smaller activation energies than that of a single molecule. However, the MSD retains its single-file $\sqrt{t}$ signature because all of the adsorbates in a file do not collapse to form a single supramolecular cluster.

These MD simulations of unidirectional and single-file systems confirm the lattice gas prediction that the MSD is proportional to $\sqrt{t}$. They also show that whenever a certain crossing probability exists, this single-file behavior disappears at long times, to be replaced by normal diffusion. Similar "anomalous" diffusion regimes, with the MSD proportional to t at long times and to t^{α} with $\alpha < 1$ at short times, have also been found in other systems that do not satisfy the single-file criteria, such as *n*-butane in silicalite-1 at high loadings (248). Therefore, one should be very careful to define exactly the time scale of interest when working with single-file or other highly correlated systems.

3. Transition State Theory and Dynamical Corrections

As discussed above in Sec. V.A.2, the smallest diffusivity that can be simulated by MD methods is well above most measured values in cation-containing zeolites (5), explaining why so many MD studies focus on hydrocarbons in all-silica zeolite analogs. This issue has been addressed by several groups within the last 10 years (317), by applying reactive flux molecular dynamics (23,318) (RFMD) and TST (319), to model the dynamics of rare events in zeolites. This subject has been reviewed very recently (12,14); as a result, we give below only a brief outline of the theory.

a. Rare Event Theory

The standard *ansatz* in TST is to replace the dynamically converged, net reactive flux from reactants to products with the instantaneous flux through the transition state dividing surface. TST is inspired by the fact that, although a dynamic rate calculation is rigorously independent of the surface through which fluxes are computed (320), the duration of dynamics required to converge the net reactive flux is usually shortest when using the transition state dividing

surface. The TST approximation can be formulated for gas phase or condensed phase systems (23,318,321), using classical or quantum mechanics (322). The rate coefficient for the jump from site i to site j can be expressed classically as (23,318):

$$k_{i\to j} = k_{i\to j}^{\mathrm{TST}} \times f_{ij}, \tag{81}$$

where $k_{i\to j}^{\mathrm{TST}}$ is the TST rate constant, and f_{ij} is the dynamic correction factor also known as the classical transmission coefficient. The TST rate constant is given by:

$$k_{i\to j}^{\mathrm{TST}} = \frac{1}{2}\left(\frac{2k_{\mathrm{B}}T}{\pi m}\right)^{1/2}\frac{Q^{\ddagger}}{Q_i}, \tag{82}$$

where m is the reduced mass associated with the reaction coordinate, $Q^{\ddagger}$ is the configurational partition function on the dividing surface, and Q_i is the configurational partition function in the reactant state i. The last expression can be evaluated without recourse to dynamics, either by Monte Carlo simulation (323) or in the harmonic approximation by normal-mode analysis (324). The dynamic correction factor is usually evaluated from short MD simulations originating on the dividing surface. For classical systems, f_{ij} always takes a value between 0 and 1, and gives the temperature-dependent fraction of initial conditions on the dividing surface that initially point to products *and* eventually give rise to reaction.

When one has an educated guess regarding the reaction coordinate but no knowledge of the transition state or the dividing surface, a reliable but computationally expensive solution is to calculate the free-energy surface along a prescribed path from one free-energy minimum to another. The free-energy surface, $F(x_0)$, which is also known as the potential of mean force and as the reversible work surface, is given by:

$$F(x_0) = -k_B T \ln[L\langle\delta(x - x_0)\rangle] = -k_B T \ln Q(x_0), \tag{83}$$

where x is the assumed reaction coordinate, x_0 is the clamped value of x during the ensemble average over all other coordinates, the length L is a formal normalization constant that cancels when computing free energy differences, and $Q(x_0)$ is the partition function associated with the free energy at x_0. In terms of the free-energy surface, the TST rate constant is given by:

$$k_{i\to j}^{\mathrm{TST}} = \frac{1}{2}\left(\frac{2k_{\mathrm{B}}T}{\pi m}\right)^{1/2}\frac{e^{-\beta F(x^{\ddagger})}}{\int_i dx e^{-\beta F(x)}} \tag{84}$$

where the integral over x is restricted to the reactant region of configuration space. Computing TST rate constants is therefore equivalent to calculating free-energy differences. Numerous methods have been developed over the years for computing $e^{-\beta F(x)}$, many of which fall under the name umbrella sampling or histogram window sampling (23,284).

While Eqs. (80–83) are standard expressions of rare event theory, the exact way in which they are implemented depends strongly on the actual system of interest. Indeed, if the transition state dividing surface is precisely known (as for the case of an adatom), then $k_{i\to j}^{\mathrm{TST}}$ provides a good first approximation to the rate coefficient, and the dynamic correction factor accounts for the possibility that the particle does not thermalize in the state it has first reached but instead goes on to a different final state. This process is called *dynamic recrossing* if the final state is identical to the original state, and otherwise is called *multisite jumping*. The importance of dynamic recrossing or multisite jumping depends on a number of factors, of which the height of the energy barriers and the mechanism of energy dissipation are essential.

For example, the minimal energy path for benzene to jump from a cation site to a window site in Na-Y is shown in Fig. 20, alongside the corresponding energy plot (229). Despite benzene's anisotropy, a reasonable model for the cation↔window dividing surface turns out to

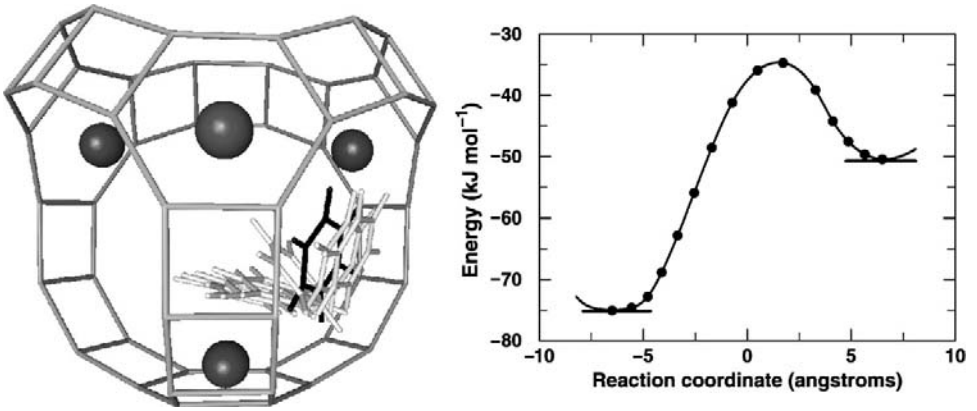

Fig. 20 Cation↔ window path for benzene in Na-Y (transition state indicated in bold), with a calculated barrier of 41 kJ mol^{-1}. (From Ref. 229.)

be the plane perpendicular to the three-dimensional vector connecting the two sites. This simple approach yields dynamic correction factors mostly above 0.5 (58).

In a complex system with many degrees of freedom it might be difficult, or even impossible, to define rigorously the dividing surface between the states. In this case, the transition state approximation may fail, requiring the calculation of f_{ij}. Indeed, TST assumes that all trajectories initially crossing the dividing surface in the direction of the product state will eventually relax in this state. This statement will be qualitatively false if the supposed surface does not coincide with the actual dividing surface. In this case, the dynamic correction factor corrects TST for an inaccurately defined dividing surface, even when dynamic recrossings through the actual dividing surface are rare. The problem of locating complex dividing surfaces has recently been addressed using topology (325), statistics (326), and dynamics (327,328).

b. Siliceous Zeolite

June *et al.* reported the first application of TST dynamically corrected with RFMD for a zeolite–guest system in 1991 (317), modeling the diffusion of Xe and "spherical SF_6" in silicalite-1. This system is sufficiently weakly binding that reasonably converged MD simulations could be performed for comparison with the rare event dynamics, showing excellent quantitative agreement in the diffusivities obtained. The dynamic correction factors obtained by June *et al.* show that recrossings can diminish rate coefficients by as much as a factor of about 3 and that multisite jumps along straight channels in silicalite-1 (53) contribute to the well-known diffusion anisotropy in MFI-type zeolites (60). Jousse and coworkers reported a series of MD studies on butene isomers in all-silica channel zeolites MEL and TON (301,329). Because the site-to-site energy barriers in these systems are comparable to the thermal energies studied in the MD simulations, rare-event dynamics need not apply. Nonetheless, Jousse and coworkers showed that even for these relatively low-barrier systems, the magnitudes and loading dependencies of the MD diffusivities could be well explained within a jump diffusion model, with residence times extracted from the MD simulations.

As discussed in Sec. V.A.1, Snurr *et al.* applied harmonic TST to benzene diffusion in silicalite-1, assuming that benzene and silicalite-1 remain rigid, by using normal-mode analysis for the six remaining benzene degrees of freedom (249). Their results underestimate

experimental diffusivities by one to two orders of magnitude, probably more from assuming a rigid zeolite than from using harmonic TST. Forester and Smith subsequently applied TST to benzene in silicalite-1 using constrained reaction coordinate dynamics on both rigid and flexible lattices (250). Lattice flexibility was found to have a very strong influence on the jump rates. Diffusivities obtained from the flexible framework simulations are in excellent agreement with experiment, overestimating the measured room temperature diffusivity (2.2×10^{-14} m^2 s^{-1}) by only about 50%. These studies suggest that including framework flexibility is very important for bulkier guest molecules, which may require framework distortions to move along zeolite channels or through windows separating zeolite cages.

c. Cation-Containing Zeolites

Mosell *et al.* reported a series of TST and RFMD calculations on Xe in Na-Y (330,331) in 1996, and benzene and *p*-xylene in Na-Y (240,241) in 1997. They calculated the reversible work of dragging a guest species along the cage-to-cage (110) axis of Na-Y and augmented this version of TST with dynamic corrections. In addition to computing the rate coefficient for cage-to-cage motion through Na-Y, Mosell *et al.* confirmed that benzene window sites are free-energy local minima, while *p*-xylene window sites are free-energy maxima, i.e., cage-to-cage transition states (240,241). Mosell *et al.* also found relatively small dynamic correction factors, ranging from 0.08 to 0.39 for benzene and 0.24 to 0.47 for *p*-xylene.

At about the same time in 1997, Jousse and Auerbach reported TST and RFMD calculations of specific site-to-site rate coefficients for benzene in Na-Y (58), using Eq. (81) with jump-dependent dividing surfaces. As with Refs. 240 and 241, Jousse and Auerbach found that benzene jumps to window sites could be defined for all temperatures studied. Jousse and Auerbach were unable to use TST to model the window → window jump because they could not visualize simply the anisotropy of the window → window-dividing surface. For jumps other than window → window, they found dynamic correction factors mostly above 0.5, suggesting that these jump-dependent dividing surfaces coincide closely with the actual ones. Although the flavors of the two approaches for modeling benzene in Na-Y differed, the final results were remarkably similar considering that different force fields were used. In particular, Mosell *et al.* used MD to sample dividing surface configurations, whereas Jousse and Auerbach applied the Voter displacement-vector Monte Carlo method (323) for sampling dividing surfaces. The apparent activation energy for cage-to-cage motion in our study is 44 kJ mol^{-1}, in very reasonable agreement with 49 kJ mol^{-1} obtained by Mosell *et al.*

d. Finite Loadings

Tunca and Ford reported TST rate coefficients for Xe cage-to-cage jumps at high loadings in ZK-4 zeolite, the siliceous analog of Na-A (structure LTA) (332). These calculations deserve several remarks. First, because this study treats multiple Xe atoms simultaneously, defining the reaction coordinate and dividing surface can become quite complex. Tunca and Ford addressed this problem by considering averaged cage sites, instead of specific intracage sorption sites, which is valid because their system involves relatively weak zeolite–guest interactions. They further assume a one-body reaction coordinate and dividing surface regardless of loading, which is tantamount to assuming that the window separating adjacent α cages in ZK-4 can only hold one Xe at a time and that cooperative many-Xe cage-to-cage motions are unlikely. Second, Tunca and Ford advocate separate calculations of $Q^{\ddagger}$ and Q_i for use in Eq. (82), as opposed to the conventional approach of calculating ratios of partition functions, i.e., free energies (323). It is not yet obvious whether separation of these calculations is worth the effort. Third, Tunca and Ford developed a recursive algorithm for building up $(N + 1)$-body partition functions from N-body partition functions, using the "test particle" method developed for

modeling the thermodynamics of liquids. Although the approach of Tunca and Ford has a restricted regime of applicability, it nonetheless seems promising in its direct treatment of many-body diffusion effects.

e. Free Energy Surfaces

Maginn *et al.* performed reversible work calculations with a TST flavor on long-chain alkanes in silicalite-1 (171), finding that diffusivities monotonically decrease with chain length until about *n*-C_8, after which diffusivities plateau and become nearly constant with chain length. Bigot and Peuch calculated free-energy surfaces for the penetration of *n*-hexane and isooctane into a model of H-mordenite zeolite with an organometallic species, $Sn(CH_3)_3$, grafted to the pore edge (333). Bigot and Peuch found that $Sn(CH_3)_3$ has little effect on the penetration barrier of *n*-hexane, but they predict that the organometallic increases the penetration barrier of isooctane by 60 kJ mol^{-1}. Sholl computed the free-energy surface associated with particle exchange of Ar, Xe, methane, and ethane in $AlPO_4-5$, a one-dimensional channel zeolite (334), suggesting time scales over which anomalous single-file diffusion is expected in such systems.

Jousse *et al.* modeled benzene site-to-site jumps in H-Y zeolite (Si:Al = 2.43) using a force field that explicitly distinguishes Si and Al, as well as oxygens in Si-O-Si, Si-O-Al, and Si-OH-Al environments (227). Such heterogeneity creates many distinct adsorption sites for benzene in H-Y. Multiple paths from site to site open as the temperature increases. To simplify the picture, Jousse *et al.* computed the free-energy surface for benzene motion along the (110) axis in H-Y, which produces cage-to-cage migration. Due to the multiplicity of possible cage-to-cage paths, the temperature dependence of the cage-to-cage rate constant as computed by umbrella sampling exhibits strong non-Arrhenius behavior. These calculations may help to explain intriguing NMR correlations times for benzene in H-Y, which also exhibit striking non-Arrhenius temperature dependencies (195).

f. Quantum Dynamics

Of all the dynamics studies performed on zeolites, very few have explored the potentially quantum mechanical nature of nuclear motion in micropores (335–338). Quantum modeling of proton transfer in zeolites (336,338,339) seems especially important because of its relevance in catalytic applications. Such modeling will become more prevalent in the near future, partially because of recent improvements in quantum dynamics approaches (338), but mostly because of novel electronic structure methods developed by Sauer and coworkers (340,341), which can accurately compute transition state parameters for proton transfer in zeolites by embedding a quantum cluster in a corresponding classical force field.

To facilitate calculating quantum rates for proton transfer in zeolites, Fermann and Auerbach developed a novel semiclassical transition state theory (SC-TST) for truncated parabolic barriers (338), based on the formulation of Hernandez and Miller (342). Our SC-TST rate coefficient is stable to arbitrarily low temperatures as opposed to purely harmonic SC-TST, and has the form $k^{\text{SC-TST}} = k^{\text{TST}} \cdot \Gamma$ where the quantum transmission coefficient, Γ, depends on the zero-point corrected barrier and the barrier curvature. To parameterize this calculation, Fermann *et al.* performed high-level cluster calculations (339) yielding an O(1) $\rightarrow$ O(4) zero-point corrected barrier height of 86.1 kJ mol^{-1}, which becomes 97.1 kJ mol^{-1} when including long-range effects from the work of Sauer *et al.* (340). Using this new approach, Fermann and Auerbach calculated rate coefficients and crossover temperatures for the O(1) $\rightarrow$ O(4) jump in H-Y and D-Y zeolites, yielding crossover temperatures of 368 K and 264 K, respectively. These results suggest that *tunneling dominates proton transfer* in H-Y up to and slightly above room temperature, and that true proton transfer barriers are being underestimated as a result of neglect of tunneling in the interpretation of experimental mobility data.

B. Lattice Models

When modeling strongly binding or tight-fitting guest–zeolite systems, theoretical methods specialized for rare event dynamics such as TST and kinetic Monte Carlo (KMC) are required. These methods are applied by coarse graining the molecular motions, keeping only their diffusive character. In zeolites, the well-defined cage and channel structure naturally orients this coarse-graining toward *lattice models*, which are the focus of this section.

The simplest such model was proposed by Ising in 1925 (343). Many variants of the Ising model have since been applied to study activated surface diffusion (57). Although in principle a lattice can be regarded simply as a numerical grid for computing configurational integrals required by statistical mechanics (344), the grid points can have important physical meaning for dynamics in zeolites, as shown schematically in Fig. 21. Applying lattice models to diffusion in zeolites rests on several (often implicit) assumptions on the diffusion mechanism; here we recall those assumptions and analyze their validity for modeling dynamics of sorbed molecules in zeolites.

1. Basic Assumptions

a. Temperature-Independent Lattice

Lattice models of transport in zeolites begin by assuming that diffusion proceeds by activated jumps over free-energy barriers between well-defined adsorption sites, i.e., that site residence times are much longer than travel times between sites. These adsorption sites are positions of high probability, constructed either from energy minima, e.g., next to cations in cation-containing zeolites, and/or from high volume, e.g., channel intersections in silicalite-1. Silicalite-1 provides a particularly illustrative example (249): its usual description in terms of adsorption sites involves two distinct channel sites, where the adsorbate is stabilized by favorable energy contacts with the walls of the 10R channels; and an intersection site at the

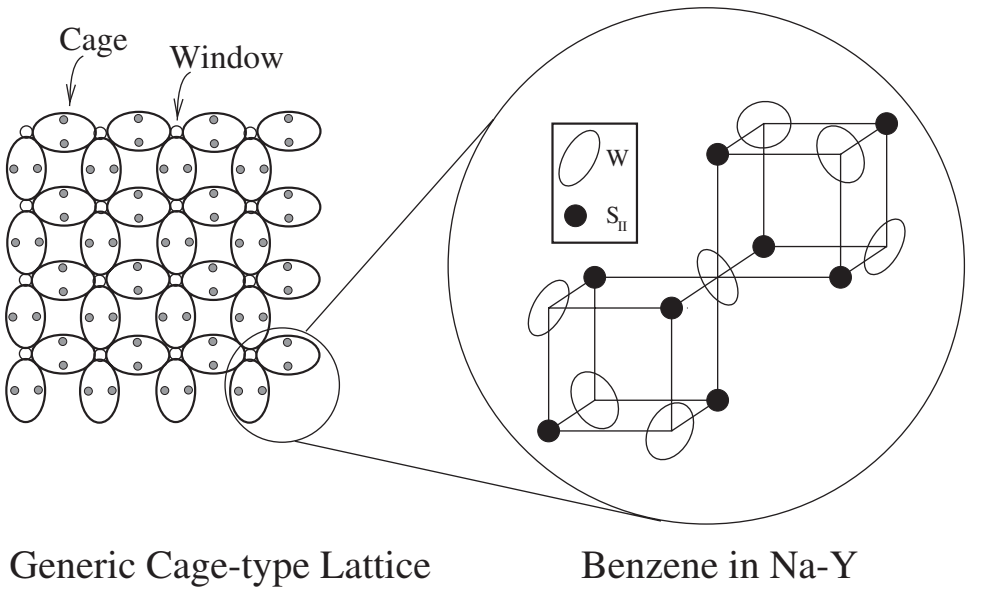

Fig. 21 Schematic lattice model for molecules in cage-type zeolites, showing cages, intracage sites, and window sites (left), as well as the specific lattice geometry for benzene in Na-Y zeolite (right).

crossing between the two-channel systems, where the large accessible volume compensates entropically for less favorable contacts (see Fig. 2). Depending on the temperature, one or both types of sites can be populated simultaneously.

The silicalite-1 example points to the breakdown of the first assumption inherent in lattice models, namely, that adsorption and diffusion of guests in zeolites proceeds on a fixed lattice of sites, independent of external thermodynamic variables such as temperature. Clearly this is not the case. Indeed, when k_BT becomes comparable with the activation energy for a jump from site i to site f, a new lattice that subsumes site i into site f may be more appropriate (53). Alternatively, one may retain site i with modifications to the lattice model discussed below, taking into account so-called kinetic correlations that arise from the relatively short residence times in site i (53,54,301).

b. Poisson Statistics

The second assumption inherent in most lattice models of diffusion, which is related to the first, is that subsequent jumps of a given molecule are uncorrelated from each other, i.e., that a particular site-to-site jump has the same probability to occur at any time. This assumption results in a site residence time distribution that follows the exponential law associated with Poisson statistics (345). In Fig. 18 we have seen that such a law can result from the analysis of MD trajectories. Consequently, lattice models can often be mapped onto master rate equations such as those in the chemical kinetics of first-order reactions (345,346). This fact highlights the close connection between reaction and diffusion in zeolites, when modeled with lattice dynamics.

Deviations from Poisson statistics would also arise if a molecule were most likely to jump in phase with a low-frequency zeolite framework vibration, such as a window breathing mode (347), or if a molecule were more likely to jump in concert with another guest molecule. An extreme case of this latter effect was predicted by Sholl and Fichthorn (84,245), wherein strong adsorbate–adsorbate interactions in single-file zeolites generated transport dominated by correlated cluster dynamics instead of single-molecule jumps. In this case, a consequence of Poisson statistics applied to diffusion in zeolites at finite loadings ceases to hold, namely, there no longer exists a time interval sufficiently short that only one molecule can jump at a time.

c. Loading-Independent Lattice

The final assumption, which is typically invoked by lattice models of diffusion at finite loadings, is that the sites do not qualitatively change their nature with increasing adsorbate loading. This assumption holds when adsorption sites are separated by barriers such as windows between large cages (332), and also when host–guest interactions dominate guest–guest interactions. This loading-independent lattice model breaks down when the effective diameter of guest molecules significantly exceeds the distance between adjacent adsorption sites, as high loadings create unfavorable excluded-volume interactions between adjacent guests. This effect does not arise for benzene in Na-Y (52), which involves site-to-site distances and guest diameters both around 5 Å, but is predicted for Xe in Na-A by classical density functional theory calculations (348).

Despite these many caveats, lattice models have proven extremely useful for elucidating qualitatively and even semiquantitatively the following physical effects regarding (a) host structure: pore topology (56,349,350), diffusion anisotropy (27,60), pore blockage (351), percolation (352), and open-system effects (27,83); (b) host–guest structure: site heterogeneity (31,32) and reactive systems (353); and (c) guest–guest structure: attractive interactions (329,349,350), phase transitions (354,355), concerted cluster dynamics (84,245), single-file diffusion (9,83), and diffusion of mixtures (309,356,357). In what follows, we outline the theory and simulation methods used to address these issues.

2. Equilibrium and Nonequilibrium Kinetic Monte Carlo

Kinetic Monte Carlo (KMC) models diffusion on a lattice as a random walk composed of uncorrelated, single-molecule jumps as discussed above, thereby providing a stochastic solution to the dynamics associated with the lattice model. Although KMC models transport as sequences of uncorrelated events in the sense that jump times are extracted from Poisson distributions, KMC does account for spatial correlations at finite loadings. Indeed, when a molecule executes a jump at higher loadings, it leaves behind a vacancy that is likely to be occupied by a successive jump, thereby diminishing the diffusivity from the mean field theory estimate, as discussed in Sec. III.B.

KMC is isomorphic to the more conventional Monte Carlo algorithms (262), except that in a KMC simulation random numbers are compared to ratios of rate coefficients, instead of ratios of Boltzmann factors. However, if the pre-exponential factors cancel in a ratio of rate coefficients, then a ratio of Boltzmann factors arises, where the relevant energies are *activation energies*. KMC formally obeys detailed balance, meaning that all thermodynamic properties associated with the underlying lattice Hamiltonian can be simulated with KMC. In addition to modeling transport in zeolites, KMC has been used to model adsorption kinetics on surfaces (358), and even surface growth itself (359).

a. Algorithms

KMC can be implemented with either constant time-step or variable time-step algorithms. Variable time-step methods are efficient for sampling jumps with widely varying time scales, while fixed time-step methods are convenient for calculating ensemble averaged correlation functions. In the constant time-step technique, jumps are accepted or rejected based on the kinetic Metropolis prescription, in which a ratio of rate coefficients, $k_{\text{hop}}/k_{\text{ref}}$, is compared with a random number (198,360). Here k_{ref} is a reference rate that controls the temporal resolution of the calculation according to $\Delta t_{\text{bin}} = 1/k_{\text{ref}}$. The probability to make a particular hop is proportional to $k_{\text{hop}}/k_{\text{ref}}$, which is independent of time, leading naturally to a Poisson distribution of jump times in the simulation. In the fixed time-step algorithm, all molecules in the simulation attempt a jump during the time Δt_{bin}. In order to accurately resolve the fastest molecular jumps, k_{ref} should be greater than or equal to the largest rate constant in the system, in analogy with choosing time steps for MD simulations. However, if there exists a large separation in time scales between the most rapid jumps, e.g., intracage motion, and the dynamics of interest, e.g., cage-to-cage migration, then one may vary k_{ref} to improve efficiency. The cost of this modification is detailed balance; indeed, tuning k_{ref} to the dynamics of interest is tantamount to simulating a system where all the rates larger than k_{ref} are replaced with k_{ref}.

A useful alternative for probing long-time dynamics in systems with widely varying jump times is variable time-step KMC. In the variable time-step technique, a hop is made every KMC step and the system clock is updated accordingly (351,361). For a given configuration of random walkers, a process list of possible hops from occupied to empty sites is compiled for all molecules. A particular jump from site i to j is chosen from this list with a probability of $k_{i\rightarrow j}/k_{\text{tot}}$, where k_{tot} is the sum of all rate coefficients in the process list. In contrast to fixed time-step KMC, where *all* molecules *attempt* jumps during a KMC step, in variable time-step KMC a *single* molecule *executes* a jump every KMC step and the system clock is updated by an amount $\Delta t_n = -\ln(1 - x)/k_{\text{tot}}$, where $x \in [0,1)$ is a uniform random number and n labels the KMC step. This formula results directly from the Poisson distribution, suggesting that other formulas may be used in variable time-step KMC to model kinetic correlations (301). In general, we suggest that simulations be performed using the variable time-step method, with data analyses carried

out by mapping the variable time-step KMC trajectories onto a fixed time-step grid (346), as discussed in Sec. V.B.2.

b. Ensembles

Guest–zeolite systems at equilibrium are inherently multicomponent systems at constant temperature and pressure. Since guest molecules are continually adsorbing and desorbing from more or less fixed zeolite particles, a suitable ensemble would fix N_z = amount of zeolite, μ_G = chemical potential of guest, p = pressure, and T = temperature, keeping in mind that μ_G and p are related by the equation of state of the external fluid phase. However, constant-pressure simulations are very challenging for lattice models, since constant pressure implies volume fluctuations, which for lattices involve adding or deleting whole adsorption sites. As such, constant-volume simulations are much more natural for lattice dynamics. Since both the volume and amount of zeolite is virtually fixed during intracrystalline adsorption and diffusion of guests, we need to specify only one of these variables. In lattice simulations it is customary to specify the number of adsorption sites, N_{sites}, which plays the role of a unitless volume. We thus arrive at the natural ensemble for lattice dynamics in zeolites: the grand canonical ensemble, which fixes μ_G, N_{sites}, and T.

The overwhelming majority of KMC simulations applied to molecules in zeolites have been performed using the canonical ensemble, which fixes N_G = number of guest molecules, N_{sites}, and T. Although the adsorption-desorption equilibrium discussed above would seem to preclude using the canonical ensemble, fixing N_G is reasonable if zeolite particles are large enough to make the relative root-mean-square fluctuations in N_G rather small. Such closed-system simulations are usually performed with periodic boundary conditions, in analogy with atomistic simulations (262,284). Defining the fractional loading, θ, by $\theta \equiv N_G/N_{sites}$, typical KMC calculations produce the self-diffusion coefficient D_s as a function of T at fixed θ for Arrhenius analysis, or as a function of θ at fixed T, a so-called diffusion isotherm.

There has recently been renewed interest in grand canonical KMC simulations for three principal reasons: to relax periodic boundary constraints to facilitate exploration of single-file diffusion with lattice dynamics (83), to study nonequilibrium permeation through zeolites membranes (27), and in general to explore the interplay between adsorption and diffusion in zeolites (305,362,363). Grand canonical KMC requires that the lattice contain at least one edge that can exchange particles with an external phase. In contrast to grand canonical MC used to model adsorption, where particle insertions and deletions can occur anywhere in the system, grand canonical KMC must involve insertions and deletions only at the edges in contact with external phases, as shown in Fig. 1a–c.

The additional kinetic ingredients required by grand canonical KMC are the rates of adsorption to and desorption from the zeolite (364). Because desorption generally proceeds with activation energies close to the heat of adsorption, desorption rates are reasonably simple to estimate. However, adsorption rates are less well known because they depend on details of zeolite crystallite surface structure. Qualitative insights on rates of penetration into microporous solids are beginning to emerge (365,366), as well as zeolite-specific models of such penetration phenomena (299,333,367). Calculating precise adsorption rates may not be crucial for parameterizing qualitatively reliable simulations because adsorption rates are typically much larger than other rates in the problem. For sufficiently simple lattice models, adsorption and desorption rates can be balanced to produce the desired loading according to the adsorption isotherm (27). If one assumes that the external phase is an ideal fluid, then insertion frequencies are proportional to pressure p. As such, equilibrium grand canonical KMC produces the self-diffusion coefficient as a function of p and T. Alternatively, for nonequilibrium systems involving different insertion frequencies on either site of the membrane, arising from a pressure

(chemical potential) gradient across the membrane, grand canonical KMC produces the Fickian or transport diffusion coefficient, D, as a function of T and the local loading in the membrane.

c. Models of Finite Loading

The great challenge in performing KMC simulations at finite loadings is that the rate coefficients $\{k_{i\to j}\}$ should depend on the local configuration of molecules because of guest–guest interactions. That is, in compiling the process list of allowed jumps and associated rate constants on the fly of a KMC simulation, TST or related calculations should be performed to account for the effect of specific guest configurations on the jump rate coefficients. To date, this "*ab initio* many-body KMC" approach has not been employed because of its daunting computational expense. Instead, researchers either ignore how guest–guest interactions modify rate coefficients for site-to-site jumps; or they use many-body MD at elevated temperatures when guest–guest interactions cannot be ignored (327,328).

A popular approach for modeling many-body diffusion in zeolites with KMC is thus the "site-blocking model," whereby guest–guest interactions are ignored, except for exclusion of multiple-site occupancy. This model accounts for entropic effects of finite loadings but not energetic effects. Calculating the process list and available rate coefficients becomes particularly simple; one simply sums the available processes using rates calculated at infinite dilution (368). This model is attractive to researchers in zeolite science (369) because blocking of cage windows and channels by large, aromatic molecules that form in zeolites, i.e., "coking," is a problem that zeolite scientists need to understand and eventually control.

The site-blocking model ignores guest–guest interactions that operate over medium- to long-length scales, which modify jump activation energies for site-to-site rate coefficients depending on specific configurations of neighboring adsorbates. By incorporating these additional interactions, diffusion models reveal the competition between guest–zeolite adhesion and guest–guest cohesion (329,370,371). Qualitatively speaking, the diffusivity is generally expected to increase initially with increasing loading when repulsive guest–guest interactions decrease barriers between sites and to decrease otherwise. At very high loadings, site blocking lowers the self-diffusivity regardless of the guest–guest interactions.

To develop a quantitative model for the effects of guest–guest attractions, Saravanan *et al.* proposed a "parabolic jump model," which relates binding energy shifts to transition state energy shifts (31,55). This method was implemented for lattice gas systems whose thermodynamics is governed by the following Hamiltonian:

$$H(\vec{n}) = \sum_{i=1}^{M} n_i f_i + \frac{1}{2}\sum_{i,j=1}^{M} n_i J_{ij} n_j \tag{85}$$

where M is the number of sites in the lattice, $\vec{n} = (n_1, n_2, \cdots, n_m)$ are site occupation numbers listing a configuration of the system, and $f_i = \varepsilon_i - T_{Si}$ is the free energy for binding in site i. In Eq. (85), J_{ij} is the nearest neighbor interaction between sites i and j, i.e., $J_{ij} = 0$ if sites i and j are not nearest neighbors.

Saravanan *et al.* assumed that the minimal energy hopping path connecting adjacent sorption sites is characterized by intersecting parabolas, shown in Fig. 22, with the site-to-site transition state located at the intersection point. For a jump from site i to site j, with $i, j = 1,\ldots, M$, the hopping activation energy including guest–guest interactions is given by:

$$E_a(i,j) = E_a^{(0)}(i,j) + \Delta E_{ij}\left(\frac{1}{2} + \frac{\delta E_{ij}^{(0)}}{k_{ij}a_{ij}^2}\right) + \Delta E_{ij}^2\left(\frac{1}{2k_{ij}a_{ij}^2}\right) \tag{86}$$

where $E_a{}^{(0)}(i, j)$ is the infinite dilution activation energy calculated using the methods of Sec. V.A.3, and a_{ij} is the jump distance. ΔE_{ij} is the *shift* in the energy difference between sites i and j

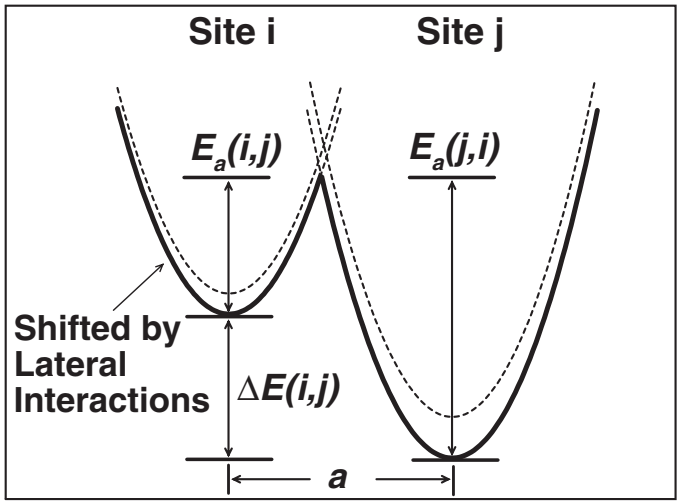

Fig. 22 Site-to-site jump activation energies perturbed by guest–guest interactions, approximated with parabolic jump model.

resulting from guest–guest interactions, and is given by $\Delta E_{ij} = (E_j - E_i) - (\varepsilon_j - \varepsilon_i)$, where $E_k = \varepsilon_k + \sum_{l=1}^{M} J_{kl} n_l$. This method allows the rapid estimation of configuration-dependent barriers during a KMC simulation, knowing only infinite dilution barriers and the nearest-neighbor interactions defined above. The parabolic jump model is most accurate when the spatial paths of jumping molecules are not drastically changed by guest–guest interactions, although the energies can change as shown in Fig. 22. The influences of nearest-neighbor attractions have also been considered in the analytical treatment of tracer exchange and particle conversion in single-file systems (371).

d. Infinite Dilution Simulations

Most KMC simulations of diffusion in zeolites are performed at high guest loadings to explore the effects on transport of guest–guest interactions. A handful of KMC studies have been reported at infinite dilution to relate fundamental rate coefficients with observable self-diffusivities for particular lattice topologies. June *et al.* augmented their TST and RFMD study with KMC calculations of Xe and SF_6 self-diffusivities in silicalite-1 (317). They obtained excellent agreement among apparent activation energies for Xe diffusion calculated using MD, KMC with TST jump rates, and KMC with RFCT jump rates. The resulting activation energies fall in the range 5–6 kJ mol^{-1}, which is much lower than the experimentally determined values of 15 and 26 kJ mol^{-1} (117,372). van Tassel *et al.* reported a similar study in 1994 on methane diffusion in zeolite A, finding excellent agreement between self diffusivities calculated with KMC and MD (373).

Auerbach *et al.* reported KMC simulations of benzene diffusion in Na-Y showing that the cation → window jump (see Fig. 20) controls the temperature dependence of diffusion, with a predicted activation energy of 41 kJ mol^{-1} (229). Because benzene residence times at cation sites are so long, these KMC studies could not be compared directly with MD but nonetheless yield reasonable agreement with the QENS barrier of 34 kJ mol^{-1} measured by Jobic *et al.* (179). Auerbach and Metiu then reported KMC simulations of benzene orientational randomization in various models of Na-Y with different numbers of supercage cations, corresponding to different Si:Al ratios (198). Full cation occupancy gives randomization rates controlled by intracage

motion, whereas one-half cation occupancy gives rates sensitive to *both* intracage and intercage motion. This finding prompted Chmelka and coworkers to perform exchange-induced sidebands NMR experiments on labeled benzene in the corresponding Ca-Y (Si:Al = 2.0), finding that they were able to measure both the cation → cation and cation → window jump rates within a single experiment (1). Finally, when Auerbach and Metiu modeled benzene orientational randomization with one-quarter cation occupancy, they found *qualitative sensitivity* to different spatial patterns of cations, suggesting that measuring orientational randomization in zeolites can provide important information regarding cation disorder and possibly Al distributions.

e. Finite Loadings

Theodorou and Wei used KMC to explore a site-blocking model of reaction and diffusion with various amounts of coking (356). They showed that xylene isomerization catalyzed by ZSM-5 is biased toward production of the most valuable isomer, *p*-xylene, because the diffusivity of *p*-xylene is much greater than that of *m*-xylene and *o*-xylene, thus allowing the para product to diffuse selectively out of the zeolite particle. This seminal study exemplifies the potential benefits of understanding and controlling transport in zeolites.

Nelson and coworkers developed similar models to explore the relationship between the catalytic activity of a zeolite and its lattice percolation threshold (374,375). In a related study, Keffer *et al.* modeled binary mixture transport in zeolites, where one component diffuses rapidly while the other component is trapped at sites, e.g., methane and benzene in Na-Y (352). They used KMC to calculate percolation thresholds of the rapid penetrant as a function of blocker loading and found that these thresholds agree well with predictions from simpler percolation theories (376).

Coppens *et al.* used KMC to calculate the loading dependence of self diffusion for a variety of lattices for comparison with mean field theories (MFTs) of diffusion (56). These theories usually predict $D_s(\theta) \cong D_0(1 - \theta)$, where θ is the fractional occupancy of the lattice and D_0 is the self diffusivity at infinite dilution. Coppens *et al.* found that the error incurred by MFT is greatest for lattices with low coordination numbers, such as silicalite-1 and other MFI-type zeolites. Coppens *et al.* then reported KMC simulations showing that by varying the concentrations of weak and strong binding sites (32), their system exhibits most of the loading dependencies of self-diffusion reported by Kärger and Pfeifer (30). Bhide and Yashonath also used KMC to explore the origins of the observed loading dependencies of self-diffusion, finding that most of these dependencies can be generated by varying the nature and strength of guest–guest interactions (349,350).

f. Benzene in Na-X

Auerbach and coworkers reported a series of studies modeling the concentration dependence of benzene diffusion in Na-X and Na-Y zeolites (31,52,55,72,368). These studies were motivated by persistent, qualitative discrepancies between different experimental probes of the coverage dependence of benzene self diffusion in Na-X (5), as shown in Fig. 12. PFG NMR diffusivities decrease monotonically with loading for benzene in Na-X (377), while tracer zero-length column (TZLC) data *increase* monotonically with loading for the same system (147).

Saravanan *et al.* performed KMC simulations using the parabolic jump model to account for guest–guest attractions (31,55). The KMC results for benzene in Na-X are in excellent qualitative agreement with the PFG NMR results, and in qualitative disagreement with TZLC. Other experimental methods yield results for benzene in Na-X that also agree broadly with these PFG NMR diffusivities (378–380). Although the evidence appears to be mounting in favor of the PFG NMR loading dependence for benzene in Na-X, it remains unclear just what is being observed by the TZLC measurements. To address this issue, Brandani *et al.* reported

TZLC measurements for benzene in various Na-X samples with different particle sizes. They found tracer exchange rates that exhibit a normal dependence on particle size, suggesting that their diffusivities are free from artifacts associated with unforeseen diffusion resistances at zeolite crystallite surfaces (147).

Noting that molecular transport in TZLC measurements samples longer length scales than that in PFG NMR experiments, Chen *et al.* have suggested that the TZLC method may be more sensitive than is PFG NMR to electrostatic traps created by random Al and cation distributions (148). By performing a field theory analysis of an augmented diffusion equation, Chen *et al.* estimate that such charge disorder can diminish the self diffusivity by roughly two orders of magnitude from that for the corresponding ordered system. This effect is remarkably close to the discrepancy in absolute magnitudes between PFG NMR and TZLC diffusivities for benzene in Na-X at low loadings (147). This intriguing prediction by Chen *et al.* suggests that there should be a striking difference between benzene diffusion in Na-X (Si:Al = 1.2) and in Na-LSX (Si:Al = 1), since the latter is essentially an ordered structure. We are not aware of self-diffusion measurements for benzene in Na-LSX, but we can turn to NMR spin-lattice relaxation data for deuterated benzene in these two zeolites (196,381). Unfortunately, such data typically reveal only short length scale, intracage dynamics (198), and as a result may not provide such a striking effect. Indeed, the activation energy associated with the NMR correlation time changes only moderately, decreasing from 14.0 ± 0.6 kJ mol^{-1} for Na-X (196) to 10.6 ± 0.9 kJ mol^{-1} for Na-LSX (381), in qualitative agreement with the ideas of Chen *et al.* (148). It remains to be seen whether such electrostatic traps can explain the loading dependence observed by TZLC for benzene in Na-X.

By varying fundamental energy scales, the model of Saravanan and Auerbach for benzene in FAU-type zeolites exhibits four of the five loading dependencies of self-diffusion reported by Kärger and Pfeifer (30), in analogy with the studies of Coppens *et al.* (32) and Bhide and Yashonath (349,350). However, in contrast to these other KMC studies, Saravanan and Auerbach explored the role of phase transitions (354,355) in determining the loading dependencies of self diffusion (31). In particular, they found that Kärger and Pfeifer's type III diffusion isotherm, which involves a nearly constant self diffusivity at high loadings, may be characteristic of a cluster-forming, subcritical adsorbed phase where the cluster of guest molecules can extend over macroscopic length scales. Such cluster formation suggests a diffusion mechanism involving "evaporation" of particles from clusters. Although increasing the loading in subcritical systems increases cluster sizes, Saravanan and Auerbach surmised that evaporation dynamics remains essentially unchanged by increasing loading. As such, the subcritical diffusivity is expected to obtain its high loading value at low loadings and to remain roughly constant up to full loading.

In addition, Saravanan and Auerbach found that Kärger and Pfeifer's types I, II, and IV are characteristic of supercritical diffusion and can be distinguished based on the loading that gives the maximum diffusivity, θ_{max}. For example, the PFG NMR results discussed above for benzene in Na-X are consistent with $\theta_{max} \lesssim 0.3$, while the TZLC data give $\theta_{max} \gtrsim 0.5$ (see Fig. 12). The KMC simulations of Saravanan and Auerbach predict that θ_{max} will decrease with increasing temperature, increasing strength of guest–guest attractions, decreasing the free-energy difference between site types, and in general with anything that makes sites more equally populated (31).

g. Reactive Systems

Trout *et al.* applied electronic structure methods to calculate thermodynamic parameters for possible elementary reactions in the decomposition of NO_x over Cu-ZSM-5 (382). Based on these insights, they developed a KMC model of reaction and diffusion in this system, seeking

the optimal distribution of isolated reactive Cu centers (353). This hierarchical approach to realistic modeling of complex systems presents an attractive avenue for future research.

h. Open Systems

Gladden *et al.* developed a versatile open-system KMC program that allows them to study adsorption, diffusion, and reaction in zeolites simultaneously (363). They have applied their algorithm to model ethane and ethene binary adsorption in silicalite-1 (363), finding excellent agreement with the experimental binary isotherm.

Nelson and Auerbach reported open-system KMC simulations of anisotropic diffusion (27) and single-file diffusion (83) (infinitely anisotropic) through zeolite membranes. They defined an anisotropy parameter, η, according to $\eta = k_y/k_x$, where k_x and k_y are the elementary jump rates in the transmembrane and in-plane directions, respectively. For example, the $\eta < 1$ case models *p*-xylene permeation through a silicalite-1 membrane (see Fig. 2) oriented along the the straight channels (*b* axis), while $\eta > 1$ corresponds to the same system except oriented along the zig-zag (*a* axis) or "corkscrew" channels (*c* axis) (289). The limiting case $\eta = 0$ corresponds to single-file diffusion.

Nelson and Auerbach have studied how the self-diffusivity depends on membrane thickness L and anisotropy η. However, the long-time limit of the MSD may not be accessible in a membrane of finite thickness. Furthermore, the natural observable in a permeation measurement is steady-state flux rather than the MSD. To address these issues, they simulated two-component, equimolar counterpermeation of identical, labeled species—i.e., tracer counterpermeation—which has been shown to yield transport identical to self diffusion (25). Such a situation is closely related to the tracer zero-length column experiment developed by Ruthven and coworkers (147). When normal diffusion holds the self diffusivity is independent of membrane thickness, while anomalous diffusion is characterized by an L-dependent self diffusivity. For $\eta \gg 1$, Nelson and Auerbach found that diffusion is normal and that MFT becomes exact in this limit (27), i.e. $D_s(\theta) = D_0(1 - \theta)$. This is because sorbate motion in the plane of the membrane is very rapid, thereby washing out any correlations in the transmembrane direction. As η is reduced, correlations between the motion of nearby molecules decrease the diffusivity. For small values of η, a relatively large lattice is required to reach the thick membrane limit such that particle exchange becomes probable during the intracrystalline lifetime. The extreme case of this occurs when $\eta = 0$, for which diffusion is strictly anomalous for all membrane thicknesses.

As discussed in Sec. III.B, Nelson and Auerbach applied open-system KMC to study the nature of anomalous diffusion through single-file zeolites of finite extent (83). They found that open, single-file systems have diffusivities that depend on file length, L, according to Eq. (44). The intracrystalline lifetime during normal, one-dimensional tracer exchange obeys:

$$\tau_{\text{intra}} = \frac{L^2}{12D_{\text{T}}} \propto L^2, \tag{87}$$

where the proportionality follows from the fact that, in normal diffusion, the diffusivity is independent of system size. However, to describe the intracrystalline lifetime during single-file self-diffusion, D_{T} in Eq. (87) must be replaced by D_{SF} from Eq. (44), giving (80,82,83):

$$\tau_{\text{intra}} = \frac{L^2}{12D_{\text{SF}}} \overset{L\to\infty}{\rightarrow} \frac{L^3\theta}{12aD_0(1-\theta)} \propto L^3, \tag{88}$$

where D_0 is the infinite dilution jump diffusivity, and a is the nearest-neighbor site-to-site or cage-to-cage distance. The L^3 scaling in Eq. (88) plays an important role in the discussion below of molecular traffic control.

Direct experimental verification of the L-dependence of the single-file self-diffusion coefficient [Eq. (44)] will require careful tracer counterpermeation experiments on single-file zeolites of various particle sizes. Before this daunting task is achieved, more indirect means of verification may prove useful. Along these lines, de Gauw *et al.* recently interpreted reaction-diffusion experiments on *n*-hexane and 2,2-dimethylbutane in Pt/H-mordenite (383). They found that the only way they could interpret their data was by assuming an intracrystalline lifetime scaling as L^3, thus providing support for the ideas above. Rodenbeck *et al.* also found it necessary to interpret activation energies for reactions catalyzed in zeolites in light of single-file diffusion (384). The general correlation between chemical reaction and molecular propagation in single-file systems is a challenging task of current experimental (314,385,386) and theoretical (384,387,388) research.

i. Molecular Traffic Control

The possibility of enhancing reactivity by "molecular traffic control" (389,390) (MTC) emerges when considering diffusion and reaction in networks of single-file systems (391–393). The effective reactivity can be enhanced by MTC if reactant and product molecules are adsorbed along different diffusion paths in the interior of zeolite crystallites. Recent MD simulations have confirmed that this assumption, which underlines MTC, can be realized for two components in an MFI-type zeolite (394).

To explore the possible consequences of MTC, Kärger and coworkers have developed lattice models that simulate the basic MTC assumption (392,393,395). In particular, the extreme case has been considered where channels of one type can accommodate only reactant molecules (A), while channels of a second type, perpendicular to those of the first type, can accommodate only product molecules (B). Within this channel network, the channel intersections are assumed to give rise to an irreversible reaction, A→B. It is further assumed that the

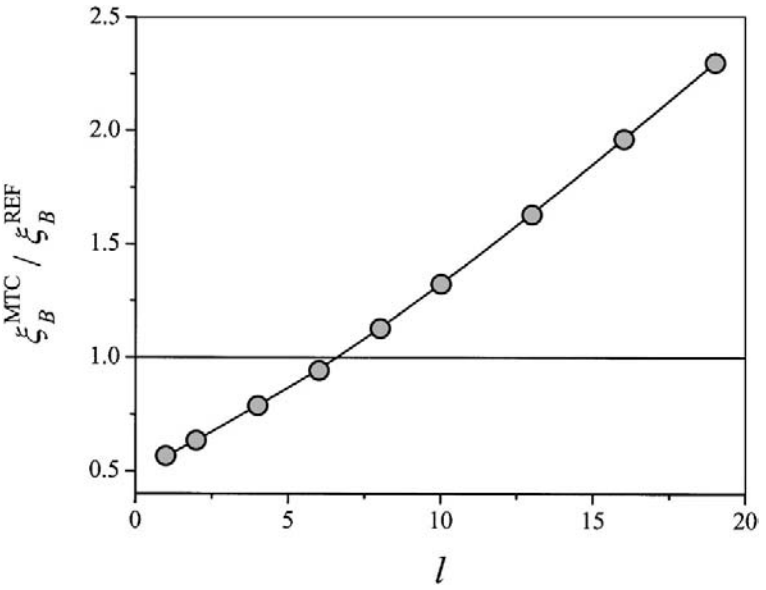

Fig. 23 Ratio of overall reaction rates in MTC and reference (REF) systems, ξ_B^{MTC}/ξ_B^{REF} for five channels as a function of the number l of sites in the channel segments between two neighboring intersections. (From Ref. 392.)

network is in contact with a gas phase containing A molecules at a certain constant pressure and that there is no reentrance of B molecules. Figure 23 shows that the effective reactivity in such a system can dramatically exceed the reactivity in a reference system, where both channels are equally accessible to both types of molecules.

This enhanced reactivity can be understood by considering the mean lifetime in single-file systems as provided by Eq. (88). We imagine using this relation to estimate the mean time required for reactant and product molecules to diffuse from one-channel intersection to an adjacent one, with L being proportional to the number of sites between intersections. However, this estimate applies only to the reference system, where the total concentration (sum of reactant and product concentrations) is constant throughout the system. But under the condition of molecular traffic control, the concentration of reactant molecules is found to drop from outside to the interior, while the concentration of product molecules (along the other set of parallel channels) drops from inside to outside. Under the influence of such concentration gradients, molecular transport in single-file systems proceeds under the conditions of normal diffusion (75,396), with mean lifetimes given by Eq. (87) rather than by Eq. (88). Thus, with an increasing number of sites between intersections, transport inhibition will become progressively more significant because of the proportionality to L^3 rather than to L^2, leading to the observed reactivity enhancement with molecular traffic control in comparison to that with the reference system.

C. Mean Field and Continuum Theories

Mean field and continuum theories provide a way to analyze the behavior of systems on length scales that are too large for even coarse-grained models to handle (208). In the end, we come full circle to the Fickian and Maxwell-Stefan formulations of diffusion.

1. Lattice Topology

The diffusion theory discussed above relies on the tetrahedral topology of FAU-type zeolites. Developing such a theory for general frameworks remains challenging. Braun and Sholl developed a Laplace-Fourier transformation method for calculating exact self-diffusion tensors in generalized lattice gas models (397), expanding on the matrix formalism originally introduced by Fenzhe and Kärger (398). These methods generally involve quite heavy matrix algebra, which can sometimes hide the underlying physical meaning of the parameters. Jousse *et al.* developed an alternative method for deriving analytical self-diffusion coefficients at infinite dilution for general lattices by partitioning the trajectory of a tracer into uncorrelated sequences of jumps (54). This approach can be used to analyze both geometrical correlations due to the nonsymmetrical nature of adsorption sites in zeolite pores and kinetic correlations arising from insufficient thermalization of a molecule in its final site. This method was applied to benzene diffusion in Na-Y (geometrical correlations) and to ethane diffusion in silicalite-1 (geometrical and kinetic correlations), yielding quantitative agreement with KMC simulations (54). The new method was also extended to finite loadings using MFT, yielding a completely analytical approach for modeling diffusion in any guest–zeolite system.

2. Maxwell-Stefan and Fick

Krishna and van den Broeke modeled the transient permeation fluxes of methane and *n*-butane through a silicalite-1 membrane using both the Fick and Maxwell-Stefan formulations (399). Transient experiments showed that initially the permeation flux of methane is higher than that of *n*-butane but that this methane flux eventually reduces to a lower steady-state value. The Maxwell-Stefan formulation succeeded in reproducing this nonmonotonic evolution to steady state for methane; the Fick formulation failed qualitatively in this regard. This is attributed to

the fact that multicomponent systems pose a challenge to the Fick formulation of diffusion, as discussed in Sec. II.D. van de Graaf *et al.* used the Maxwell-Stefan formulation to interpret permselectivity data for the separations of ethane/methane and propane/methane mixtures with a silicalite-1 membrane (38). Based only on separately determined single-component adsorption and diffusion parameters, the Maxwell-Stefan model gave permselectivities in excellent agreement with their experimental data.

3. Membrane Disorder

Nelson *et al.* computed steady-state solutions of the diffusion equation to evaluate the influence of defects, voids, and diffusion anisotropy on permeation fluxes through model zeolite membranes (28). Nelson *et al.* augmented the lattice configuration shown in Fig. 1a with various kinds of defect structures and used a time-dependent, numerical finite difference approach for computing steady-state fluxes in a variety of situations. They found that with a reasonable anisotropy and with a moderate density of voids in the membrane, permeation fluxes can be controlled by jumps perpendicular to the transmembrane direction. This suggests that oriented zeolite membranes may not behave with the intended orientation if there is a sufficient density of defects in the membrane.

4. Charge Disorder

As discussed in Sec. V.B.2, Chen *et al.* explored the extent to which static charge disorder in zeolites influences self-diffusivities on different length and time scales. They focused on the effects from random charge–polarization interactions for benzene in Na-Y zeolite using Debye-Hückel correlation functions. Chen *et al.* augmented the standard diffusion equation [Fick's second law, *cf.* Eq. (9)] with terms representing the effects of these fluctuating interactions. They analyzed the resulting equation in the hydrodynamic limit using time-dependent renormalization group theory (23), finding that such disorder can diminish benzene self-diffusivities in Na-Y by one to two orders of magnitude.

This field theory approach appears promising for explaining qualitatively the data in Fig. 16, which shows that PFG NMR self-diffusivities can depend sensitively on the length scales probed. However, to explain quantitatively the data in Fig. 16, this approach will require much more accurate input from correlation functions describing the static charge disorder in zeolites. Such information can only come from careful, atomistic simulations, which in turn must be validated by experiments capable of measuring disorder in zeolites.

VI. SUMMARY AND PROSPECTS FOR THE FUTURE

In this chapter we have reviewed the basic ideas underlying diffusion in microporous solids, and have explored recent efforts over the last two decades to measure and model the dynamics of molecules sorbed in zeolites. These studies have revealed many important insights regarding diffusion in zeolites; here we summarize a subset of these ideas. The basic theories of diffusion on two-dimensional surfaces and in dense solids have been successfully modified to produce new insights regarding transport in microporous materials. The relationships between the many diffusivities, including the Fickian, Maxwell-Stefan, Onsager, corrected, transport, and self-diffusivities, have been elucidated. The temperature dependence of diffusion in zeolites most often exhibits Arrhenius behavior. Reliable activation energies for diffusion can be measured nowadays with increasingly sophisticated experimental techniques, such as those based on NMR or neutron scattering. The loading dependence of diffusion in zeolites is less predictable, although recent calculations have revealed how the interplay between host–guest and guest–

guest interactions can give rise to different loading dependencies. Regarding multicomponent diffusion in zeolites at high loadings, one generally expects that the faster diffusing component is slowed down to the mobility of the more slowly diffusing component. Good to very good agreement among various experiments and simulations has been obtained for the simplest zeolite–guest systems, often involving all-silica zeolites (e.g., silicalite) and simple hydrocarbons (e.g., methane or butane).

For each of the generalizations above, myriad zeolite–guest systems exist that break the rules. This underscores the fact that, despite our increasing level of understanding, much remains unknown regarding diffusion in zeolites. For example, it is not clear whether permeation through zeolites occurs in the linear response regime for typical concentration drops and particle sizes. In addition, we do not generally know whether transport is diffusion or desorption limited in present applications of zeolites. We have much to learn about the coupling between reaction and diffusion in zeolites, especially in single-file systems capable of producing molecular traffic control. Particularly intriguing are the persistent discrepancies among different experimental probes of diffusion for certain zeolite–guest systems. For example, PFG NMR and tracer zero length column (TZLC) self diffusivities are in very good agreement for methanol in Na-X but in total disagreement for benzene in the same zeolite. Despite the careful experiments performed to validate the TZLC data, there appears to be mounting evidence in favor of the PFG NMR diffusivities. This raises the question: what exactly is TZLC measuring for this particular system? Furthermore, as simulation methods have become more reliable over the past decade, it becomes timely to ask what causes persistent discrepancies between certain experiments and simulations, e.g., between quasi-elastic neutron scattering and kinetic Monte Carlo self diffusivities for benzene in Na-Y? We must answer these questions before our knowledge of diffusion in zeolites can be used generally to develop new and improved processes in zeolite science.

Many zeolite scientists have suggested that defects and disorder in zeolites can lead to the observed discrepancies discussed above. Given the intricate topologies that zeolites purportedly adopt, it seems highly unlikely that they do so without error. Discovering the nature of framework defects, and their role in influencing diffusion in zeolites, represents an important area for future zeolite research. In addition to framework defects, most zeolites are riddled with disordered charge distributions arising from disordered framework aluminum and accompanying charge-compensating ions. Measurement of correlations in these disordered charge distributions will be crucial for quantifying their impact on diffusion in zeolites. We can also consider external zeolite surfaces as defects, providing different transport resistances that need to be understood. In general, such defects and disorder patterns can produce different diffusivities depending on the length scales probed. Elucidating these effects remains one of the great challenges for future zeolite research.

In addition to thoroughly understanding diffusion in the more commonly studied host–guest systems, it is important to explore the properties of future diffusion systems as well. One can imagine remarkable properties of polymers or biomolecules intercalated into large-pore zeolites. Also of interest is the transport behavior of electronically active species in zeolites, such as metals or charge-transfer complexes. Much can be learned from drawing analogies between zeolite–guest systems and other nanoporous systems such as biological ion channels, which also exhibit intricate structures and impressive selectivities. We hope that this chapter provides the necessary launching point for the next generation to solve the mysteries we have discussed, as well as those we have not yet imagined.

ACKNOWLEDGMENTS

We gratefully acknowledge our research coworkers for their invaluable contributions and for many stimulating discussions. S.M.A. especially thanks Dr. Fabien Jousse with expert assistance

in preparing this manuscript. J.K. and S.V. are obliged to the Deutsche Forschungsgemeinschaft and Fonds der Chemischen Industrie for financial support. S.M.A. acknowledges support from the University of Massachusetts at Amherst Faculty Research Grant Program, the Petroleum Research Fund (ACS-PRF 30853-G5), the National Science Foundation (CHE-9403159, CHE-9625735, CHE-9616019, and CTS-9734153), a Sloan Foundation Research Fellowship (BR-3844), a Camille Dreyfus Teacher-Scholar Award (TC-99-041), the National Environmental Technology Institute, and Molecular Simulations, Inc.

REFERENCES

1. DE Favre, DJ Schaefer, SM Auerbach, BF Chmelka. Phys Rev Lett 81:5852, 1998.
2. J Caro, M Bülow, W Schirmer, J Kärger, W Heink, H Heink, H Pfeifer, SP Zhdanov. J Chem Soc Faraday Trans I 81:2541, 1985.
3. F Stallmach, J Kärger. Adsorption 5:117, 1999.
4. J Kärger, DM Ruthven. Diffusion and adsorption in porous solids. In: *Handbook of Porous Solids*. Edited by F Schüth, K Sing, and J Weitkamp. Weinheim: Wiley-VCH, 2002, pp. 2089–2173.
5. J Kärger, DM Ruthven. *Diffusion in Zeolites and Other Microporous Solids*. New York: Wiley, 1992.
6. NY Chen, TF Degnan, CM Smith. *Molecular Transport and Reaction in Zeolites*. New York: VCH, 1994.
7. CRA Catlow. ed. *Modelling of Structure and Reactivity in Zeolites*. London: Academic Press, 1992.
8. J Kärger, DM Ruthven. Self diffusion and diffusive transport in zeolite crystals. In: *Studies in Surface Science and Catalysis*. Edited by H Chon, SK Ihm, and YS Uh, Vol. 105. Amsterdam: Elsevier, 1997, pp 1843–1851.
9. J Kärger. Single-file diffusion in zeolites. In: *Molecular Sieves—Science and Technology, Vol. 7, Sorption and Diffusion*. Edited by HG Karge and J Weitkamp. Berlin: Springer-Verlag, (in press).
10. DN Theodorou, RQ Snurr, AT Bell. Molecular dynamics and diffusion in microporous materials. In: *Comprehensive Supramolecular Chemistry, Vol. 7*. Edited by G Alberti and T Bein. Oxford: Pergamon Press, 1996, pp 507–548.
11. P Demontis, GB Suffritti. Chem Rev 97:2845, 1997.
12. SM Auerbach. Int Rev Phys Chem 19:155, 2000.
13. F Keil, R Krishna, M-O Coppens. Rev Chem Eng 16:71, 2000.
14. SM Auerbach, F Jousse, DP Vercauteren. Dynamics of sorbed molecules in zeolites. In: *Computer Modelling of Microporous and Mesoporous Materials*. Edited by CRA Catlow, RA van Santen, B Smit. London: Academic Press (in press).
15. W Jost. *Diffusion in Solids, Liquids and Gases*. New York: Academic Press, 1960.
16. P Heitjans, J Kärger. *Diffusion in Condensed Matter–From the Elementary Step to Transport in Complex Systems*. Heidelberg: Springer, 2003.
17. RS Berry, SA Rice, J Ross. *Physical Chemistry: Part 2.-Matter in Equilibrium*. New York: Wiley, 2000.
18. LD Landau, EM Lifshitz. *Fluid Mechanics*. Oxford: Pergamon Press, 1987.
19. CN Satterfield. *Heterogeneous Catalysis in Practice*. New York: McGraw-Hill, 1980.
20. H Mehrer, F Wenwer. Diffusion and adsorption in porous solids. In: *Diffusion in Condensed Matter*. J Kärger, P Heitjans, R. Haberlandt, eds. Braunschweig: Vieweg, 1998, pp 1–39.
21. A Dyer, H Faghihian. Micropor Mesopor Mater 21:27, 1998.
22. SR DeGroot, P Mazur. *Non-Equilibrium Thermodynamics*. Amsterdam: Elsevier, 1962.
23. D Chandler. *Introduction to Modern Statistical Mechanics*. New York: Oxford University Press, 1987.
24. R Krishna. Chem Eng Sci 48:845, 1993.
25. PH Nelson, J Wei. J Catal 136:263, 1992.
26. R Kutner. Phys Lett A81:239, 1981.
27. PH Nelson, SM Auerbach. Chem Eng J 74:43, 1999.

28. PH Nelson, M Tsapatsis, SM Auerbach. J Membrane Sci 184:245, 2001.
29. J Kärger. Langmuir 4:1289, 1988.
30. J Kärger, H Pfeifer. Zeolites 7:90, 1987.
31. C Saravanan, SM Auerbach. J Chem Phys 110:11000, 1999.
32. MO Coppens, AT Bell, AK Chakraborty. Chem Eng Sci 54:3455, 1999.
33. R Krishna, JA Wesselingh. Chem Eng Sci 52:861, 1997.
34. JA Wesslingh, R Krishna. *Mass Transfer in Multicomponent Mixtures*. Delft: University Press, 2000.
35. EJ Maginn, AT Bell, DN Theodorou. J Phys Chem 97:4173, 1993.
36. DM Ruthven. *Principles of Adsorption and Adsorption Process*. New York: John Wiley & Sons, 1984.
37. AI Skoulidas, DS Sholl. J Phys Chem B 105:3151, 2001.
38. JM van de Graaf, F Kapteijn, JA Moulijn. AIChE J 45:497, 1999.
39. F Kapteijn, JA Moulijn, R Krishna. Chem Eng Sci 55:2923, 2000.
40. G Xomeritakis, S Nair, M Tsapatsis. Micropor Mesopor Mater 38:61, 2000.
41. S Nair, ZP Lai, V Nikolakis, G Xomeritakis, G Bonilla, M Tsapatsis. Micropor Mesopor Mater 48:219, 2001.
42. R Krishna. Chem Eng Sci 1779, 1990.
43. A Vignes. Ind Eng Chem Fund 5:189, 1966.
44. D Paschek, R Krishna. Phys Chem Phys 3:3185, 2001.
45. TLM Maesen, M Schenk, TJH Vlugt, JP de Jonge, B Smit. J Catal 188:403, 1999.
46. JA Martens, G Vanbutsele, PA Jacobs, J Denayer, R Ocakoglu, G Baron, JAM Arroyo, J Thybaut, GB Marin. Catal Today 65:111, 2001.
47. L Onsager. Phys Rev 37:405, 1931.
48. JAW Elliott, HY Elmoazzen, LE McGann. J Chem Phys 113:6573, 2001.
49. SM Auerbach, HI Metiu. J Chem Phys 105:3753, 1996.
50. DG Levitt. Phys Rev A8:3050, 1973.
51. AN Fitch, H Jobic, A Renouprez. J Phys Chem 90:1311, 1986.
52. C Saravanan, SM Auerbach. J Chem Phys 107:8120, 1997.
53. J Kärger, P Demontis, GB Suffritti, A Tilocca. J Chem Phys 110:1163, 1999.
54. F Jousse, SM Auerbach, DP Vercauteren. J Chem Phys 112:1531, 2000.
55. C Saravanan, F Jousse, SM Auerbach. Phys Rev Lett 80:5754, 1998.
56. MO Coppens, AT Bell, AK Chakraborty. Chem Eng Sci 53:2053, 1998.
57. R Gomer. Rep Prog Phys 53:917, 1990.
58. F Jousse, SM Auerbach. J Chem Phys 107:9629, 1997.
59. NK Bär, J Kärger, H Pfeifer, H Schäfer, W Schmitz. Microp Mesop Mat 22:289, 1998.
60. J Kärger. J Phys Chem 95:5558, 1991.
61. J Kärger, H Pfeifer. Zeolites 12:872, 1992.
62. RL June, AT Bell, DN Theodorou. J Phys Chem 94:8232, 1990.
63. SD Pickett, AK Nowak, JM Thomas, BK Peterson, JFP Swift, AK Cheetham, CJJ den Ouden, B Smit, MFM Post. J Phys Chem 94:1233, 1990.
64. P Demontis, ES Fois, G Suffritti, S Quartieri. J Phys Chem 94:4329, 1990.
65. SJ Goodbody, K Watanabe, D MacGowan, JPB Walton, N Quirke. J Chem Soc Faraday Trans 87:1951, 1991.
66. U Hong, J Kärger, H Pfeifer, U Müller, KK Unger. Z Phys Chem 173:225, 1991.
67. U Hong, J Kärger, R Kramer, H Pfeifer, G Seiffert, U Müller, KK Unger, HB Lück, T Ito. Zeolites 11:816, 1991.
68. GE Murch. In: *Diffusion in Crystalline Solids*. Edited by GE Murch and AS Nowick. Orlando: Academic Press, 1984, p 379.
69. RA Tahir-Kheli, RJ Elliott. Phys Rev B 27:844, 1983.
70. RA Tahir-Kheli, N El-Meshad. Phys Rev B 32:6166, 1985.
71. D Paschek, R Krishna. Chem Phys Lett 333:278, 2001.
72. C Saravanan, F Jousse, SM Auerbach. J Chem Phys 108:2162, 1998.
73. PA Fedders. Phys Rev B 17:40, 1978.

74. J Kärger. Phys Rev A 45:4173, 1992.
75. KW Kehr, K Mussawisade, T Wichmann. *Diffusion in Condensed Matter*. J Kärger, P Heitjans, R Haberlandt, eds. Braunschweig: Vieweg, 1998, pp. 265–306.
76. J Kärger. Phys Rev E 47:1427, 1993.
77. V Gupta, SS Nivarthi, AV McCormick, HT Davis. Chem Phys Lett 247:596, 1995.
78. K Hahn, J Kärger, V Kukla. Phys Rev Lett 76:2762, 1996.
79. H Jobic, K Hahn, J Kärger, M Bée, A Teul, M Noack, I Girnus, GJ Kearley. J Phys Chem B 101:5834, 1997.
80. K Hahn, J Kärger. J Phys Chem B 102:5766, 1998.
81. HL Tepper, JP Hoogenboom, NFA van der Vegt, WJ Briels. J Chem Phys 110:11511, 1999.
82. C Rödenbeck, J Kärger. J Chem Phys 110:3970, 1999.
83. PH Nelson, SM Auerbach. J Chem Phys 110:9235, 1999.
84. DS Sholl, KA Fichthorn. Phys Rev Lett 79:3569, 1997.
85. D Forster. *Hydrodynamic Fluctuations, Broken Symmetry and Correlation Functions*. Reading, MA: W. A. Benjamin, 1975.
86. JP Hansen, IR McDonald. *Theory of Simple Liquids*. London: Academic Press, 1976.
87. JP Hoogenboom, HL Tepper, NFA van der Vegt, WJ Briels. J Chem Phys 113:6875, 2000.
88. DS Sholl. Ind Eng Chem Res 39:3737, 2000.
89. G Arya, HC Chang, EJ Maginn. J Chem Phys 115:8112, 2001.
90. HL Tepper, WJ Briels. J Chem Phys 116:9464, 2002.
91. MJ Sanborn, RQ Snurr. Sep Purif Tech 20:1, 2000.
92. MJ Sanborn, RQ Snurr. AIChE J 47:2032, 2001.
93. WJ Briels. *Theory of Simple Liquids (Lecture Notes)*. Uppsala University, 1993.
94. DM Ruthven, M Post. In: *Introduction to Zeolite Science and Practice*. Edited by EMFH van Bekkum, JC Jansen. Amsterdam: Elsevier, 2000.
95. ER Gues, H van Bekkum, WJH Bakker, JA Mouljin. Micropor Mater 1:131, 1993.
96. JC Jansen, GM Rosmalen. J Cryst Growth 128:1150, 1993.
97. LC Boudreau, JA Kuck, M Tsapatsis. J Membrane Sci 152:41, 1999.
98. DT Hayhurst, A Paravar. Zeolites 8:27, 1988.
99. J Caro, M Noack, D Peterson, M Griepenstrog, JJ Kornatowski. J Phys Chem 97:13685, 1993.
100. O Talu, MS Sun, DB Shah. AIChE J 44:681, 1998.
101. J Caro, M Noack, P Kolsch, R Schafer. Micropor Mesopor Mater 38:3, 2000.
102. WO Haag, RM Lago, PB Weisz. Faraday Disc 72:317, 1982.
103. MFM Post, J van Amstel, HW Kouwenhoeven. Proc Sixth Int Zeolite Conf. Guildford: Butterworth, 1984, pp. 517–527.
104. L Riekert. Adv Catal 21:281, 1970.
105. J Crank. *Mathematics of Diffusion*. Oxford: Clarendon Press, 1956.
106. RM Barrer. *Diffusion In and Through Solids*. Cambridge UK: Cambridge University Press, 1951.
107. M Bülow, A Micke. Adsorption 1:29, 1995.
108. DM Ruthven, LK Lee, H Yucel. AIChE J 26:16, 1980.
109. L Sun, F Meunier. Chem Eng Sci 42:1585, 1987.
110. R Haul, H Stremming. J Coll Interf Sci 97:348, 1984.
111. J Kärger, M Bülow, BR Millward, JM Thomas. Zeolites 6:146, 1986.
112. J Kärger. AIChE J 28:417, 1982.
113. J Kärger, H Pfeifer, R Richter, H Fürtig, W Roscher, R Seidel. AIChE J 34:1185, 1988.
114. J Caro, M Bülow, H Jobic, J Kärger, B Zibrowius. Adv Catal 39:351, 1993.
115. D Prinz, L Riekert. Ber Bunsenges Phys Chem 90:413, 1986.
116. M Bülow and A Micke. Z Phys Chem 189:195, 1995.
117. M Bülow, U Härtel, U Müller, KK Unger. Ber Bunsenges 94:74, 1990.
118. A Micke and M Bülow. Chem Eng Sci 48:2777, 1993.
119. S Brandani. Adsorption 4:17, 1998.
120. M Kocirik, A Zikanova. Z Phys Chem (Leipzig) 250:360, 1972.
121. MM Dubinin, IT Erashko, VI Ulin, AM Voloschuk, PP Zolotarev. Carbon 13:193, 1975.

122. M Eic and DM Ruthven. Zeolites 8:40, 1988.
123. DM Ruthven, M Eic. Am Chem Soc Symp Ser 368:362, 1988.
124. DM Ruthven, P Stapleton. Chem Eng Sci 48:89, 1993.
125. L Boulicaut, S Brandani, DM Ruthven. Micropor Mater 25:81, 1998.
126. Y Yasuda. Heterogen Chem Rev 1:103, 1994.
127. LVC Rees, DH Shen. J Chem Soc Faraday Trans I 86:3687, 1990.
128. LVC Rees, L Song. Frequency response methods for the characterization of microporous solids. In: *Recent Advances in Gas Separation by Microporous Ceramic Membranes*. Edited by NK Kanellopoulos. Amsterdam: Elsevier, 2000, pp. 139–186.
129. LM Sun, V Bourdin. Chem Eng Sci 48:3783, 1993.
130. V Bourdin, P Grenier, F Meunier, LM Sun. AIChE J 42:700, 1996.
131. V Bourdin, A Germanus, P Grenier, J Kärger. Adsorption 2:205, 1996.
132. W Niessen, HG Karge. Stud Surf Sci Catal 60:213, 1991.
133. HG Karge, W Niessen, H Bludau. Appl Catal A 146:339, 1996.
134. HG Karge. Proc Third Polish-German Zeolite Coll. In: *Studies in Surface Science Catal.* Edited by M Rozwadowski. Torun: Nicolas Copernicus Univ. Press, 1998, pp. 11–32.
135. HW Haynes, PN Sarma. Adv Chem 133:205, 1974.
136. BG Anderson, RA van Santen, LJ Ijzendoorn. Appl Catal A 160:125, 1997.
137. RR Schumacher, BG Anderson, NJ Noordhoek, FJMM de Gauw, AM de Jong, MJA de Voigt, RA van Santen. Micropor Mesopor Mater 35–36:315, 2000.
138. OP Kleipert, M Baerns. Chem Eng Sci 53:3623, 1998.
139. TA Nijhuis, LJP van den Broeke, JM van de Graaf, F Kapteijn, M Makkee, JA Moulijn. Chem Eng Sci 52:3401, 1997.
140. W Heink, J Kärger, H Pfeifer. Chem Eng Sci 33:1019, 1978.
141. NK Bär, BJ Balcom, DM Ruthven. Direct measurement of transient concentration profiles in molecular sieve particles and columns by MRI. In: *Adsorption Science and Technology*. Edited by DD Do. Singapore: World Scientific, 2000, pp. 1935–1937.
142. S Brandani, DM Ruthven. Chem Eng Sci 55:1935, 2000.
143. TA Nijhuis, JM van der Graaf, F Kapteijn, M Makkee, JA Moulijn. Chem Eng Sci 55:1938, 2000.
144. M Goddard, DM Ruthven. Zeolites 6:445, 1986.
145. S Brandani, JR Hufton, DM Ruthven. Micropor Mater 15:624, 1995.
146. DM Ruthven, S Brandani. Measurement of diffusion in porous solids by zero length column methods. In: *Zeolites*. Edited by NK Kanellopoulos. Amsterdam: Elsevier, 2000, pp 187–212.
147. S Brandani, Z Xu, D Ruthven. Micropor Mater 7:323, 1996.
148. L Chen, M Falcioni, MW Deem. J Phys Chem B 104:6033, 2000.
149. S Vasenkov, W Bohlmann, P Galvosas, O Geier, H Liu, J Kärger. J Phys Chem B 105:5922, 2001.
150. A Dyer, AM Yusof. Zeolites 7:191, 1987.
151. RM Rynders, MB Rao, S Sircar. AIChE J 43:2456, 1997.
152. RJ Mohr, D Varkapic, MB Rao, S Sircar. Adsorption 5:145, 1999.
153. C Förste, J Kärger, H Pfeifer. J Am Chem Soc 112:7, 1990.
154. DL Wernick, EJ Osterhuber. Proc Sixth Int. Zeolite Conf. Guildford: Butterworth, 1984, pp 130–133.
155. DT Hayhurst, A Paravar. Direct measurement of diffusivity for butane across a single large silicate crystal. In: *Proc Sixth Int. Zeolite Conf.* Edited by D Olson and A Bisio. Guildford: Butterworth, 1984, pp 217–224.
156. J Caro, M Noack, P Kölsch, R Schäfer, Micropor Mesopor Mater 38:3, 2000.
157. U Schemmert, J Kärger, C Krause, RA Rakoczy, J Weitkamp. Europhys Lett 46:204, 1999.
158. U Schemmert, J Kärger, J Weitkamp. Micropor Mesopor Mater 32:101, 1999.
159. C Weidenthaler, RX Fischer, RD Shannon, O Medenbach. J Phys Chem 98:12687, 1994.
160. ER Geus, JC Jansen, H van Bekkum. Zeolites 14:82, 1994.
161. O Geier, S Vasenkov, E Lehmann, J Kärger, U Schemmert, RA Rakoczy, J Weitkamp. J Phys Chem B 105:10217, 2001.

162. C Herzig, Y Mishin. Grain boundary diffusion in metals. In: *Diffusion in Condensed Matter*. J Kärger, P Heitjans, R Haberlandt, eds. Braunschweg: Vieweg, 1998, pp 90–115.
163. M Kocirik, J Kornatowski, V Masarik, P Novak, A Zikanova, J Maixner. Micropor Mater 23:295, 1998.
164. H Jobic. Diffusion studies using quasi-elastic neutron scattering. In: *Recent Advances in Gas Separation by Microporous Ceramic Membranes*. Edited by NK Kanellopoulos. Amsterdam: Elsevier, 2000, pp 109–138.
165. H Jobic. Applications of neutron scattering to catalysis. In: *Catalyst Characterization: Physical Techniques for Solid Materials*. New York: Plenum, 1994, pp 347–376.
166. M Gaub, S Fritzsche, R Haberlandt, DN Theodorou. J Phys Chem B 103:4721, 1999.
167. PL Hall and DK Ross. Mol Phys 42:673, 1981.
168. H Jobic, J Kärger, M Bee. Phys Rev Lett 82:4260, 1999.
169. W Heink, J Kärger, H Pfeifer, KP Datema, AK Nowak. J Chem Soc Faraday Trans 88:3505, 1992.
170. RC Runnebaum and EJ Maginn. J Phys Chem B 101:6394, 1997.
171. EJ Maginn, AT Bell, DN Theodorou. J Phys Chem 100:7155, 1996.
172. M Eic and D Ruthven. Stud Surf Sci Catal 49B:897, 1989.
173. R Tsekov, E Ruckenstein. J Chem Phys 100:3808, 1994.
174. R Tsekov, PG Smirniotis. J Phys Chem B 102:9385, 1998.
175. D Schuring, APJ Jansen, RA van Santen. J Phys Chem B 104:941, 2000.
176. R Kimmich. *NMR Tomography, Diffusometry, Relaxometry*. Berlin: Springer-Verlag, 1997.
177. PT Callaghan. *Principles of Nuclear Magnetic Resonance Microscopy*. New York: Oxford University Press, 1991.
178. J Kärger, W Heink. *J Magn Reson* 51:1, 1983.
179. H Jobic, AN Fitch, J Combet. J Phys Chem B 104:8491, 2000.
180. V Kukla, J Kornatowski, D Demuth, I Gimus, H Pfeifer, LVC Rees, S Schunk, KK Unger, J Kärger. Science 272:702, 1996.
181. J Kärger, H Pfeifer, G Vojta. Phys Rev A 37:4514, 1988.
182. SS Nirvarthi, AV McCormick. J Phys Chem 99:4661, 1995.
183. U Hong, J Kärger, H Pfeifer. J Am Chem Soc 113:4812, 1991.
184. RQ Snurr, J Kärger. J Phys Chem B 101:6469, 1997.
185. S Jost, NK Bär, S Fritzsche, R Haberlandt, J Kärger. J Phys Chem B 102:6375, 1998.
186. U Hong, J Kärger, NN Feoktistova, SP Zhdanov. J Catal. 137:243, 1991.
187. RQ Snurr, A Hagen, H Ernst, HB Schwarz, S Ernst, J Weitkamp, J Kärger. J Catal. 163:130, 1996.
188. HB Schwarz, H Ernst, S Ernst, J Kärger, T Roser, RQ Snurr, J Weitkamp. Appl. Catal. A 130:227, 1995.
189. K Schmidt-Rohr and HW Spiess. *Multidimensional Solid-State NMR and Polymers*. London: Academic Press, 1994.
190. H Pfeifer. Phys Rep 26:293, 1976.
191. B Boddenberg, R Burmeister. Zeolites 8:488, 1988.
192. B Boddenberg, B Beerwerth. J Phys Chem 93:1440, 1989.
193. V Voss, B Boddenberg. Surf Sci 298:241, 1993.
194. LM Bull, NJ Henson, AK Cheetham, JM Newsam, SJ Heyes. J Phys Chem 97:11776, 1993.
195. JA Sousa-Gonçalves, RL Portsmouth, P Alexander, LF Gladden. J Phys Chem 99:3317, 1995.
196. SM Auerbach, LM Bull, NJ Henson, HI Metiu, AK Cheetham. J Phys Chem 100:5923, 1996.
197. DE Favre, DJ Schaefer, BF Chmelka. J Magnet Reson 134:261, 1998.
198. SM Auerbach, HI Metiu. J Chem Phys 106:2893, 1997.
199. M Wilhelm, A Firouzi, DE Favre, LM Bull, DJ Schaefer, BF Chmelka. J Am Chem Soc 117:2923, 1995.
200. DJ Schaefer, DE Favre, M Wilhelm, SJ Weigel, BF Chmelka. J Am Chem Soc 119:9252, 1997.
201. O Isfort, B Boddenberg, F Fujara, R Grosse. Chem Phys Lett. 288:71, 1998.
202. J Kärger, J Caro. J Chem Soc Faraday Trans 73:1363, 1977.
203. LVC Rees. Exciting new advances in diffusion of sorbates in zeolites and microporous materials. In: *Zeolites and Related Microporous Materials: State of the Art 1994*. Edited by J Weitkamp, HG

Karge, H Pfeifer, and W Holderich. Studies in Surface Science and Catalysis. Amsterdam: Elsevier, 1994, pp 1133–1150.
204. J Kärger. Diffusion in zeolites. In: *Proc. 12th Int. Zeolite Conf.* Edited by MMJ Treacy, BK Marcus, ME Bisher, and JB Higgins. Warrendale, PA: Materials Research Society, 1999, pp 35–42.
205. W Heink, J Kärger, H Pfiefer, F Stallmach. J Am Chem Soc 112:2175, 1990.
206. J Kärger, H Pfeifer, M Rauscher, A Walter. J Chem Soc Faraday Trans 176:717, 1980.
207. P Galvosas, F Stallmach, G Seiffert, J Kärger, U Kaess, G Majer. J Magn. Reson 151:260, 2001.
208. MW Deem. AICHE J 44:2569, 1998.
209. WM Meier, DH Olson. *Atlas of Zeolite Structure Types, 3rd Revised Ed*. London: Butterworth-Heinemann, 1992.
210. *InsightII 4.0.0 User Guide*. San Diego: MSI, 1996.
211. B Herreros. 1996, http://suzy.unl.edu/Bruno/zeodat/zeodat.html.
212. EB Webb III, GS Grest. Catal Lett 56:95, 1998.
213. C Hansenne, F Jousse, L Leherte, DP Vercauteren. J Mol Catal A Chem 166:147, 2001.
214. F Jousse, E Cohen De Lara. J Phys Chem 100:233, 1996.
215. DE Akporiaye, IM Dahl, HB Mostad, R Wendelbo. J Phys Chem. 100:4148, 1996.
216. D. Ding, B. Li, P. Sun, Q. Jin, J. Wang, Zeolites 15:569, 1995.
217. AJ Vega. J Phys Chem 100:833, 1996.
218. CP Herrero, R. Ramírez. J Phy Chem 96:2246, 1992.
219. CP Herrero, J. Phys. Chem. 95:3282, 1991.
220. J. Klinowski, S. Ramdas, JM Thomas, CA Fyfe, JS Hartman. J Chem Soc Faraday Trans. 2 78:1025, 1982.
221. EJP Feijen, JL Lievens, JA Martens, PJ Grobet, PA Jacobs. J Phys Chem 100:4970, 1996.
222. JM Newsam. J Phys Chem 93:7689, 1989.
223. CF Mellot, AM Davidson, J Eckert, AK Cheetham. J Phys Chem B 102:2530, 1998.
224. CF Mellot, AK Cheetham, S Harms, S Savitz, RJ Gorte, AL Myers. J Am Chem Soc 120:5788, 1998.
225. G Vitale, CF Mellot, LM Bull, AK Cheetham. J Phys Chem B 101:4559, 1997.
226. DA Faux. J Phys Chem B 102:10658, 1998.
227. F Jousse, SM Auerbach, DP Vercauteren. J Phys Chem B 104:2360, 2000.
228. P Santikary, S Yashonath. J Phys Chem 98:9252, 1994.
229. SM Auerbach, NJ Henson, AK Cheetham, HI Metiu. J Phys Chem 99:10600, 1995.
230. NJ Henson, AK Cheetham, A Redondo, SM Levine, JM Newsam. Computer simulations of benzene in faujasite-type zeolites. In: *Zeolites and Related Microporous Materials: State of the Art 1994*. Edited by J Weitkamp, HG Karge, H Pfeifer, and W Hölderich. Amsterdam: Elsevier, 1994, pp 2059–2066.
231. E Jaramillo, SM Auerbach. J. Phys. Chem. B 103:9589, 1999.
232. JM Newsam, CM Freeman, AM Gorman, B. Vessal, Chem. Commun 16:1945, 1996.
233. CRA Catlow, CM Freeman, B. Vessal, SM Tomlinson, M. Leslie. J Chem Soc, Faraday Trans. 87:1947, 1991.
234. P. Demontis, GB Suffritti, ES Fois, S. Quartieri, J Phys Chem 96:1482, 1992.
235. KS Smirnov. Chem Phys Lett 229:250, 1994.
236. A Bouyermaouen, A Bellemans. J Chem Phys 108:2170, 1998.
237. S Fritzsche, M Wolfsberg, R Haberlandt, P Demontis, GB Suffritti, A Tilocca. Chem Phys Lett 296:253, 1998.
238. G Schrimpf, M Schlenkrich, J Brickmann, P Bopp. J Phys Chem 96:7404, 1992.
239. G Sastre, CRA Catlow, A Corma. J Phys Chem B 103:5187, 1992.
240. T Mosell, G Schrimpf, J Brickmann. J Phys Chem B 101:9476, 1997.
241. T Mosell, G Schrimpf, J Brickmann. J Phys Chem B 101:9485, 1997.
242. F Jousse, DP Vercauteren, SM Auerbach. J Phys Chem B 104:8768, 2000.
243. KT Thomson, AV McCormick, HT Davis. J Chem Phys 112:3345, 2000.
244. LA Clark, GT Ye, A. Gupta, LL Hall, RQ Snurr. J Chem Phys 111:1209, 1999.

245. DS Sholl, CK Lee. J Chem Phys 112:817, 2000.
246. DS Sholl, Chem Phys Lett 305:269, 1999.
247. EB Webb, III, GS Grest, M Mondello. J. Phys Chem B 103:4949, 1999.
248. LN Gergidis, DN Theodorou. J Phys Chem B 103:3380, 1999.
249. RQ Snurr, AT Bell, DN Theodorou. J Phys Chem 98:11948, 1994.
250. TR Forester, W. Smith. J Chem Soc Faraday Trans 93:3249, 1997.
251. RJ-M Pellenq, D Nicholson. J Phys Chem 98:13339, 1994.
252. D Nicholson, A Boutin, RJ-M Pellenq. Mol Simul 17:217, 1996.
253. AV Larin, E Cohen de Lara. Mol Phys 88:1399, 1996.
254. F Jousse, AV Larin, E Cohen De Lara. J Phys Chem 100:238, 1996.
255. MD Macedonia, EJ Maginn. Mol Phys 96:1375, 1999.
256. F Jousse, SM Auerbach, H Jobic, DP Vercauteren. J Phys IV Proc 10:147, 2000.
257. LN Gergidis, DN Theodorou, H Jobic. J Phys Chem B 104:5541, 2000.
258. V Lachet, A Boutin, R J-M Pellenq, D Nicholson, AH Fuchs. J Phys Chem 100:9006, 1996.
259. N Raj, G Sastre, CRA Catlow. J Phys Chem B 103:11007, 1999.
260. G Sastre, N Raj, CRA Catlow, R Roque-Malherbe, A Corma. J Phys Chem B 102:3198, 1998.
261. PP Ewald. Ann Physik 64:253, 1921.
262. MP Allen, DJ Tildesley. *Computer Simulation of Liquids*. Oxford: Clarendon Press, 1987.
263. L Greengard, V Rokhlin. J Comp Phys 73:325, 1987.
264. HG Petersen, D Soelvason, JW Perram, ER Smith. J. Chem Phys 101:8870, 1994.
265. DK Remler, PA Madden. Mol. Physics 70:921, 1990.
266. G Galli, A Pasquarello. *First-Principles Molecular Dynamics*. Dordrecht: Kluwer Academic, 1993, pp 261–313.
267. S Bolton, WL Hase, Peshlerbe. Direct dynamics simulations of reactive systems. In: *Modern Methods for Multidimensional Dynamics for Computations in Chemistry*. Edited by DL Thompson. New York: World Scientific, 1998.
268. R Car, M Parrinello. Phys Rev Lett 55:2471, 1985.
269. K Schwarz, E Nusterer, PE Blöchl. Catal Today 50:501, 1999.
270. E Fois, A Gamba. J Phys Chem B 103:1794, 1999.
271. I Štich, JD Gale, K Terakura, MC Payne. J Am Chem Soc 121:3292, 1999.
272. E Nusterer, PE Blöchl, K Schwarz. Angew Chem Int Ed Engl 35:175, 1996.
273. E Nusterer, PE Blöchl, K Schwarz. Chem Phys Lett 253:448, 1996.
274. Y Jeanvoine, JG Ángyán, G Kresse, J Hafner. J Phys Chem B 102:7307, 1998.
275. R Shah, MC Payne, M-H Lee, JD Gale. Science 271:1395, 1996.
276. R Shah, JD Gale, MC Payne. J Phys Chem 100:11688, 1996.
277. F Filippone, FA Gianturco. J Chem Phys 111:2761, 1999.
278. D Alfè, MJ Gillan. Phys Rev Lett 81:5161, 1998.
279. GA de Wijs, G Kresse, L Vocadlo, D Dobson, D Alfe, MJ Gillan, GD Price. Nature 392:805, 1998.
280. P Demontis, GB Suffritti, A Alberti, S Quartieri, ES Fois, A Gamba. Gazz Chim Ital 116:459, 1986.
281. D Nicholson, K Travis. Molecular simulation of transport in a single micropore. In: *Recent Advances in Gas Separation by Microporous Ceramic Membranes*. Edited by NK Kanellopoulos. Amsterdam: Elsevier, 2000, pp 257–286.
282. R Haberlandt, S Fritzsche, H-L Vörtler. Simulation of microporous systems: Confined fluids in equilibrium and diffusion in zeolites. In: *Handbook of Surfaces and Interfaces of Materials*. Edited by HS Nalwa. San Diego: Academic Press, 2001, pp 357–443.
283. R Haberlandt, S Fritzsche, G Peinel, K Heinzinger. *Molekulardyanmik*. Braunschweig: Vieweg, 1995.
284. D Frenkel, B Smit. *Understanding Molecular Simulations*. San Diego: Academic Press, 1996.
285. CJ Mundy, S Balasubramanian, K Bogchi, ME Tuckerman, ML Klein. Rev Comp Chem 14:291, 2000.
286. ME Tuckerman, GJ Martyna. J Phys Chem B 104:159, 2000.
287. WG Hoover. Physica A 194:450, 1993.

288. WG Hoover, O Kum. Mol Phys 86:685, 1995.
289. MC Lovallo, M Tsapatsis. AIChE J 42:3020, 1996.
290. X Lin, JL Falconer, RD Noble. Chem Mater 10:3716, 1998.
291. S Fritzsche, R Haberlandt, J Kärger. Z Phys Chem 189:211, 1995.
292. GS Heffelfinger, F van Swol. J Chem Phys 100:7548, 1994.
293. D. Nicholson. Supramol Sci 5:275, 1998.
294. KP Travis, KE Gubbins. Langmuir 15:6050, 1999.
295. L. Xu, TT Tsotsis, M. Sahimi. J Chem Phys 111:3252, 1999.
296. I Wold, B Hafskjold. Int J Thermophys 20:847, 1999.
297. KP Travis, KE Gubbins. J Chem Phys 112:1984, 2000.
298. L. Xu, MG Sedigh, TT Tsotsis, M Sahimi, J Chem Phys 112:910, 2000.
299. MG Martin, AP Thompson, TM Nenoff. J Chem. Phys 114:7174, 2001.
300. RL June, AT Bell, DN Theodorou. J Phys Chem 96:1051 1992.
301. F Jousse, L Leherte, DP Vercauteren. J Phys Chem B 101:4717, 1997.
302. AK Nowak, CJJ Den Ouden, SD Pickett, B Smit, AK Cheetham, MFM Post, JM Thomas. J Phys Chem 95:848, 1991.
303. F Jousse, L Leherte, DP Vercauteren. J Mol Catal A Chemical 119:165, 1997.
304. V Lachet, A Boutin, B Tavitian, AH Fuchs. Faraday Disc 106:307, 1997.
305. R Krishna, B Smit, TJH Vlugt. J Phys Chem 102:7727, 1998.
306. V Lachet, A Boutin, B Tavitian, AH Fuchs. J Phys Chem B 103:9224, 1999.
307. MD Macedonia, EJ Maginn. Grand canonical Monte Carlo simulation of single component and binary mixture adsorption in zeolites. In: *Proc 12th Int Zeolite Conf. Materials Research Society*. 1999, pp 363–370.
308. TJH Vlugt, R Krishna, B Smit. J Phys Chem B 103:1102, 1999.
309. DS Sholl, KA Fichthorn. J Chem Phys 107:4384, 1997.
310. H van Beijeren, KW Kehr, R Kutner. Phys Rev B 28:5711, 1983.
311. PA Fedders. Phys Rev B 17:40, 1978.
312. V Kukla, K Hahn, K Kärger, J Kornatowski, H Pfeifer. Anomalous diffusion in $AlPO_4$-5. In: *Proceedings of the 2nd Polish-German Zeolite Colloquium*. Edited by M Rozwadowski. Torun: Nicholas Copernicus University Press, 1995, pp 110–119.
313. C Rödenbeck, J Kärger, K Hahn, J Catal 157:656, 1995.
314. GD Lei, BT Carvill, WMH Sachtler. Appl Catal 142:347, 1996.
315. D. Keffer, AV McCormick, HT Davis. Mol Phys 87, 367 1996.
316. K Hahn, J Kärger. J Phys Chem 100:316, 1996.
317. RL June, AT Bell, DN Theodorou. J Phys Chem 95:8866, 1991.
318. D Chandler. J Chem Phys 68:2959, 1978.
319. P Pechukas. Transition state theory. Dynamics of Molecular Collisions. Edited by W Miller. New York: Plenum, 1976, p 269.
320. WH Miller. J Chem Phys 61:1823, 1974.
321. AF Voter, JD Doll. J Chem Phys 82:80, 1985.
322. GA Voth, D. Chandler, WH Miller. J Chem Phys 91:7749, 1989.
323. A Voter. J Chem Phys. 82:1890, 1985.
324. GH Vineyard. J Phys Chem Solids 3:121, 1957.
325. EM Sevick, AT Bell, DN Theodorou. J Chem Phys 98:3196, 1993.
326. H Jonsson, G Mills, KW Jacobsen. Nudged elastic band method for finding minimum energy paths of transitions. In: *Classical and Quantum Dynamics in Condensed Phase Simulations*. Edited by BJ Berne, G Ciccotti, and DF Coker. Singapore: World Scientific, 1998, pp 385–404.
327. A Voter. J Chem Phys 106:4665, 1997.
328. C Dellago, PG Bolhuis, FS Csajka, D. Chandler. J Chem Phys 108:1964, 1998.
329. F Jousse, SM Auerbach, DP Vercauteren. J Phys Chem B 102:6507, 1998.
330. T Mosell, G. Schrimpf, C. Hahn, J. Brickmann. J Phys Chem 100:4571, 1996.
331. T Mosell, G. Schrimpf, J. Brickmann. J Phys Chem 100:4582, 1996.
332. C Tunca, DM Ford. J Chem Phys 111:2751, 1999.

333. B Bigot, VH Peuch. J Phys Chem B 102:8696, 1998.
334. DS Sholl. Chem Eng J 74:25, 1999.
335. MJ Murphy, GA Voth, ALR Bug. J Phys Chem B 101:491, 1997.
336. TN Truong. J Phys Chem B 101:2750, 1997.
337. Q Wang, SR Challa, DS Sholl, JK Johnson. Phys Rev Lett 82:956, 1999.
338. JT Fermann, SM Auerbach. J Chem Phys 112:6787, 2000.
339. JT Fermann, C Blanco, SM Auerbach. J Chem Phys 112:6779, 2000.
340. J Sauer, M Sierka, F Haase. In: *Transition State Modeling for Catalysis*. Edited by DG Truhlar and K Morokuma. Volume 721 in ACS Symposium Series. Washington, DC: ACS, 1999, pp 358–367.
341. M Sierka, J Sauer. J Chem Phys 112:6983, 2000.
342. R Hernandez, WH Miller. Chem Phys Lett 214:129, 1993.
343. E Ising. Z Phys 31:253, 1925.
344. AZ Panagiotopoulos. J Chem Phys 112:7132, 2000.
345. NG van Kampen. *Stochastic Processes in Physics and Chemistry*. Amsterdam: North-Holland, 1981.
346. C Blanco, C Saravanan, M Allen, SM Auerbach. J Chem Phys 113:9778, 2000.
347. MW Deem, JM Newsam, JA Creighton. J Am Chem Soc 114:7198, 1992.
348. MC Mitchell, AV McCormick, HT Davis. Z Phys B 97:353, 1995.
349. SY Bhide, S Yashonath. J Chem Phys 111:1658, 1999.
350. SY Bhide, S Yashonath. J Phys Chem B 104:2607, 2000.
351. PH Nelson, AB Kaiser, DM Bibby. J Catal 127:101, 1991.
352. D Keffer, AV McCormick, HT Davis. J Phys Chem 100:967, 1996.
353. BL Trout, AK Chakraborty, AT Bell. Chem Eng Sci 52:2265, 1997.
354. C Saravanan, SM Auerbach. J Chem Phys 109:8755, 1998.
355. I Dukovski, J Machta, C Saravanan, SM Auerbach. J Chem Phys 113:3697, 2000.
356. DN Theodorou, J Wei. J Catal 83:205, 1983.
357. LF Gladden, JA Sousa-Gonçalves, P Alexander. J Phys Chem B 101:10121, 1997.
358. KA Fichthorn, WH Weinberg. J Chem Phys 95:1090, 1991.
359. HI Metiu, YT Lu, ZY Zhang, Science 255:1088, 1992.
360. C Saravanan, PhD thesis, University of Massachusetts, Amherst, 1999.
361. P Maksym. Semicond Sci Technol 3:594, 1988.
362. R Krishna, TJH Vlugt, B Smit. Chem Eng Sci 54:1751, 1999.
363. LF Gladden, M. Hargreaves, P Alexander. Chem Eng J 74:57, 1999.
364. RM Barrer. J Chem Soc, Faraday Trans 86:1123, 1990.
365. DM Ford, ED Glandt. J Phys Chem 99:11543, 1995.
366. DM Ford, ED Glandt. J Membrane Sci 107:47, 1995.
367. L. Whitmore, B. Slater, CRA Catlow. Phys Chem Chem Phys 2:5354, 2000.
368. C Saravanan, SM Auerbach. J Chem Phys 107:8132, 1997.
369. RQ Snurr. Chem Eng J 74:1, 1999.
370. I Kuscer, JJM Beenakker. J Stat Phys 87:1083, 1997.
371. C Rodenbeck, J Kärger, K Hahn. Phys Rev E 55:5697, 1997.
372. D Shen, LVC Rees. J Chem Soc Faraday Trans 86:3687, 1990.
373. PR van Tassel, SA Somers, HT Davis, AV McCormick. Chem Eng Sci 49:2979, 1994.
374. PH Nelson, AB Kaiser, DM Bibby. Zeolites 11:337, 1991.
375. PH Nelson, DM Bibby. Stud Surf Sci Catal 68:407, 1991.
376. D Stauffer, A Aharony. *Introduction to Percolation Theory*. Bristol PD: Taylor & Francis, 1991.
377. A Germanus, J Kärger, H Pfeifer, NN Samulevic, SP Zdanov. Zeolites 5:91, 1985.
378. M Bülow, W Mietk, P Struve, P Lorenz. J Chem Soc, Faraday Trans I 79:2457, 1983.
379. H Jobic, M Bée, J Kärger, H Pfeifer, J Caro. J Chem Soc, Chem Commun 341, 1990.
380. DM Shen, LVC Rees. Zeolites 11:666, 1991.
381. G Vitale, LM Bull, RE Morris, AK Cheetham, BH Toby, CG Coe, JE Macdougall. J Phys Chem 99:16087, 1995.
382. BL Trout, AK Chakraborty, AT Bell, J Phys Chem 100:17582, 1996.

383. FJMM de Gauw, J van Grondelle, RA van Santen. J Catal 204:53, 2001.
384. C Rödenbeck, J Kärger, K Hahn. J Catal 176:513, 1998.
385. GD Lei, WMH Sachtler. J Catal 140:601, 1993.
386. Z Kapinski, SN Ghandi, WMH Sachtler. J Catal 141:337, 1993.
387. C Rödenbeck, J Kärger, H Schmidt, T Rother, M Rödenbeck. Phys Rev E 60:2737, 1999.
388. C Rödenbeck, J Kärger, K Hahn, W Sachtler. J Catal 183:409, 1999.
389. EG Derouane, Z Gabelica. J Catal 65:486, 1980.
390. EG Derouane. Appl Catal A 115:N2, 1994.
391. J Kärger, P Bräuer, H Pfeifer. Z Phys Chem 214:1707, 2000.
392. N Neugebauer, P Bräuer, J Kärger. J Catal 194:1, 2000.
393. P Bräuer, J Kärger, N Neugebauer. Europhys Lett 53:8, 2001.
394. LA Clark, GT Ye, RQ Snurr, Phys Rev Lett 84:2893, 2000.
395. P Bräuer, N Neugebauer, J Kärger. Coll Surf A 187:459, 2001.
396. J Kärger, M Petzold, H Pfeifer, S Ernst, J Weitkamp. J Catal 136:283, 1992.
397. OM Braun, CA Sholl. Phys Rev B 58:14870, 1998.
398. D Fenzke, J Kärger. Z Phys D 25:345, 1993.
399. R Krishna, LJP van den Broeke. Chem Eng J Biochem Eng J 57:155, 1995.
400. L Forni, CF Viscardi. J Catal 97:480, 1986.
401. P Lorenz, M Bülow, J Kärger. Izv Akad Nauk SSSR, Ser Khim, 1741, 1980.
402. R Burmeister, H Schwarz, B Boddenberg. Ber Bunsenges Phys Chem 93:1309, 1989.
403. H Jobic, M Bée, J Caro. Translational mobility of *n*-butane and *n*-hexane in ZSM-5 measured by quasi-elastic neutron scattering. In: *Proc. 9th Int. Zeolite Conf*. Edited by R vonr Ballmoos et al. Boston: Butterworth-Heinemann, 1993, pp 121–128.
404. JB Nicholas, FR Trouw, JE Mertz, LE Iton, AF Hopfinger. J Phys Chem 97:4149, 1993.
405. VA Ermoshin, V Engel. J Phys Chem A 103:5116, 1999.
406. E Hernández, CRA Catlow. Proc Roy Soc Lond A 448:143, 1995.